Regenerative bioadhesives for intervertebral disc repair

Xuan Li

Doctor of Philosophy

Department of Mechanical Engineering

McGill University

Montreal, Quebec

January 2024

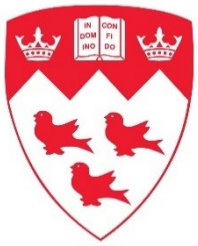

A thesis submitted to McGill University in partial fulfillment of the requirements for the degree of Doctor of Philosophy

Abstract

Intervertebral disc (IVD) herniation is a leading cause of chronic lower back pain and disability, affecting people's daily lives and causing a substantial economic burden. Current surgical interventions, involving discectomy with or without nucleotomy. Though pain could be alleviated, damages to native nucleus pulposus (NP) and annulus fibrosus (AF) were inevitable, which heighten the risks of recurrent herniations. Bioadhesives hold promise as an alternative solution for IVD repair due to their capacity to fill the NP cavity while sealing defects in the AF, yet existing options are inadequate in restoring the biomechanical properties and fail to effectively prevent re-herniation under loading. Challenges in advancing bioadhesives for IVD repair and regeneration include weak adhesion performance between bioadhesives and tissues, restricted regenerative capacities of the implanted biomaterials, and mechanical and structural mismatching with the native tissue. Moreover, the heterogeneous nature of IVD makes repair difficult using a single material solution.

To address these challenges, this thesis presents hybrid bioadhesives, integrating an injectable glue and a tough sealant, to concurrently repair and regenerate IVD following nucleotomy. The glue fills NP cavities, while the sealant repairs AF defects. The bioadhesive exhibits robust adhesion with IVD tissues and can withstand extreme disc loads. The glue also matches native NP mechanics, supporting cell viability and matrix deposition, serving as an effective cell delivery carrier for NP regeneration. In vitro and ex vivo assessments confirm the efficacy of regeneration and repair. Biomechanical evaluations on bovine IVD motion segments verify the capacity of hybrid bioadhesive to restore disc biomechanics and prevent permanent herniation under demanding loading conditions. Furthermore, the AF sealant was optimized to mimic human AF tissues mechanically and structurally. A composite hydrogel sealant was developed by embedding 3D-printed thermoplastic polyurethane (TPU) mesh into the tough hydrogel adhesive. The mesh design reinforces the mechanical properties of the sealant and can match those of human AF tissue. This composite hydrogel sealant forms tough adhesion and matches the curvature of human IVD. Ex vivo tests on bovine IVD segments validates its efficacy in preventing herniation and enhancing biomechanical recovery. Moreover, preliminary ex vivo studies are conducted on a human IVD model with a bioreactor with cyclic loading for four weeks. As a result, the bioadhesive exhibits robust integrity, effectively preventing the recurrence of disc herniation and preserving crucial biomechanical properties. Additionally, there is an enhancement in regeneration indicators,

including notable increases in hydration levels and proteoglycan content. This initial validation marks the efficacy of hybrid bioadhesives towards translational applications and sets the stage for subsequent preclinical studies.

The reported hybrid bioadhesive strategy for the treatment of IVD post-nucleotomy demonstrates tough adhesion, mimics native tissue mechanics, and supports cell growth. Through biomechanical assessments and ex vivo tests, it shows promise in preventing re-herniation and enhancing biomechanical recovery. This finding holds potentials to advance IVD repair and regenerative medicine applications.

Résumé

La hernie discale intervertébrale (DIV) est l'une des principales causes de douleurs lombaires chroniques et d'invalidité, affectant la vie quotidienne des personnes et entraînant un fardeau économique substantiel. Les interventions chirurgicales actuelles consistent en une discectomie avec ou sans nucléotomie. Bien que la douleur puisse être soulagée, des dommages au noyau pulpeux (NP) et à l'anneau fibreux (AF) sont inévitables, ce qui augmente les risques de hernies récurrentes. Les bioadhésifs sont prometteurs en tant que solution alternative pour la réparation des DIV en raison de leur capacité à remplir la cavité du NP tout en scellant les défauts de l'AF, mais les options existantes sont inadéquates pour restaurer les propriétés biomécaniques et ne parviennent pas à prévenir efficacement la ré-hernie sous charge. Parmi les défis posés par les progrès des bioadhésifs, citons les faibles performances d'adhésion, les capacités de régénération restreintes et l'inadéquation mécanique et structurelle avec le tissu natif. En outre, la nature hétérogène des DIV rend la réparation difficile en utilisant une solution à base d'un seul matériau.

Pour relever ces défis, cette thèse présente des bioadhésifs hybrides, intégrant une colle injectable et un produit d'étanchéité résistant, pour réparer et régénérer simultanément les DIV après une nucléotomie. La colle remplit les cavités des NP, tandis que le scellant répare les défauts de la FA. La bioadhésive présente une forte adhérence avec les tissus de la DIV et peut résister à des charges discales extrêmes. La colle correspond également à la mécanique native des NP, favorisant la viabilité cellulaire et le dépôt de la matrice, et servant de vecteur cellulaire efficace pour la régénération des NP. Des évaluations in vitro et ex vivo confirment l'efficacité de la régénération et de la réparation. Des évaluations biomécaniques sur des segments de mouvement de DIV bovins vérifient la capacité du bioadhésif hybride à restaurer la biomécanique du disque et à prévenir une hernie permanente dans des conditions de charge exigeantes. En outre, le mastic AF a été optimisé pour imiter les tissus AF humains d'un point de vue mécanique et structurel. Un scellant composite à base d'hydrogel a été mis au point en incorporant un filet en polyuréthane thermoplastique (TPU) imprimé en 3D dans l'adhésif hydrogel résistant. La conception de la maille renforce les propriétés mécaniques de l'agent d'étanchéité et peut correspondre à celles du tissu AF humain. Ce scellant hydrogel composite forme une adhésion solide et correspond à la courbure de la DIV humaine. Des essais ex vivo sur des segments de DIV bovins ont validé son efficacité dans la prévention des hernies et l'amélioration de la récupération biomécanique. En outre, des études préliminaires ex vivo ont été menées sur un modèle humain de DIV à l'aide d'un bioréacteur avec une charge cyclique

pendant quatre semaines. En conséquence, le bioadhésif présente une intégrité robuste, empêchant efficacement la récurrence de l'hernie discale et préservant les propriétés biomécaniques cruciales. En outre, on observe une amélioration des indicateurs de régénération, y compris des augmentations notables des niveaux d'hydratation et de la teneur en protéoglycanes. Cette validation initiale démontre l'efficacité des bioadhésifs hybrides pour les applications translationnelles et ouvre la voie à des études précliniques ultérieures.

La stratégie bioadhésive hybride rapportée pour le traitement de la DIV après une nucléotomie démontre une adhésion solide, imite la mécanique du tissu natif et soutient la croissance cellulaire. Grâce à des évaluations biomécaniques et à des tests ex vivo, elle s'avère prometteuse pour prévenir la ré-hernie et améliorer la récupération biomécanique. Cette découverte est susceptible de faire progresser la réparation des DIV et les applications de médecine régénérative.

Acknowledgments

Throughout the last four and a half years, my time at McGill in Montreal has been filled with immense joy and unforgettable moments. I am incredibly fortunate and appreciative to have crossed paths and collaborated with such exceptional individuals in this vibrant city.

Firstly, I would like to thank Professor Jianyu Li, my advisor and mentor, for his support throughout my doctoral journey. I am deeply grateful to Professor Li for providing me with a wealth of opportunities and resources to access facilities and expertise, conduct collaborative projects, and participate in conferences, all of which I have greatly benefited from and which I treasure. I am grateful for his understanding of the challenges I faced during my PhD studies and for all the understanding and support he provided. His patient guidance and generous support not only encouraged me to overcome these research obstacles, but also facilitated my continuous growth. It was an honor to work with him, and our friendship and invaluable experience will always inspire me in the future.

I wish to thank all the fantastic collaborations and communications I had with our lab members. I would like to thank Dr. Zhenwei Ma, who was the first person to train me on how to synthesize alginate hydrogels in the laboratory. He not only helped me with the project but also encouraged me when I encountered difficulties in scientific research. His passion for and exploration of scientific research constantly inspires me to become a better researcher. I am sincerely grateful to Dr. Guangyu Bao for his invaluable guidance and support during my time in the laboratory whose extensive knowledge has incredibly inspired me. His generous assistance and exemplary character have left a lasting impression, for which I hold deep respect and gratitude. I would like to thank Dr. Farshid Ghezelbash for his assistance with biomechanics and for his valuable advice on the research project and career development. I want to express my gratitude to Dr. Baolin Huang for his invaluable support in the bioreactor experiment. I am delighted to have collaborated with him to complete this challenging task. Thanks to Ran Huo for being my best co-worker in the lab, whose seamless collaboration on experiments and positive attitude have been pivotal in making our work enjoyable. Many thanks to Shiyu Liu for being so helpful in the lab. His encouragement and expertise in mechanics have boosted my research. Many thanks to Shuaibing Jiang for always showing patience and support during our chemical synthesis experiments and beyond. I also like to thank Christopher Chuang for being my best deskmate and

providing selfless help for the lab. I would like to thank Alex Nottegar for helping in the lab and cheering up in the office. Thank Portia Rayner for sharing popcorn in the office. Thank Aram Bahmani very much for his help on the mechanical test and advice on the presentation. Thanks to Dr. Zhen Yang for his help and insights on mechanics in the bioadhesive experiments. Thanks to Yin Liu for her kind help on cell culture and bioassay experiments. Thanks to Evan Johnston for his assistance with lab duties and for taking care of freeze dryer together. Thank Justin Puma for living up the atmosphere in the lab with cute insects. Thanks to Tianqin Ning for creating a relaxing vibe during the experiment with background music. Thank Ting Wang for bovine intervertebral disc isolation. Thank Yixun Cheng for answering my chemical questions. Thank David-Michael Phillips for sharing the chili in the office. Thank Dr. Malvika Nagrath for providing advice on my group presentation. Thank Dr. Michelle Lan for her advice on my career development. Thank Xiang Ni, Louis-Jacques and Dr. Shengyun Huang for their kind support in the lab.

I would like to thank my collaborators outside our lab for their support and contributions to various research projects. I am grateful to Professor Lisbet Haglund from the Department of Surgery at McGill for providing mentoring on our collaborative projects of bioadhesives for intervertebral disc repair. Many thanks to Prof. Haglund for her responsible supervision and for providing access to sources related to the project. It was a great pleasure to work with Professor Haglund's group members at Montreal General Hospital (MGH), especially with Li Li and Dr. Hosni Cherif. Thank Li Li so much for her detailed training, selfless assistance, and professional collaboration on our project. Her encouragements and kind support also helped me getting though the difficult time during the Covid-period. Many thanks to Hosni Cherif for his help on the bioreactor experiments and providing insights on the bioadhesive projects. I also like to thank Professor Derek H. Rosenzweig from Department of Surgery at McGill for his support and for his advice on the 3D printing materials design. Thank Professor Rahul Gawri from Department of Surgery at McGill for allowing me access to the equipment in his lab at MGH. Thank Dr. Michael H. Weber from Department of Surgery at McGill for providing expertise on clinical-related questions and for training on the procedure of nucleotomy. Thank Professor Mark Driscoll from Department of Mechanical Engineering at McGill for the helpful discussion on the project and thank Siril Dukkipati from Department of Mechanical Engineering at McGill and Lorne Beckman for assistance on biomechanics tests in the Orthopaedic Research Laboratory (ORL) at McGill. Thank Professor Nicole Y. K. Li-Jessen from School of Communication Sciences and Disorders at McGill

for serving as my Advisory Committee member with guidance and for her kind support on journal manuscript writing. Thank Professor Luc Mongeau from Department of Mechanical Engineering for allowing me access to the equipment in the lab, for providing support as my Advisory Committee member, for helping me when I was a teaching assistant in MECH 315. Thank Sepideh Mohammadi, Sareh Taheri, Sara Nejati, Alicia Reyes, Zixin He, Dr. Kaustuv Basu from Professor Mongeau's group for always being supportive and helpful in the lab.

I acknowledge Life Sciences Complex Advanced BioImaging Facility (ABIF) at McGill for collecting and processing fluorescence images. Thank Jérémie Fouquet and Mila Urosevic for the assistance on MRI scanning at Brain at Douglas Mental Health Institute. Thank Dr. Sam Alexandre Selmani from Oligo Medic for providing fresh bovine tails for lap shear tests. Thank. This work was supported by the Canadian Institutes of Health Research (grants PJT 165995, PJT 180232)) and the Natural Sciences and Engineering Research Council of Canada (grant NCE-ALLRP 548623-19). I acknowledge support from the Québec Cell, Tissue and Gene Therapy (ThéCell) Network and the McGill Regenerative Medicine Network. I also like to acknowledge financial support from Fonds de recherche du Québec – Nature et technologies (FRQNT) Doctoral Research Scholarship and McGill Engineering International Tuition Award.

Finally, I would like to thank my husband Yufei Fu for his unconditional love and understanding, and my parents Liping Ding and Manjin Li for their endless love and support. Thank my dear friends Delin Li, Le Fan, Yijie Gong, and Xiumei Jiang for their mental support. Thank Xinyi Wang for her support with food and love. Thanks to Lina and Bigking for reminding me about happiness by slowing down my writing speed. Thank Patrick Star for giving me the power to be fearless and joyful.

Contribution to Original Knowledge

The research reported within this dissertation contributes to the advancement of original knowledge to the field of bioadhesive in four aspects: a tissue-mimicking hybrid bioadhesive strategy that prevents disc reherniation; an injectable viscoelastic bioadhesive that supports cellular function to promote nucleus pulposus regeneration; a composite-reinforced hydrogel bioadhesive for local-specific annuals fibrosus repair; and an ex vivo model of the human intervertebral disc after nucleotomy for validation of translational potential.

A **tissue-mimicking hybrid bioadhesive strategy** was developed to prevent reherniation of intervertebral discs (IVD). It consists of two components: a viscoelastic hydrogel adhesive that fills the nucleus pulposus (NP) cavity and a tough adhesive that seals the annulus fibrosus (AF) defect. This hybrid bioadhesive allows for simultaneous regeneration and repair the heterogeneous IVD tissue with the ability to withstand loading by adhering strongly to the substructure of the IVD tissue.

An **injectable viscoelastic bioadhesive** was developed that supports cellular function and promotes NP regeneration. The bioadhesive features tunable viscoelasticity which can match the native NP property while affect cellular metabolic activity and matrix deposition, enabling cell regeneration function at the target site.

A **composite-reinforced hydrogel bioadhesive** was designed considering the specific geometry and angle-ply structures at AF defects. Reinforced by a 3D-printed thermoplastic polyurethane mesh, the designed composite sealant successfully regained high modulus values matching those of natural AF tissue. The modified composite sealant patch also achieved restoration of disc biomechanical function.

An **ex vivo model of the human IVD after nucleotomy** was developed for translational potential validation. The assessment based on this platform revealed that the hybrid bioadhesive successfully prevented reherniation through a 28-day incubation, while promoting regeneration within the NP region under physiologic loading conditions.

The aforementioned contributions have been consolidated in the preparation or publication of the following peer-reviewed journal articles:

- Peer-reviewed journal articles

1. **Xuan Li**, Yin Liu, Li Li, Ran Huo, Farshid Ghezelbash, Zhenwei Ma, Guangyu Bao, Shiyu Liu, Zhen Yang, Michael H. Weber, Nicole Y. K. Li-Jessen, Lisbet Haglund*, Jianyu Li*, Tissue-mimetic hybrid bioadhesives for intervertebral disc repair. *Materials Horizons*, 10 (5), 1705-1718 (2023).

   ***Contributions*:** X. L., L. H., and J. L. conceived the idea and designed the research. X. L., Y. L., Z. M., and S. L. performed the lap-shear test; Z. Y. analyzed the lap-shear test results; X. L., R. H., F. G., S. L., and Z. M. performed the biomechanical test. F. G. and X. L. processed the data of biomechanical tests; L. H., L. L., and M. H. W. provided the human IVD tissues and cells. X. L., L. L., Y. L., and G. B. performed cytotoxicity tests, cell culture, bioassays, and imaging; L. H. and J. L. supervised the work. X. L., Y. L., L. H., and J. L. drafted the manuscript, and all authors contributed to the writing of the manuscript.

2. **Xuan Li**, Yin Liu, Shiyu Liu, Baolin Huang*, Nicole Li-Jessen, Lisbet Haglund, Jianyu Li*, Designing Regenerative Bioadhesives for Tissue Repair and Regeneration, *Advanced Therapeutics*, 2300139 (2023).

   ***Contributions*:** X. L., Y. L., J. L., and B. H. conceived the idea and concept of the review article; X. L., Y. L., J. L., and B. H. drafted the manuscript; S. L., X. L., and B. H. prepared the figures; N. L. J. and L. H. provided insights of the writing, and all authors contributed to the writing of the manuscript.

3. **Xuan Li**, Ran Huo, Farshid Ghezelbash, Li Li, Hosni Cherif, Lisbet Haglund, Jianyu Li*, Composite hydrogel adhesives for annulus fibrosus repair, Preparation for submission (2024).

   ***Contributions*:** X. L. and J. L. contributed to the idea of the research; L. H., L. L., and H. C. provided insights into the design of the study and provided human AF tissues for mechanical tests; X. L., R. H., and F. G. contributed to the hydrogel design, fabrication, and all mechanical tests; X. L. and R. H. conducted the ex vivo biomechanical tests; X. L. and F. G. processed the biomechanical test data; J. L. and L. H. supervised the work. X. L. and J. L. drafted the manuscript, and all authors contributed to the writing of the manuscript.

- Selected conference proceedings

1. **Xuan Li**, Baolin Huang, Li Li, Hosni Cherif, Yin Liu, Lisbet Haglund, Jianyu Li, "Bioadhesives for intervertebral disc repair and regeneration after nucleotomy", 38th Canadian Biomaterials Society Annual Meeting, Oral presentation, 2023.
2. **Xuan Li**, Yin Liu, Li Li, Farshid Ghezelbash, Ran Huo, Zhenwei Ma, Shiyu Liu, Zhen Yang, Lorne Beckmen, Lisbet Haglund, Jianyu Li, "Hybrid bioadhesive strategy for intervertebral disc repair and regeneration after nucleotomy", Annual Meeting of Orthopedic Research Society, Accepted poster, 2022.
3. **Xuan Li**, Jianyu Li, "Regulating mechanotransduction of intervertebral disc cells via engineered biomaterials". Annual Meeting of Biomedical Engineering Society, Poster presentation, 2020

In addition to this thesis, I have contributed to other projects, and be the co-author for collaboration publications during my Ph.D. study period:

1. H. Cherif, Li Li, J Snuggs, **Xuan Li**, C Sammon, Jianyu Li, L Beckman, Lisbet Haglund, C.L. Le Maitre, Injectable hydrogel induces regeneration of naturally degenerate human intervertebral discs in a loaded organ culture model, *Acta Biomaterialia* (2023), doi: https://doi.org/10.1016/j.actbio.2023.12.041.

   Contributions: Processed and analyzed the mechanical loading data from the bioreactor experiment and contributed to the interpretation of the biomechanical data.

2. Ran Huo, Guangyu Bao, Zhenwei Ma, Zixin He, Roozbeh Moakhar, Zhen Yang, Shuaibing Jiang, **Xuan Li**, Christopher Chung, Alexander Nottegar, Changhong Cao, Sara Mahshid, Jianyu Li*, Tough transient ionic junctions printed with ionic microgels, *Advanced Functional Materials*, 2213677 (2023).

   Contributions: Fabricated the ionic touchpad based on triboelectric nanogenerators, implemented the detection circuit, and carried out the experiment of demonstration of the touchpad performance.

3. Zhenwei Ma, Claire Bourquard, Qiman Gao, Shuaibing Jiang, Tristan De Iure-Grimmel, Ran Huo, **Xuan Li**, Zixin He, Zhen Yang, Galen Yang, Yixiang Wang, Edmond Lam, Zu-Hua Gao, Outi Supponen*, Jianyu Li*, Controlled tough bioadhesion mediated by ultrasound, *Science*, 377, 751-755 (2022).

Contributions: Carried out the experiment to measure the depth of penetration of the bioadhesive agent in the skin and analyzed it with confocal fluorescence imaging.

4. Patrick Coburn, **Xuan Li**, Jianyu Li, Yo Kishimoto, Nicole Li-Jessen*, Progress in vocal fold regenerative biomaterials: An immunological perspective, *Advanced NanoBiomed Research*, 2100119 (2021).

   Contributions: Graphed the schematic of the effects of biomaterial parameters on immune cells and modified the writing.

Contribution of Authors

I, Xuan Li, confirm that I am the primary author and contributor to all work contained within this thesis, with the responsibility for the conceptualization, study design, experimentation, data analysis, visualization, and writing of all the chapters. All work was done under the supervision of Prof. Jianyu Li and under the guidance of Prof. Lisbet Haglund. This section outlines the scientific contributions of all authors for each of the thesis chapters presented herein.

In Chapter 1, under the guidance of Prof. Jianyu Li, I conceptualized the idea of this study and wrote about the background, challenges, rationale, and objectives of this study.

In Chapter 2, I provided a literature review of mechanical design considerations and a case study of a bioadhesive used for intervertebral disc (IVD) repair. In addition, I did the literature survey on the background of this study in Sections 2.2 through 2.6. Yin Liu contributed to the part of the literature review on biological design considerations for regenerative bioadhesives in Section 2.1. Shiyu Liu contributed to the schematic preparation. Dr. Baolin Huang contributed to part of the literature search on biological and mechanical design considerations in Section 2.1.

In Chapter 3 and Chapter 4, I, Prof. Jianyu Li and Prof. Lisbet Haglund contributed to the idea and design of the research. I, Yin Liu, Dr. Zhenwei Ma, Shiyu Liu, and Dr. Zhen Yang contributed to the performance and analysis of the lap-shear test of NP glue on bovine IVD. I, Dr. Guangyu Bao, Dr. Zhenwei Ma, and Yin Liu contributed to the rheology test of alginate hydrogel and human NP tissue. I and Dr. Zhenwei Ma contributed to the primer penetration characterization. I, Ran Huo, Dr. Farshid Ghezelbash, Shiyu Liu, and Dr. Zhenwei Ma contributed to the performance of biomechanical tests of bovine IVD. I and Dr. Farshid Ghezelbash contributed to the processing of biomechanical test data. Prof. Lisbet Haglund, Li Li, Dr. Hosni Cherif, and Dr. Michael H. Weber contributed to the preparation of the human IVD tissue and cells for all the experiments. I, Ran Huo, Dr. Baolin Huang, and Aram Bahmani contributed to the human IVD biomechanical tests. I, Li Li, Yin Liu, and Dr. Guangyu Bao contributed to the cytotoxicity tests, cell culture, bioassays, and imaging. I, Dr. Baolin Huang, Li Li, Dr. Hosni Cherif and Yin Liu contributed to the human IVD bioreactor experiments.

In Chapter 3 and Chapter 5, I and Prof. Jianyu Li contributed to the idea of the research. Prof. Lisbet Haglund, Li Li, and Dr. Hosni Cherif provided insights into the design of composite hydrogel patches and provided human AF tissues for the mechanical test. I, Ran Huo and Dr. Farshid

Ghezelbash contributed to the design and fabrication of the composite hydrogel patch. I, Ran Huo, Dr. Farshid Ghezelbash, and Aram Bahmani contributed to the mechanical test of the composite hydrogel patch. I and Ran Huo contributed to the biomechanical test on the bovine IVD with composite hydrogel patches.

Under the guidance of Dr. Jianyu Li, I critically discuss the findings in Chapter 6. And I summarized the thesis in Chapter 7. Dr. Jianyu Li contributed to improvement of the writing. Ran Huo contributed to the proofreading of the thesis.

Abbreviations

3D	three dimensional
AA	6-aminocaproic acid
AA-NHS	AA-g-N-hydroxysuccinimide
AF	annulus fibrosus
BME	basement membrane extract
BMP-2	bone morphogenetic protein-2
CTL	control
DAPI	4′,6-diamidino-2-phenylindole
DDA	degree of deacetylation
DMMB	1,9-dimethyl methylene blue
DMEM	Dulbecco's modified eagle's medium
ECM	extracellular matrix
EDC	ethyl-3-(3-dimethylaminopropyl) carbodiimide hydrochloride
FibGen	Genipin-crosslinked fibrin
GAG	glycosaminoglycan
GF	growth factor
HA	hyaluronic acid
IAF	inner annulus fibrosus
IVD	intervertebral disc
LBP	lower back pain
MMPs	matrix metalloproteinases
MSCs	mesenchymal stem/stromal cells
MW	molecular weight
NHS	N-hydroxysulfosuccinimide
NP	nucleus pulposus
NZ	neutral zone
OAF	outer annulus fibrosus
PBS	phosphate buffered saline
PEG	poly (ethylene glycol)
PLGA	poly (lactic-co-glycolic acid)
PLLA	poly (L-lactic acid)
PTMC	poly (trimethylene carbonate)
PVA	poly (vinyl alcohol)
RGD	Arg-Gly-Asp
ROM	range of motion
SDF-1α	stromal cell-derived factor-1α
sGAG	sulfated glycosaminoglycan
TPU	thermoplastic polyurethane

Table of Contents

List of Figures

List of Tables

Chapter 1
Introduction

This chapter begins with an overview of the structure and organization of the dissertation, followed by an in-depth discussion of the background of intervertebral disc (IVD) repair and regeneration. Then the challenges of bioadhesives for IVD repair are outlined. The chapter then describes the rationale for initiating this project and concludes with a clear statement of specific research objectives.

1.1 Thesis organization

This thesis is written in traditional monograph style, structured into seven chapters: Introduction, Literature Review, Materials and Methods, Tissue-mimetic Hybrid Bioadhesives for IVD Repair, Composite Hydrogel Sealant for Annulus Fibrosis (AF) Repair, Discussions, and Concluding Remarks.

Chapter 1 provides an introduction to the whole thesis. First, the background of bioadhesive development targeting the needs of IVD repair after nucleotomy is described, followed by the challenges in the existing bioadhesives for IVD treatment. Next, rationale underlying the study design are outlined and the main objectives of this study are stated.

Chapter 2 provides a comprehensive literature review on bioadhesives for applications in IVD tissue repair and regeneration. The chapter explores design aspects of regenerative bioadhesives, covering mechanical and biological design and examining case studies related to musculoskeletal tissue repair. Additionally, it summarizes the structure, properties, and functions of the IVD. The chapter then focuses on biological strategies and biomaterials for nucleolus pulposus (NP) and AF regeneration and IVD culture models.

In Chapter 3, materials and methods used in the thesis are detailed. The experimental methodology is categorized into seven sections, the first five being material synthesis, mechanical characterization, cell culture and bioassays, biomechanical testing with IVD tissues, and evaluation on human IVD bioreactor. Ethical statements and statistical analysis are presented at last.

Chapter 4 and Chapter 5 present the results of the experiments conducted in the thesis, which contains two subsequent studies towards the objectives. Chapter 4 covers the design of tissue-

mimetic hybrid bioadhesives for IVD repair and regeneration, highlighting their adhesion and biomechanical performance characteristics. The chapter then discusses the capacity to enhance failure strength and prevent re-herniation, and their cytocompatibility with native and delivered cells. Preliminary ex vivo validation on a human IVD model demonstrates the clinical translation potential of the developed bioadhesive strategy. In Chapter 5, the focus shifts to the modification of bioadhesives for AF repair. A three dimensional (3D)-printed mesh is incorporated into the pristine hydrogel AF sealant, creating a composite hydrogel sealant with enhanced moduli. Strong adhesion of the modified sealant is demonstrated through lap shear and in-situ peeling tests on human and bovine AF tissues, and biomechanical properties are investigated to confirm the recovery of IVD mechanical functions.

Chapter 6 provides an extensive discussion on the results of the study. The chapter covers seven key topics: the development of tissue-mimetic hybrid bioadhesives, adhesion performance within IVD niche, biomechanical performance, cytocompatibility, ex vivo evaluation of IVD in bioreactor, mesh-reinforced composite hydrogel sealant, the limitations of the reported technologies, and identification of future opportunities for improvement.

The final chapter, Chapter 7, is the conclusion and remarks of the thesis. The chapter summarizes the findings corresponding to the proposed objectives and the contribution of this study to the field of IVD repair and regeneration.

1.2 Background

Lower back pain (LBP) is a leading cause of disability globally, with far-reaching consequences for both the economy and quality of life of the patients.[1,2] Studies anticipate that more than 80% of adults worldwide will experience LBP at some point in their lives.[3] In Canada, a survey of 2,400 individuals revealed that the lifetime prevalence of LBP as high as 83% in Alberta and Saskatchewan, with 61.8% reporting experiencing back pain in 2006.[4] Apart from pain and activity limitations, LBP has broader social implications, including participation restrictions and economic burdens.[5] The economic burden alone is significant, pertaining to medical expenses, compensation, lost productivity, employee retraining, administrative expenses, and litigation costs.[6,7] In Canada, healthcare costs associated with LBP are estimated to be between 6 and 12 billion dollars annually.[8,9] The prevalence increases with the aging population.

LBP is a multi-factorial condition. One of the main factors is the IVD degeneration.[10–12] IVD degeneration can occur across IVD components: the NP and the AF.[13] A tear in the AF may lead to extrusion of the NP through the defects, which leads to compression of spinal cord and/or nerve roots with resulting neurological injury.[14–16] The factors causing IVD degeneration include genetic predisposition, abnormal biomechanical loading, infection, decreased nutrient transport across the vertebral endplates, and aging.[17,18] As the IVD degenerates, NP loses water and changes from a gelatinous substance to a fibrous structure with the appearance of fissures in both NP and AF.[19,20] Due to the low nutrients and low pH microenvironment caused by avascularity, IVD has limited ability to recover and regenerate from degeneration or injury, especially for the NP tissue with extremely low cell density.[21,22]

Current preventive approaches include pain relief, physical health maintenance, and exercises to avoid excessive stress on the spine. Conservative clinical treatments target pain management, such as medication, analgesics, and physiotherapy.[23,24] For advanced degenerated IVD cases, surgery treatment (i.e., disc excision and vertebral fusion) may need to be considered following the failure of appropriate conservative treatments.[23,25] The current standard of care, a discectomy with a partial nucleotomy, removes the extruded and degenerated NP tissue from the epidural space to decompress the neural element.[26] This treatment is largely for treating the resulting neurological injury and is only palliative for disc degeneration as it fails to replenish the loss of NP tissue or repair the AF defect.[27–29] Although chondroid metaplasia may occur and close the inner AF defect, the structure at the AF/NP interface is still disrupted and the IVD remains malfunctioning.[27] Thereby, recurrent herniation (re-herniation) often occurs, leading to recurrent symptoms and repeat surgery. Study shows that the annual incidence of additional surgery for adjacent segment degeneration after lumbar arthrodesis is 2.5%, with a predicted 10-year prevalence of 22.2%. These incidence rates vary widely depending on specific risk factors. Patients who underwent fusion of three or four levels were at three times the risk of undergoing subsequent surgery than single-layer surgery, with a projected 10-year prevalence of 40%.[30] To avoid re-herniation post-nucleotomy, mechanical devices such as Barricaid® have been developed to close the AF defect. Nonetheless, they cause damage to adjacent vertebrae and cannot biologically regenerate the injured IVD tissues.[31] Therefore, great demands exist for novel regenerative strategies for biologically restoring IVD microenvironment and mechanically supporting the disc function.

For regenerative purposes, hydrogels are appealing due to their biocompatibility and capacity to deliver and support cells in injury sites. Existing hydrogels, however, are mechanically inferior against the disc loading and lack adhesiveness to IVD tissues, resulting in displacement and extrusion of the hydrogel from the AF defect.[32] Recent advances in bioadhesive hydrogels highlight their ability to adhere strongly to biological tissues and to tolerate biomechanical loadings.[33–38] A notable example is a bioinspired tough adhesive consisting of tough alginate-polyacrylamide hydrogel, achieving extremely high adhesion energy on various biological tissue surfaces.[39] Despite the advances, few bioadhesive hydrogels have been optimized or validated for IVD repair and regeneration. As such, IVD-mimetic bioadhesives continue to be sought.

The design of IVD-mimetic bioadhesives should account for the heterogeneity among the IVD substructures. NP and AF are different in terms of mechanical, structural, biochemical, and cellular properties.[40] Specifically, the AF consists of less water and proteoglycan (approximately 70% and 5% of the wet weight, respectively), compared to NP (around 80% and 15% of the wet weight, respectively) in immature human IVDs. Besides, native NP cells reside within the NP for homeostasis and regeneration.[41] The AF contains AF cells and laminates of organized collagen fibers, providing tensile strength to withstand the circumferential pressure from NP bulging.[42] Although the hallmarks between AF and NP become less apparent in mature human IVD, a clear difference in IVD remains by visual inspection of the horizontal bisected human IVDs.[43] These features lead to the highly viscoelastic nature of the NP and the high mechanical strength of the AF.[44] The heterogeneity among the IVD substructures poses different requirements for the IVD-mimetic bioadhesives. That is, they should exhibit viscoelastic behavior and support cells in the NP region while excelling in mechanical properties in the AF region.[45]

These requirements of IVD-mimetic bioadhesives are challenging to address under the conventional paradigm of bioadhesives, which are primarily based on a single hydrogel matrix. The single bioadhesive is difficult to meet the heterogeneity of the IVD. Achieving high adhesion performance to repair mechanically strong AF likely involves cytotoxic chemicals and harsh reaction conditions, which sacrifice the ability of bioadhesives to encapsulate and deliver viable cells to regenerate NP. These challenges are apparent in a recently reported bioadhesive hydrogel designed for IVD repair post-nucleotomy. It proved unsuitable for cell encapsulation and delivery due to its requirement for in-situ free-radical polymerization. Lack of mechanical robustness also caused extrusion of the hydrogel and the NP (re-herniation) under physiological disc loading.[46]

1.3 Challenges

Bioadhesive strategy is a promising approach for IVD repair post-nucleotomy, yet two challenges remain. First, the heterogeneity between different substructures of the IVD poses a challenge for the design of bioadhesives. The AF and NP of the disc differ in mechanical, structural, biochemical, and cellular properties, making it difficult for a conventional single bioadhesive to meet the requirements in these different regions. To address this challenge, IVD bioadhesives need to exhibit viscoelasticity and be able to support cells in the NP region, while possessing superior mechanical properties in the AF region. However, the current single hydrogel matrix bioadhesives do not satisfy the requirement for heterogeneity. This is because improving adhesion to repair the mechanically strong AF often sacrifices the bioadhesive's ability to encapsulate and release regenerating NP cells, leading to the re-herniation problems after repair. Therefore, effective repair and regeneration of the IVD necessitate a bioadhesive that can simultaneously restore the functions of different regions of the IVD.

Second, existing hydrogel bioadhesives for IVD repair are challenged by deficiencies in mechanical properties and structural functionality. Specifically, current hydrogel bioadhesives for NP repair lack strong adhesion to IVD tissue, leading to hydrogel displacement and extrusion when the disc is under load. For AF repair, hydrogel bioadhesives require higher modulus and toughness to prevent implant bulging. In addition, the complex fiber-layer structure of AF tissue needs to be considered in development for tissue-mimicking, and the specific defect shape of the AF itself poses challenges to accurately designing the geometry of the bioadhesive. These complexities are difficult to replicate accurately. Thus, conventional hydrogels need further enhancement to meet the specific requirements for repairing NP and AF.

1.4 Research rationale

IVD degeneration poses a significant challenge in orthopedic medicine, necessitating innovative solutions to enhance surgical outcomes and patient well-being. Current strategies for IVD repair face limitations, prompting the need for a paradigm shift in biomaterial design and application. This research aims to address these limitations by developing hydrogels that combine mechanical functionality and biological compatibility to serve as effective IVD bioadhesives. The focus on viscoelasticity, adhesive properties, biomechanical performance, and cell-delivery strategies represents a pioneering approach to improve the repair and regeneration of the IVD.

1.5 Research objectives

The research objectives of this thesis are divided into the following three subsequent aims.

Objective 1: Developing viscoelastic cell-laden bioadhesives for NP regeneration.

An injectable bioadhesive is designed to be viscoelastic to mimic and match the natural mechanical properties of NP tissue, providing the appropriate support and environment for cell growth and regeneration, named NP glue. By adjusting the molecular weight (MW) of the alginate and the concentration of cross-linking agent, the viscoelasticity can be matched to natural human NP. The adhesion of NP glue can be achieved by applying a bridging polymer as a primer between the glue and the tissue, and the adhesion performance is evaluated on specific IVD substructures. Next, the cytocompatibility of human IVD tissues can be evaluated by co-culture experiments with NP glue encapsulating stem cells. The response of primary human NP cells in different viscoelastic environments can be assessed by in vitro evaluations. Overall, the proposed NP glue is designed to strongly adhere to the NP region and support cellular functional regeneration to fulfill the complex needs of the NP.

Objective 2: Developing the biomimetic bioadhesive sealant for AF repair.

This objective aims to develop an AF sealant for repairing AF defects following nucleotomy and injection of the developed NP glue. The design criteria for the AF sealant is to replicate the complex angle-ply structure of AF in order to match its mechanical properties, and to maintain strong adhesion in a dynamic environment. First, an alginate-polyacrylamide double-network tough adhesive hydrogel is used. The adhesion property of this tough adhesive sealant is evaluated specific on IVD tissues. Next, the mechanical properties of the sealant are enhanced by incorporating a 3D-printed thermoplastic polyurethane (TPU) mesh. The configuration and volume fraction of the TPU mesh are tailored to mimic the modulus, tensile strength, and toughness of natural AF. Geometry of the AF sealant is further optimized based on the AF defect shape and IVD curvature. The performance of the developed composite hydrogel bioadhesives is validated by in-situ adhesion testing.

Objective 3: Assessing NP glue and AF sealant for biomechanical recovery and herniation prevention.

In this objective, the developed NP glue and AF sealant are combined to create a hybrid bioadhesive strategy designed for simultaneous IVD repair and regeneration. In this approach, the cell-laden NP glue is injected to fill the NP cavity and promote regeneration, while the AF sealant secures the injected NP glue by forming strong adhesion at the AF defect. Expected outcomes include prevention of recurrent herniation, restoration of biomechanical functions and stimulation of regeneration. To assess the efficacy of this hybrid bioadhesive strategy, compressive and tensile cyclic loading tests on bovine IVD motion segment model are performed to evaluate biomechanical performance. Subsequent ramp-to-failure compression testing verifies strength enhancement to prevent NP extrusion. Moreover, preliminary experiment utilizing an ex vivo human IVD culture model is conducted with a bioreactor to evaluate the performance of the hybrid bioadhesive under physiological conditions.

Chapter 2
Literature Review

Chapter 2 provides a comprehensive overview of the use of bioadhesives in the field of tissue repair and regeneration. It begins with a detailed review of existing regenerative bioadhesive designs, covering mechanical and biological design considerations, and highlights case studies of musculoskeletal tissue repair. Subsequent sections explore the complexity of intervertebral disc (IVD), revealing its intricate structure, cellular composition, functional dynamics, and the effects of mechanical loading. The chapter further delves into the multiple biological strategies for IVD repair, followed by biomaterials designed specifically for nucleus pulposus (NP) regeneration and annulus fibrosus (AF) repair. Finally, a survey of culture models employed in IVD research is presented.

2.1 Regenerative bioadhesives for tissue repair and regeneration

Bioadhesives are natural or synthetic polymers that act as “glue” in the provision of adhesion with living tissues. Since the introduction of fibrin glues, the bioadhesive repertoire has expanded substantially to various material systems, including hydrogels, plastics, and elastomers.[33] Bioadhesives are widely applicable in clinical and engineering fields, such as for wound closure, surgical sealants, regenerative medicine, drug delivery, trauma care, and implantable wearable devices. Many of these applications are associated with a critical and immediate need to regenerate the lost tissues. Since the introduction of fibrin hydrogels as bioadhesives,[47] researchers have made significant advancements in the development of hydrogel-based bioadhesives. Hydrogels have emerged as an attractive choice for this application compared to other material systems due to their biocompatibility, degradability, tunable mechanical properties, and biomimetic characteristics.[48,49] Among these advantages, a key benefit of hydrogels is their ability to engineer both chemical and physical bonds with biological systems, making them a versatile platform for bioadhesion. They can exist in various forms and be delivered using administration routes depending on the clinical needs. Also, hydrogels have been adapted for delivering bioactive components such as therapeutics and cells that further enhance their capacity for tissue regeneration. As a result, hydrogels hold immense promise as bioadhesives in tissue repair and regeneration, across diverse clinical settings, ranging from surgical excision, and blunt trauma, to tissue degeneration.

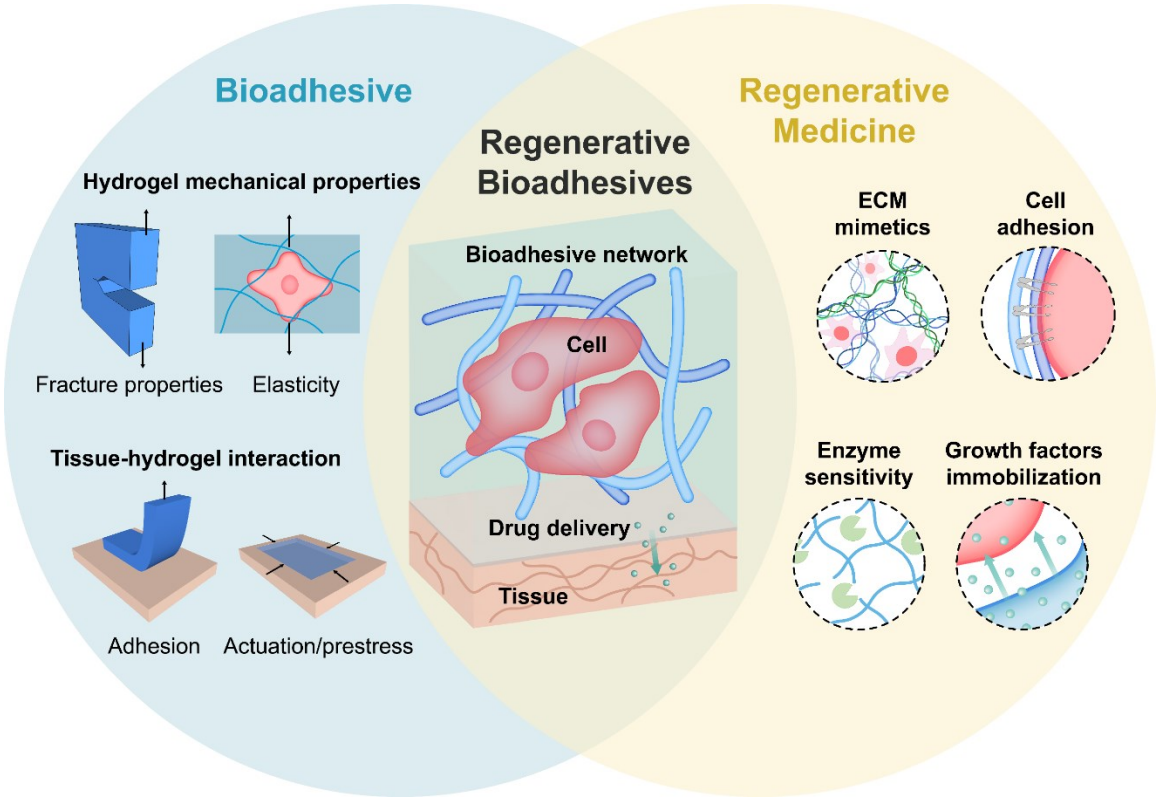

Figure 2.1 Mechanical and biological design considerations of regenerative bioadhesives for tissue repair and regeneration. Among the mechanical considerations, the elasticity and fracture properties mainly contribute to the intrinsic mechanical properties of hydrogel bioadhesives, whereas the adhesion and actuation properties affect the tissue-hydrogel interaction. ECM mimetics, cell adhesion, enzyme sensitivity, and group factors immobilization of bioadhesives are essential aspects to consider for improving the biological regenerative efficacy. Adapted with permission.[50] Copyright 2023, The Authors. Advanced Therapeutics published by Wiley-VCH GmbH.

Whereas many bioadhesives commercially available or under development focus on mechanical functions, their potential role in regeneration is underappreciated and thus opens many opportunities in the field. Regenerative bioadhesives could meet multifaceted requirements in regenerative medicine, that is, restoring both mechanical and biological functions of tissues and organs for better therapeutic outcomes. The main considerations for traditional hydrogel bioadhesives include biocompatibility, biodegradability, and remodeling abilities. However, only optimizing the biological aspect of bioadhesives is insufficient to achieve a desirable hydrogel system needed for the reconstruction of tissue structure and function. In particular, for load-bearing applications such as bone and IVD, the mechanical properties of bioadhesives offer critical means of providing physical strength and support for injured tissues[44,51] The mechanical performance also plays a vital role in the regeneration function by instructing cellular modulation from environmental

cues. For example, it has been demonstrated that mechanical properties provide instructive cues to stem cells in regenerative processes for cartilage repair.[52] Furthermore, the stiffness and cell adhesion ligands of hydrogels can affect cellular activities, such as IVD cell-cell interactions[53] and the stiffness effects on immune cells[54], although the cell-matrix mechanical interactions have not been fully understood to date. Apart from the static mechanical properties, the dynamic mechanical behaviors of the hydrogel bioadhesives should be properly adjusted to mimic the properties of the native extracellular matrix (ECM), which has stress relaxation behaviour can provide a dynamic microenvironment for cells.[55,56]

Regenerative bioadhesives from a integrated perspective of bioadhesives and regenerative medicine need key design considerations in terms of mechanical and biological properties (**Figure 2.1**).[50] Regenerative bioadhesives with pre-defined mechanical properties can help engineer a tailored tissue microenvironment and exert specific stress/strains on cells and tissues, thus serving as a mechanobiological tool to guide tissue regeneration by modulating cell activities. Harnessing the bulk matrix of the bioadhesive can also enable targeted delivery of therapeutic payloads such as stem cells and GFs to specific tissues.

2.1.1 Mechanical design considerations

Regenerative bioadhesives directly interface with injured tissues and their surrounding microenvironment. This direct contact exposes the tissues to specific mechanical cues, which could be predefined and modulated over time. Mechanical cues play critical roles in restoring the mechanical function of injured tissues and modulating the fate and activities of local cells. Recent advances in mechanobiology have gradually revealed the importance of mechanical cues, and are now approaching the same level of importance as the long-known biochemical cues.[57] Variation of the mechanical cues of the cellular microenvironment can lead to significant differences in cellular responses, ranging from simple adhesion, morphology, and matrix deposition to more complex differentiation.

Considering the complexity and open questions surrounding mechanobiological interactions, researchers could engineer the bioadhesives to emulate the specific mechanics of target tissues, both in static and dynamic states.[44,53,56,58] Similar strategies have been adopted in the field of regenerative medicine. At the early stage of tissue engineering, the tissue substitutes are simply required to be able to fulfill the functions of the tissue it replaces.[59] The key mechanical properties of bioadhesive materials include stiffness, strength, viscoelasticity, poroelasticity, toughness,

adhesion, actuation, and pre-stress. Additionally, the tests and methods employed for characterizing various mechanical properties of bioadhesive hydrogels are also significant.

Elasticity. Elasticity influences bioadhesives resistive forces upon deformation. Elastic modulus is typically measured from the tangent of stress-strain curves in tensile, shear or compression tests.[51] For homogenous, isotropic materials, the elastic compressive modulus (E) is related to the elastic shear modulus (G) by the following relationship: $G = E/(2 + 2\upsilon)$, where υ is the hydrogel Poisson ratio. For polymeric hydrogels, υ is approximately 0.5, and thus $G = E/3$.[51] Closely related to elastic modulus, stiffness is defined as the ratio between the load applied to the structure and the resulting deformation, corresponding to the load required to achieve a certain deformation.[60] Although these terms are frequently used as synonyms, it should be noted that stiffness is a property of a structured object, whereas modulus is a property of the material that constitutes the structure, from a mechanical point of view.[61] Bioadhesive elastic moduli vary widely, from 1 kPa in hydrogel-based adhesives to 1 GPa in plastic adhesives like cyanoacrylate. Adjustment of polymer concentration and crosslinker density allows tuning within suitable ranges to mimic native tissue mechanics. It is worth noting that the elastic moduli of different tissues also have a wide range, from 0.2 – 1 kPa for brain[62] to around 20 kPa for muscle[63], approximately 1 MPa for cartilage[64], and over 10 GPa for bone.[65] Stiffness and modulus define the basic mechanical response of biological tissues under small strains. When repairing the injured tissues with altered mechanics, the bioadhesives should match the stiffness or modulus of the target tissues to restore biomechanics. Additionally, the secondary effects that accompany the modulation of bioadhesive stiffness such as altering cell-adhesive ligand density, changing mesh size and porosity of hydrogel structure,[66] also need to be considered.

Viscoelasticity. Both bioadhesives and tissues are not ideally elastic solids due to the conformational changes of macromolecules, polymer networks and cells, which behave as both viscous liquid and elastic solid concurrently.[67–70] Following the same reasoning with elasticity, viscoelasticity is thus an important consideration in bioadhesive design.[70] The viscoelastic behavior exhibited by different components of human body is closely related to their specific functions, including load bearing, energy absorption, and dissipation, as well as dynamic adaptation. Such correlations are key to the overall mechanical integrity and functionality of the body's tissues and organs.[71] Rheological tests, measuring dynamic moduli of storage modulus (E') and loss modulus (E''), quantify the viscoelasticity. Time-dependent tests, such as stress relaxation and creep,

reveal characteristic viscoelastic time constants for biological tissues spanning from seconds to thousands of seconds. Tuning the viscoelasticity of regenerative bioadhesives to match that of targeted tissues is crucial, especially in load-bearing tissues like cartilage and IVDs. Also, the viscoelastic behavior of hydrogel bioadhesives is essential to recapitulate proper cellular properties. Similar to aforesaid elastic modulus, stress relaxation in engineered tissues can impact stem cell differentiation.[67] Strategies to modify the bioadhesive viscoelasticity focuses on bond strength and molecular weight (MW). Studies show that adjusting polymer chain MW,[52] crosslinking chemistries[72,73], or polymer concentration[74] alters stress relaxation, influencing cellular behaviour. Alginate hydrogels, crosslinked with calcium ions, showcase tunable viscoelastic time constants ranging from ten to thousands of seconds.

Poroelasticity. Another crucial aspect in bioadhesive design is poroelasticity, which involves the mechanical behavior of porous materials when fluid flow interacts with solid deformation. Living tissues, rich in water, exhibit poroelastic effects due to water flow within the ECM.[67,75] Similarly, hydrogel bioadhesives are composed of a significant amount of water and a polymer network, exhibiting a time-dependent mechanical response due to water flow into or out of porous network meshes when a deformation induces a change in volume. Characterizing poroelasticity involves compressive or rheology tests to capture stress relaxation or strain creep behaviors. Both viscoelasticity and poroelasticity are time-dependent parameters in bioadhesives, with the former resulting from tissue network or cell rearrangement and the latter originating from fluid movement through pores. While viscoelastic properties are independent of length scale, poroelasticity depends on it.[70,76–78] Controlling hydrogel bioadhesive porosity is essential for cell growth, mass transport, and drug delivery in regenerative medicine. The tunable polymer network mesh size, ranging from nano to micro scale, affects porosity, with recent focus on micron-sized features for improved cell migration.[79] Macroporous structures, in the micron range, enhance nutrient exchange, facilitate vascularization, and address limitations in conventional nanoscale networks.[80] Macroporous bioadhesives, with interconnected large pores, offer a 3D environment for cell activity.[81,82] A biomimetic macroporous bioadhesive with a triple-network structure has demonstrated injectability, rapid gelling, adjustable mechanical strength, and macroporous microstructure properties in full-thickness skin regeneration.[83] In vitro, ex vivo, and in vivo experiments highlight its effectiveness in sutureless wound closure and promoting wound healing, showcasing its potential for treating severe and deep wounds.

Fracture. The fracture resistance of bioadhesives is critical for their efficacy, with cohesive failure occurring when mechanical failure happens within the bulk material. Fracture strength, representing the maximum stress upon fracture, or fracture energy, measuring the energy required to extend a crack of unit area, are key parameters. Fracture strength is commonly used, while fracture energy is more suitable for cracks or similar defects. Matching the fracture properties of bioadhesives to targeted tissues is challenging due to the high strength and fracture energy of biological tissues like cartilage and skin. Commonly used bioadhesives, such as poly(ethylene glycol) (PEG)-based hydrogels, exhibit lower fracture energy. Addressing this, tough hydrogels, like alginate-polyacrylamide hydrogels, with fracture energy beyond 10,000 J m^{-2},[84,85] have emerged. These tough hydrogels, based on a stretchy network and a secondary network dissipating energy via bond breakage, serve as matrices for bioadhesives. Combined with interfacial bonding reactions, these tough hydrogel bioadhesives demonstrate unprecedented fracture properties.

Adhesion. Adhesion performance can be measured by adhesion energy or adhesion strength, with the former specifically applicable to situations involving cracks or defects. Achieving effective adhesion to wet tissue surfaces covered with biological fluids and/or mucus layers poses a persistent challenge. Ideal adhesion performance within a tissue should match its bulk properties for proper cohesive strength. However, current tissue adhesive hydrogels face limitations in terms of cytotoxicity, weak mechanical performance, or inapplicability in dynamic and wet environments. Recent advancements focus on strategies and material systems for achieving tough adhesion on tissues.[33] Notable examples include tough adhesives with a bilayer structure: a surface layer with bridging polymers forming topological and chemical links with tissues, and a bulk matrix of tough hydrogels.[39] Computational modeling attributes the obtained tough adhesion to the synergy of interfacial bonding and bulk dissipation. In vitro and in vivo experiments demonstrate biocompatible tough adhesives exhibiting high adhesion energy (up to 1100 J m^{-2}) on blood-covered animal tissues. This versatile family of adhesives holds promise for applications in tissue repair, wound dressing, and tissue adhesion.

Fatigue resistance. Cyclic loading or fatigue resistance is another mechanical consideration for bioadhesives,[86,87] especially when interfacing with mechanically active tissues in the human body, such as tendons, ligaments, the gastric wall, and vocal folds. Tissues often endure millions of cycles of mechanical loading throughout a lifetime.[88] Despite achieving strong and tough adhesion, existing bioadhesives face a challenge in withstanding cyclic loading and fatigue fracture.[89,90] For

instance, a tough adhesive may fail under critical cyclic loading, significantly smaller than monotonic loading. Researchers are exploring fatigue-resistant bioadhesives using self-healing and self-reinforced hydrogels due to their mechanical damage repair capabilities.[90–93] A recent example involves a triblock copolymer hydrogel for gastric perforation treatment with reversible hydrogel bonds exhibiting self-healing abilities in the dynamic acidic gastric environment.[94] While their performance in animals is superior to conventional approaches, the response to fatigue fracture and the fatigue threshold measured using fracture mechanics have not been reported. Recent studies on poly (vinyl alcohol) (PVA) hydrogels on rigid substrates show promising prospects for achieving hydrogel adhesion resistant to cyclic loading.[89] Rigid nanostructures at the hydrogel-substrate interface reached an interfacial fatigue threshold comparable to the fracture toughness of natural connective tissues. However, the method's harsh conditions limit practical bioadhesive applications. Another potential approach involves incorporating rigid inclusions into the bioadhesive to impede crack growth and enhance fatigue resistance, offering promising directions in the development of fatigue-resistant bioadhesives.

Actuation. Unlike passive bioadhesives, emerging mechanically active bioadhesives exert forces on tissues, promoting wound closure. For example, a temperature-responsive bioadhesive with poly(N-isopropylacrylamide) exhibits mechanical actuation, shrinking at temperatures above its critical solution temperature, accelerating wound closure in rodent skin models.[58] Similar mechanically active bioadhesives show promise in treating diabetic ulcers and chronic wounds.[95] Design considerations for mechanically active bioadhesives extend to tissue engineering areas like soft robotics, artificial muscles, biomimetics, and biohybrid materials.[96] Inspired by natural plant responses, researchers explore hydrogel actuation, although its slow diffusion limits speed.[97,98] Alternative mechanisms include the mechanical actuation of soft robotics and the shape memory behavior of alloys triggered by environmental signals.[99,100] An active bioadhesive adhering to skeletal muscles and mimicking muscle contractions has been developed, integrating fluorescence and shape memory for multifunctionality.[96] Beyond chemical compositions, structural design determines bioadhesive actuation.[101,102] Layer structures, gradient structures, and patterned structures have been explored, resulting in grippers, walkers, swimmers, artificial muscles, and valves. Inspired by drosera, a bilayer actuator of poly(acrylamide) and poly(N, N-diethylacrylamide) functions as a soft gripper in water, hinting at potential applications in adhesion or mechanical

stimulation for healing.[103] While rarely attempted, integrating soft robotics and bioadhesives presents exciting opportunities.

2.1.2 Biological design considerations

Bioadhesives with highly hydrated polymer networks can be modified with bioactive-biochemical signals to regulate cellular behaviors by mimicking the biological features from the local cell microenvironments.[104–106] This approach has yielded valuable insights into the mechanisms of cell development and their responses to various tissue regeneration conditions. In recent years, the design of hydrogel bioadhesives have incorporated many biological functions to be utilized as tissue substitutes in the field of tissue engineering and regenerative medicine.[107–109] On one hand, bioadhesives can act as a temporary substrates or scaffolds for resident cells; on the other hand, bioadhesives can provide carrier platforms for biochemical factors (e.g. bioactive molecules) and appropriate biochemical stimulations (e.g. GFs, cytokines), thus supporting cell growth and maintaining cell functions.[110,111]

Extracellular matrix mimetic cues. Regenerative bioadhesives draw inspiration from the ECM, a dynamic network supporting cells and regulating various cell functions. Many bioadhesives incorporate ECM proteins like collagen, gelatin, hyaluronic acid (HA), and chondroitin sulfate, making them biocompatible and capable of triggering biological responses. The ECM serves as both a structural scaffold and a dynamic environment for storing and releasing biomolecules, influencing cellular functions such as survival, communication, proliferation, and differentiation.[112–114] Efforts in tissue engineering aim to develop hydrogel bioadhesives that mimic the structures and biofunctions of the natural ECM. These bioadhesives, enriched with physical, chemical, and biological cues, emulate tissue-specific ECM.[111,115,116] Examples include intelligent ECM mimetic injectable hydrogels composed of methacrylate collagen building blocks demonstrating sustained release of biomolecules and maintaining biocompatibility.[117] Another approach involves a self-assembled peptide amphiphile and PEG composite bioadhesive system, offering tunable biological and mechanical properties for tissue engineering.[118] Native ECM microenvironments feature 3D networks influencing cell morphology and function. Hydrogel bioadhesives with ECM mimetic cues are particularly valuable, representing the tissue environment and providing a degradable, bioactive substrate for effective tissue regeneration. The integration of ECM mimetic features in bioadhesives aligns with the intricate dynamics of native tissue microenvironments, fostering cell development and tissue remodeling.

Cell adhesion ligands. Cellular attachment is essential for the behaviors, including migration, proliferation, and differentiation, forming a macroscopic structure.[119,120] Interactions between cellular surface receptors (e.g., integrin) and cell adhesion ligands, such as the notable Arg-Gly-Asp (RGD) peptide, play a crucial role in cell adhesion to scaffolds. Strategies like carbodiimide and polydopamine chemistry have been employed to pattern these bioactive ligands. Cell-binding peptides, inspired by specific cell-adhesive interactions, are used to modify hydrogel bioadhesives.[57,58,121,122] Clinically used synthetic bioadhesives, like PEG hydrogels in COSEAL and DURASEAL, often lack cell adhesion ligands, resulting in low cell viability. Efforts focus on functionalizing hydrogels with cell adhesion ligands like RGD, YIGSR, and IKVAV peptides.[57,123] Mesenchymal stem cells exhibit enhanced attachment and densities on RGD-linked PEG hydrogels. Integrating cell adhesion ligands into bioadhesives facilitates interactions between encapsulated cells and the substrate matrix, modulating cell functions and phenotypes. Chaudhuri et al. covalently coupled RGD peptides to viscoelastic alginate hydrogels, promoting osteogenesis in encapsulated mesenchymal stem cells.[124] This approach demonstrates the potential for incorporating cell adhesion ligands into bioadhesive systems to enhance cell-matrix interactions and guide specific cell responses.

Enzyme-sensitive cues. Incorporating autologous or exogenous enzymes into bioadhesives can enhance their bio-responsiveness and improve tissue regeneration. Enzyme-sensitive bioadhesives create a 3D environment that undergoes biodegradation, mimicking the natural remodeling of the ECM.[125,126] Matrix metalloproteinases (MMPs), elastases, plasmin, and thrombin are among the enzymes targeted for this purpose in biodegradable hydrogels.[127,128] For instance, MMPs-degradable HA hydrogels have been developed for controlled delivery of stromal cell-derived factor-1α (SDF-1α) and bone morphogenetic protein-2 (BMP-2) to enhance bone repair.[129] The degradation speed can be adjusted by tuning the polymer network composition, making the bioadhesive responsive to enzyme-mediated degradation for tissue regeneration. However, the biodegradation rate should align with the healing process; if too rapid, it may hinder tissue regeneration, while being too slow might impede new tissue formation. Ideally, the degradation rate should correspond well with new tissue formation to maintain mechanical stability. Enzyme-sensitive bioadhesives, when designed with optimal biodegradation rates and consideration for tissue regeneration, hold great potential for tissue regeneration. Strategies from

bio-responsive hydrogels for drug delivery can be applied to encapsulate payloads within the bioadhesive matrix, further enhancing their responsiveness for regenerative applications.

Ion-sensitive cues. The ion concentrations in tissue environments vary, with pH representing specific ion conditions ranging from very acidic (~1.5)[130] in the stomach to weakly basic (~7.5)[131] in chronic skin wounds. Hydrogels incorporating pH-responsive groups undergo swelling or dissolution in response to local pH changes.[132] However, these effects can be undesired as they compromise mechanical and adhesion properties and may compress adjacent tissues. To mitigate these effects, ionic crosslinks can be replaced with hydrogen bonds or covalent bonds for stability against ions.[34,91] For instance, an acid-tolerant hydrogel bioadhesive uses hydrophobic associations for physical crosslinking, inhibiting further swelling under extreme conditions and enabling instant sealing of gastric perforation without sutures.[91] In vivo studies show accelerated gastric mucosal repair. pH-responsive adhesive hydrogels, incorporating 6-aminocaproic acid (AA) and AA-g-N-hydroxysuccinimide (AA-NHS), effectively control gastric bleeding in a swine model.[92] Leveraging pH sensitivity for controlled drug delivery, injectable hydrogel bioadhesives with enhanced release in acidic pH promote skin wound healing.[133] Another hydrogel based on polyphosphate-conjugated pectin releases doxorubicin hydrochloride in different pH environments, potentially enhancing therapy efficacy in infected wounds with lower pH and chronic wounds with a relatively alkaline environment.[134] Future research may explore coupling ion sensitivity with other cues and mechanical properties to mediate local tissue environments for repair and regeneration.

Growth factors. Incorporating growth factors (GFs) into bioadhesives enhances their biological functions by modulating cellular activities. Different mechanisms, including covalent and noncovalent approaches, have been employed for loading GFs into bioadhesives.[111,135] Simple encapsulation, while easy to implement, often results in rapid release lacking controllability. Various strategies have been developed to improve GF incorporation into hydrogels, enhancing bioactivity and manipulating cell function.[136] For example, tethering epidermal GF to bone scaffolds increased mesenchymal stem cell survival,[137] and transforming GF-β1 tethering to PEG hydrogels boosted ECM production by vascular smooth muscle cells.[138] Precision in the conjugation site, such as the site-directed immobilization method for BMP-2, has addressed issues like unpredictable protein orientation, ensuring improved applicability for bone defect repair.[139] Noncovalent specific affinity interactions, achieved through direct loading, encapsulation, or interactions with other ECM

biomolecules, offer an alternative.[140] Electrostatic and van der Waals interactions naturally occurring between ECM components enable noncovalent immobilization. This approach minimizes structural changes to GFs, preserving their bioactivity.[104,141] However, challenges in controlling loading and release persist, relying largely on GF affinity to hydrogel bioadhesives. Considering both mechanical support and dynamic presentation of GFs in drug delivery, the next generation of hydrogel bioadhesives must address these aspects for effective tissue regeneration.

2.1.3 Case studies for musculoskeletal tissue repair

Regenerative bioadhesives are in high demand for repairing various musculoskeletal tissues, including tendon, IVD, cartilage, and ligaments. These tissues are associated with diseases such as low back pain and arthritis, which are leading causes of disability affecting millions of people and resulting in enormous burdens.[142] The injury and degeneration of musculoskeletal tissues often result in tissue fracture or defects, which traditionally are repaired with suturing that has been linked with microtrauma, inflammation and other complications. In addition, some musculoskeletal tissues such as IVD and tendon have low cellularity, limited vasculature, and low nutrient supply, resulting in a limited self-regenerative capacity that necessitates the intervention of regenerative approaches.

To address these issues, ideal acellular bioadhesives biomaterials should not only repair and support the mechanical properties, but also provide regenerative properties to restore biological functions in the long term. Leveraging bioadhesives for cell and drug delivery can meet the demand for tissue engineering and regeneration of musculoskeletal tissues. As such, the regenerative bioadhesive could fill the injury/degenerated defects, accommodate physiological loading and deformation of the tissue, and replenish and/or recruit cells to the degenerated sites so boosting the regeneration progress. To elaborate on the design considerations for different applications, we describe regenerative bioadhesives developed for repairing IVDs and tendon.

IVD are composed of a gelatinous and viscoelastic NP at the center and a fibrous AF at the periphery, which are subjected to physiological compression stress ranging from 0.1 MPa to 2.3 MPa.[143,144] Defects in the AF can lead to NP herniation, causing acute painful disability. Herniation will in a longer perspective also directly lead to NP degeneration and loss of mechanical properties. Discectomy is a standard surgical treatment for disc herniation, but it cannot repair AF defects or restore mechanical properties after NP tissue removal. Furthermore, re-herniation after surgery is frequently observed due to the remaining AF defect opening. The heterogeneity among the IVD substructures poses different requirements for the specific bioadhesives for repair after discectomy.

Bioadhesives for NP tissue replacement should be injectable and viscoelastic in the NP cavity region. To repair AF, they should seal the AF defect and prevent re-herniation, while excelling in mechanical strength matched with the strong and tough AF. Beyond that, cell therapy needs to be considered and incorporated into IVD bioadhesive. Thus, the bioadhesives, as cell cargos, need to support the growth and function of cells in order to achieve the purpose of regeneration of IVD tissue. Together filling the NP cavity and sealing the AF defect could restore biomechanics and homeostasis of the IVD. These factors motivate the development of regenerative bioadhesives for IVD treatment.

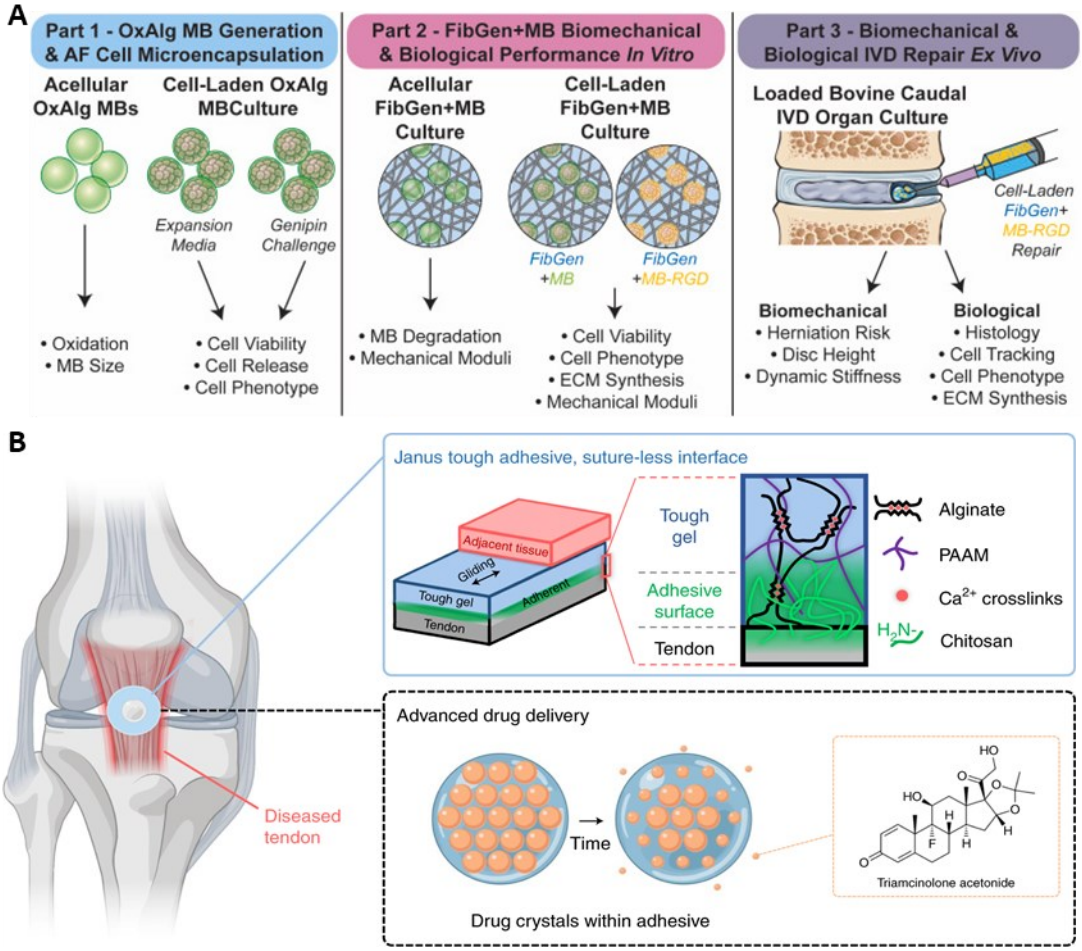

Figure 2.2. Examples of bioadhesive design for the repair of intervertebral disc and tendon. A. Bioadhesives composed of genipin-crosslinked fibrin seeded with oxidized alginate microbeads as a novel strategy for intervertebral disc cell therapy. Adapted with permission.[145] Copyright 2022 Elsevier Ltd. B.

Tough bioadhesives with the 'Janus' side to enhance tendon healing. Adapted with permission.[146] Copyright 2022, The Authors, under exclusive licence to Springer Nature Limited.

To address this complex issue of repairing IVD, a recent study proposed a composite bioadhesive strategy for IVD cell therapy. The bioadhesives is comprised of cell-seeded oxidized alginate microbeads encapsulated in genipin-crosslinked fibrin (FibGen), which fills the NP cavity and adheres to the AF tissue after discectomy (**Figure 2.2A**).[145] The biological considerations include incorporating AF cells and RGD peptides to enhance cell-matrix binding, while the mechanical design leverages the bioadhesiveness of fibrin hydrogels. In vitro studies have shown that the microbeads conjugated with RGD peptides can reduce cell apoptosis. Histology and mechanical evaluations have demonstrated that the composite hydrogel could remain biomechanically stable over three weeks and promote seeded AF cells to synthesize extracellular matrix as oxidized alginate microbeads degrade. Although the adhesion was not quantitatively measured in this study, the composites adhesive had virtually no herniation risk after approximately 96,000 cycles of compressive loading during 42-day organ culture in a customized bioreactor. Also, the adhesives can prevent injury-induced disc height loss and acute IVD stiffening.

Tendons are important components of the musculoskeletal system, responsible for connecting muscles to bones and transmitting forces generated during movement. Tendinopathies, such as tendinitis and tendinosis, are common conditions that can cause pain, inflammation, and impaired mobility. To treat tendon injuries, bioadhesives have emerged as a promising approach. Unlike cartilage and IVD, tendons are primarily subjected to tensile stress and exhibit very large elastic modulus (~100 MPa). Furthermore, strong adhesion between tendon-bone interfaces is critical for successful repair. **Figure 2.2B** highlights a tough adhesive hydrogel that combines a dissipative tough matrix on one side and a chitosan adhesive on the other. Mechanically, this adhesive hydrogel demonstrates "Janus" adhesiveness, meaning that one side could achieve strong adhesion (greater than 1000 J m^{-2}) between hydrogel-tendon interfaces and the other side is highly lubricant and friction-less, supporting tendon gliding.[146] The biomechanical stability and biointegrity of this tough adhesive hydrogel were tested with porcine and human tendon preparations during cyclic-friction loadings. Regarding the biological design considerations, researchers confer the bioadhesives with potent bioactivity by leveraging the bioadhesive matrix as a drug depot to deliver and release the corticosteroid triamcinolone acetonide. Due to the permeable and hydrated nature of hydrogel matrix, the bioadhesive features high drug loading capacity and controlled release

behavior. In a rat model of Achilles tendon rupture, the implanted bioadhesives strategy was shown to reduce inflammation, modulate chemokine secretion, recruit tendon stem and progenitor cells. This strategy was also validated to promote macrophage polarization towards an anti-inflammatory phenotype, specifically the alternatively activated macrophages (M2), rather than the pro-inflammatory classically activated phenotype (M1). These results embody the promise of regenerative bioadhesives for tendon repair and regeneration.[146]

2.2 Structure, property, and function of IVD

2.2.1 Anatomical structure and function of human IVD

The IVD is a fibrocartilaginous tissue connecting two vertebras, which provides load support, energy absorption, and flexibility in the spine.[17,147,148] There are at least 25 IVDs interposed between the adjacent surfaces of the vertebrae uniting them from the axis to the sacrum. There are 6 discs distributed in the cervical region, 12 in the thoracic region, 6 in the lumbar region, and 1 between the sacrum and coccyx, each approximately 7 to 10 mm thick and 4 cm in diameter (from anterior-posterior plane) in the lumbar region of the spine. The NP part of the discs consists of hydrated proteoglycan (35 – 65% of the dry weight of NP) which is held together loosely by an irregular network of fine collagen type II (5 – 20% of the dry weight of NP) and elastin fibers.[12,19] The major proteoglycan of the disc is aggrecan, which provides the osmotic properties needed to resist compressive loading, due to the fixed negative charge of glycosaminoglycan (GAG) content.[149,150] The NP constitutes a significant portion of the IVD and possesses distinctive mechanical characteristics crucial for its function within the spinal column. Predominantly composed of water, the NP exhibits exceptional hydrostatic pressure resistance. This attribute enables it to effectively withstand and distribute compressive loads experienced by the spine. Moreover, the NP displays viscoelastic behavior, allowing it to deform under load and gradually recover its original shape over time, thereby absorbing shock, mitigating vibrations, and adapting to varying mechanical loads during spinal movement and weight-bearing activities. Additionally, the NP demonstrates elasticity, ensuring it can promptly return to its initial configuration after deformation, essential for preserving disc height, spinal alignment, and overall biomechanical integrity. Furthermore, the gel-like consistency and water content of the NP contribute to uniform pressure distribution within the IVD, diminishing localized stress concentrations on neighboring vertebral endplates and the annulus fibrosus, thereby mitigating the risk of disc degeneration, herniation, and spinal instability.

Outside the nucleus is the AF. There is a distinct boundary between these two regions in the young individuals (less than 10 years old) and the boundary will become obscure with mature. In the healthy IVD, the AF contains 65 – 70% of water. Dry weight is approximately 20% proteoglycan, 50 – 70% collagen, and 2% elastin.[151] AF is made up of a series of 15 to 25 concentric rings, with the individual lamellae consisting primarily of collagen type I fibers passing obliquely between vertebral bodies. The orientation of the fibers is opposite in successive lamellae.[17] The complex arrangement of collagen fibers in the AF enables it to develop tensile, acting like a hoop to withstand the circumferential pressure from the NP bulging.[150,151] The cartilage endplates cover the IVDs from both the cranial and caudal ends, which bind the disc to the vertebral bodies and prevent the highly hydrated NP from bulging into the adjacent vertebrae. They are approximately 0.6 mm thick, comprising approximately 60% of water and major dry weight of collagen type II and proteoglycans.[152,153]

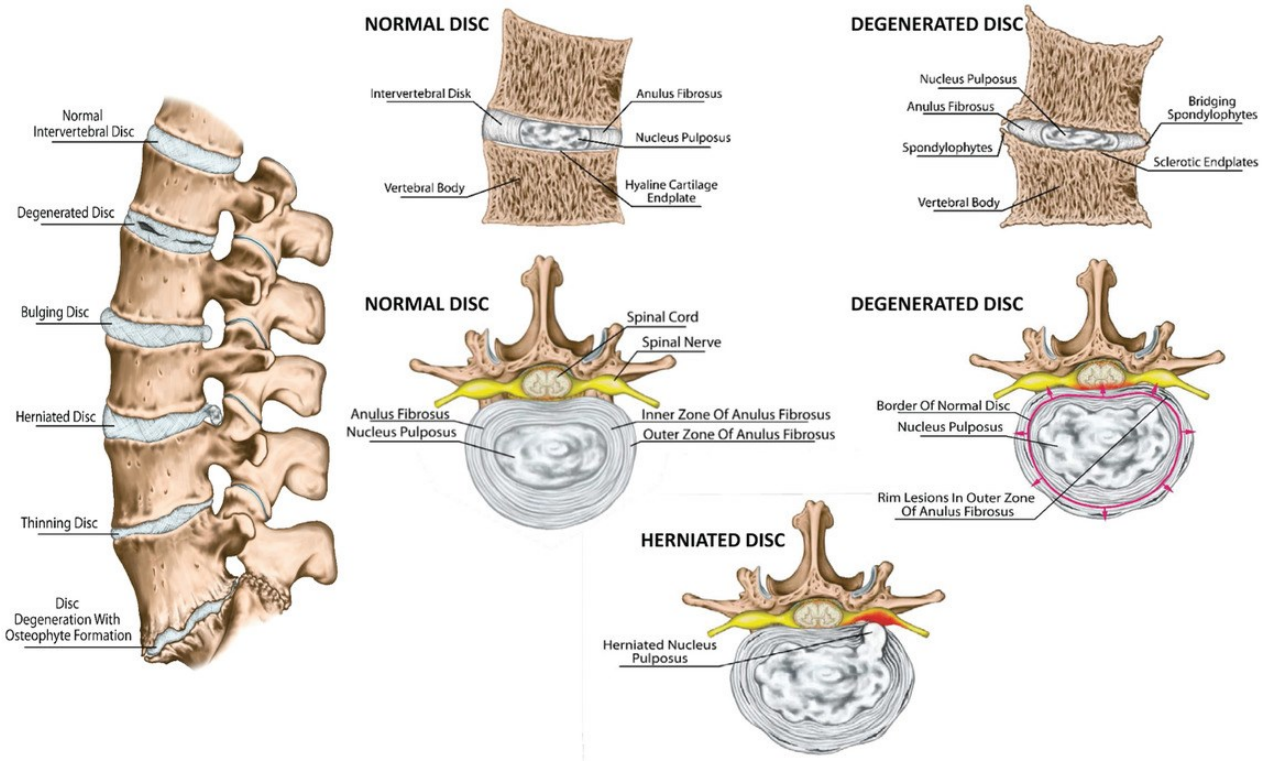

Figure 2.3. Spine and IVD anatomy in sagittal and cross-sectional. Adapted with permission.[148] Copyright 2017 New York Academy of Sciences.

The pathomechanism of disc collapse or herniation stems from various factors contributing to the structural breakdown of the intervertebral discs in the spine. Primarily, degenerative changes over time weaken the discs, making them more prone to damage. Excessive loads or traumatic

events can exceed the disc's tolerance, leading to tears in the AF or degeneration of the NP. These factors, combined with genetic predispositions, contribute to disc collapse or herniation, resulting in conditions like degenerative disc disease.

2.2.2 Cells and extracellular matrix of IVD tissues

Cells in the NP tissue are initially notochordal-derived and are gradually replaced by rounded cells, resembling chondrocytes, with a low density (~ 3000 – 5000 cells mm^{-3}).[154,155] They are highly specialized to survive in a very hypoxic environment (1% of O_2).[156,157] AF cells (~ 9000 cells mm^{-3}) are elongated parallel to the collagen fibers, with varying morphologies from the thin, fibroblast-like shapes in the outer layers to the oval shapes in the inner part.[158] The cell density within IVD declines during growth to a very low level in the adult, especially in the NP region. AF cells synthesize mostly collagen type I in the ECM in response to deformation, whereas NP cells respond to hydrostatic pressure by synthesizing mostly proteoglycans and fine collagen type II fibers.[19] Few blood vessels exist in the healthy adult disc, but some nerves are found mainly restricted to the outer annulus lamellae. The cartilaginous endplate, like other hyaline cartilages, is avascular and aneural in the healthy adult disc.[157] Essential nutrients (e.g. oxygen, glucose, amino acids etc.) are supplied through the cartilage endplates penetrating the IVD from its peripheries. Metabolic waste products are removed from the IVD via a reverse route.[22] The low oxygen tension in the center of the IVD leads to anaerobic metabolism, resulting in a harsh microenvironment with a high concentration of lactic acid and low pH. Deficiencies in metabolite transport appear to limit both the density and metabolic activity of disc cells.[20] As a result, discs exhibit insufficient ability to recover from metabolic or mechanical injuries.

2.2.3 Mechanical loading on IVD

IVDs lie between vertebras of the spine, allowing the vertebral column to bend and twist[159], and distributing compressive loadings to the adjacent vertebral bodies.[20] The mechanical loading, in turn, is important to maintain the balance of matrix turnover in the IVD.[160] The discs play the mechanical role in constantly transmitting loads arising from body weight and muscle activity through the spinal column. Axial compressive loading to the IVD gives rise to a radial deformation (outward bulge), as the disc deforms in response to the compressive load. The high tensile stiffness of the healthy AF in the circumferential direction acts to restrict this outwardly directed deformation. Tissues of the disc are variably loaded and experience a combination of compression, tension, and shear. Pressurization of the central and gelatinous NP is an important mechanism for load support

and load transfer to the AF. It also contributes to the maintenance of disc height. In a healthy lumbar disc, in vivo pressures in the NP are between 460 kPa and 1330 kPa in the seated position, 500 kPa and 870 kPa in the standing position, and 91 kPa and 539 kPa when lying either prone or supine. The highest pressure in the nucleus (2300 kPa) was recorded in a standing subject who was flexing forwards holding a 20 kg mass.[144,152,161]

As the largest avascular structure in human body, IVD exchanges nutrients and metabolic by-products with the surrounding through diffusion and convection.[22,157] Changes in interstitial pressure, balanced against osmotic pressure of NP, provide a pumping action for convective transport of large solutes such as GFs, cytokines and enzymes. However, studies have shown that excessive water movement caused by mechanical loading decreases the synthesis of ECM.[157,162–164] Biomechanical changes in the disc likely aid in degeneration, causing a significant structural alteration in both regions of the disc, leading to a decrease in height, and ultimately resulting in pain. Thus, when investigating the strategies for IVD repair, it is necessary not only to maintain the balance of the static intrinsic biochemical microenvironment of the IVD, but also to consider the impact of external dynamic loads on the IVD.

2.3 Biological strategies for IVD repair and regeneration

Formulating strategies for IVD repair should be based on the physical chemical, mechanical, and biological characteristic of the tissue. Based on the fundamentals, novel advanced therapeutic solutions to IVD degenerative problems are evolving rapidly. To overcome the limitations of conventional treatments, biological strategies are developed in accordance with the cellular, biochemical, and mechanical properties of IVD. The biological strategies such as drug delivery approaches can be classified based on the specific stage of degeneration.[165,166] The first is biomolecular therapy, with as focus on the early degeneration. Biomolecular (e.g. GF and recombinant genes) injected into the disc can enhance selective protein expression therefore maintaining the balance of anabolic and catabolic cascades in the ECM. For higher grade of degeneration, cell therapy as another repair strategy is the optimal treatment therapy, which involves the injection of autologous/allogeneic NP cells/stem cells suspension into the NP to produce desired ECM components.[167] As for advanced degeneration (e.g. herniation, fissure across the IVD), partial or whole disc replacement by acellular biomaterials (e.g. HA, silk fibroin, collagen, agarose) can restore the mechanical function of the nucleus pulposus and relieving the pain.[168] Although

extensive research has been carried out on using these strategies, there are some problems remaining to be solved among them. Using cell suspension to supplement NP will directly expose the cells to the harsh environment inside the NP (e.g. low pH, low oxygen, inflammation), which is not conducive to the survival of the implanted cells.[169] Another concern is the long-term viability maintenance for the delivered cells. Besides, acellular synthesized polymers do not have the biological regenerative ability. In addition, the mechanical mismatch between biomaterial implants and the native NP in terms of stiffness, elasticity, viscoelasticity, and hydrostatic pressure, leads to the implant extrusion, endplate failure and poor integration associated with the disc.

2.4 Biomaterials for NP regeneration

Cell-laden biomaterials for NP repair were used to enable matrix production and long-term maintenance of regenerated tissue in the past decades. According to the previous research, there are vital design criteria to follow:[168,170,171] the biomaterial is required to maintain the NP cell phenotypes and matrix biosynthesis, such as aggrecan and collagen which are quantified as 500 μg μg^{-1} DNA and 250 μg μg^{-1} DNA in mature human lumbar IVD;[172] it should be able to integrate with adjacent structure biologically and mechanically; it should adapt to the harsh microenvironment in the degenerated IVD with a stable biochemical property; it should match the material properties of healthy native NP and support the structure and function of the whole tissue; the material ideally can be injected via a needle with a minimally invasive procedure.[173,174] In some *in vitro* study, biodegradable biomaterials implants were proposed,[175] following with the additional requirements that they must generate no cytotoxic or immunogenic degradation or breakdown fragments to enable the new matrix formation.

The synergy of mechanics, chemistry, and biology is important for the design of suitable biomaterials for IVD treatment. Investigators have examined several design parameters for biomaterials to be used as cell delivery vehicles, including material type, mechanical property, and porosity.[176]

Recently, studies have shown that many polymeric biomaterials can promote cell proliferation, migration, and ECM production for NP regeneration. Those materials can be classified into three categories: naturally-derived scaffolds, synthetic and bio-synthetic polymers.[169,177] Natural scaffolds are biomaterials assembled from various natural polymers, such as silk[178,179], collagen[180], hyaluronic acid (HA)[181], chitosan[173,182], and alginate[183–185] hydrogels.

Bioactive molecules (such as GFs) that are loaded into these bio-scaffolds can effectively maintain NP cell viability and proliferation.[186] Synthetic polymers can be fabricated in various forms such as injectable and thermosensitive based on the desired application. Bio-synthetic scaffolds can be produced by physical mixing or chemically coupling of natural material and synthetic polymers, which holds the biocompatibility and the restore of the mechanical strength to the final combination.[187]

Mechanical cues provided by the biomaterial can mediate cell organization and function.[188] The mechanical properties of the biomaterial ideally should match with the native NP tissue, including stiffness, compressive elasticity, viscoelasticity and swelling pressure. In confined compression, the effective modulus of human, non-degenerate NP was 1.0 MPa,[189] and the bulk modulus was 1720 MPa,[190] Although the behavior of the NP is not linearly elastic, Cloyd et al.[191] reported a modulus from the 'linear' region of the stress-strain response obtained using unconfined compression of 5.4 kPa. A study based on porcine NP cell culture on laminin-rich basement membrane extract (BME) substrates indicated that less stiff (720 Pa), laminin-containing ECM 2D substrates promote NP cell morphologies, cell-cell interactions, and proteoglycan production *in vitro*.[188] It is evidenced that ECM production and phenotypic stability of NP cells requires cultures in a 3D format, where rounded cell morphology can be maintained.[192] A number of studies have reported that hydrogel-based constructs with complex shear modulus and phase angle similar to NP counterparts (7.4 kPa – 19 kPa, 23° – 30°)[193,194] maintained the phenotype and matrix deposition of NP. However, this shear modulus was determined prior to any matrix deposition. The liquid-solid-phase property (viscoelasticity) which defines the time dependent behavior of NP has not been widely investigated which can be quantified as the viscoelastic time.[189] It was found that the swelling pressure of NP was approximately 0.05 MPa – 3 MPa depending on loading conditions.[194] One study presented biomimetic GAG analogues polymers forming NP implant which possessed appropriate osmotic responsiveness and display the capacity to restore disc height.[175]

Pore size, porosity and density of a scaffold play important roles in tissue engineering.[168,195] When the scaffold has a highly porous structure, the microscale pores offer interconnections, 3D architecture, suitable mechanical properties and sufficient space.[196,197] The pore sizes of the scaffolds need to meet general requirements, which are sufficient spacing, compressive strength for greater stability and bioactivity for cell seeding, as well as the diffusions of nutrients and oxygen to the seeded cells within the scaffold to form new NP tissue. A study investigated the influence of

pore sizes of poly (lactic-co-glycolic acid) (PLGA) scaffolds on the compressive strength of tissue-engineered bio-discs and the screening of the suitable pore size for NP cells in vivo growth.[198] The results found that the pore size of 90 μm – 250 μm offered the better cell proliferation and ECM production of cells, which indicated that suitable space in the scaffold for cell viability is a key factor for cell metabolism.

Reduced cell numbers and phenotypic changes in the resident NP cell population in the degenerated NP requires cell supplementation using biomaterials.[12] The supplemented cells can originate from different sources, including autologous and allogeneic primary cells, as well as multiple types of progenitor cells and chondrocytes. They are all capable of synthesizing and depositing certain type of collagens and GAGs within the matrix.[199] IVD progenitor cells resemble to mesenchymal stem/stromal cells (MSCs) with multilineage potential, which are plastic adherent, express MSC markers and a unique expression profile that reflects the origin and microenvironment. They are proposed to have advantages over non-IVD-derived MSCs for IVD cell differentiation that might be better able to adapt to and engraft into the host IVD tissue after transplantation.[199,200]

Previous studies have evaluated the use of autologous MSCs, or adipose-derived stromal cells; as well as allogeneic or xenogeneic embryonic stem cells; MSCs from multiple sources; and primary cells of NP or chondrocytes.[167] Some early studies compared the effect of injection of MSCs alone and MSCs embedded with atelocollagen gels into rabbit or rat with degenerated NPs. These studies demonstrated that cells within the collagen carrier helped maintain the disc height and strengthened magnetic resonance signal intensity. The histological appearance was also more similar to that of the native tissue after long-term implantation.[201–205]

2.5 Biomaterials for AF repair

AF is prone to tearing following acute injuries like forceful waist twisting or chronic strain, leading to extrusion and wear. These tears, often responsible for compromising the integrity of the IVD's load-bearing unit, result in severe pain and dysfunction. Given this increasing prevalence of defective AF, there is a critical need to consolidate effective strategies for repairing the AF to address these challenges.

The mechanical restoration of the AF relies on maintaining its structural integrity. AF patch has attracted much attention because of its suitability for the treatment of large AF ruptures. In recent years, AF repair patches made from decellularized porcine pericardial tissue have

demonstrated superior fatigue resistance and mechanical strength compared to natural AF [206,207]. Borem et al. introduced an AF patch utilizing collagen as the raw material, which enhances the repair of AF defects by influencing cell activity and migration.[208] Ankush Dewleet al. developed an electrically densely aligned collagen type I patch, capable of generating sufficient type I collagen and extracellular matrix.[209] However, the actual efficacy of the AF patch requires validation through preclinical experiments. Therefore, further in-depth research on repair strategies based on the suture approach is essential.

The primary challenge in AF healing is achieving mechanical properties comparable to native tissue while preserving structural integrity. Over the years, numerous studies have explored the use of various adhesive biomaterials to seal AF injuries sites. Unlike traditional mechanical devices for repairing AF ruptures, hydrogels emerge as a promising option for postoperative repair due to their injectability, unique physical characteristics, and biocompatibility [210].

Previous studies have utilized cellulose, a representative of natural hydrogels, for AF healing due to its excellent formability, adjustable mechanical characteristics, and high biocompatibility [211]. Alginate, a polysaccharide polymer derived from algae, is considered an injectable biomaterial for IVD repair owing to its biocompatibility and low cytotoxicity.[212] However, natural hydrogels, including cellulose and alginate, commonly exhibit mechanical deficiencies and face challenges in inhibiting or reversing AF degeneration. To address these limitations, composite hydrogels have been developed to achieve mechanical properties closer to the natural strength of AF. Among these, covalently bound hydrogels represent the most efficient strategy for repairing AF.[213]

FibGen hydrogels stand out as highly effective biomaterials for IVD repair. Demonstrated success includes the effective repair of AF defects and prevention of secondary protrusion in a sheep IVD model for up to one month.[214] In bovine intervertebral disc (IDD) models, FibGen sustained a high level of AF with increased extracellular matrix formation.[215] Another promising biomaterial is high-density collagen (HDC) gel crosslinked with riboflavin, which has shown significant efficacy in large animal models, with attenuated microscopic AF injury and maintained the intact AF structure for up to 6 weeks.[216] Furthermore, studies have utilized microfluidic technology to prepare hydrogels, suppressing inflammatory cytokine storms and promoting AF repair and regeneration.[217] Additionally, nanocellulose-reinforced gellan-gum hydrogels have been employed for AF repair due to their mechanical characteristics comparable to those of the natural human AF.[218]

The challenge in AF repair lies in the inability of hydrogels to fully restore its biomechanical characteristics over an extended period [219]. Innovative approaches are necessary, considering the need to rebuild AF structure and composition for functional integrity restoration. Scaffolds present advantages over hydrogels, particularly in mimicking AF's microstructure and anisotropic mechanical characteristics. Silk fibroin scaffolds, extensively researched for their high biocompatibility and compatibility with AF's biochemical gradient structure, are noteworthy. A study aimed to create a multilayered, disc-like, angle-ply construct of silk fibroin laminar scaffolds, resembling AF, using a direct freezing technique. Silk fibroin scaffolds exhibit various mechanical and cell-binding characteristics that can facilitate the differentiation of mesenchymal stem cells into fibroblast-like cells and enhance the synthesis of the extracellular matrix [220]. Electrospinning technology is recognized for producing aligned nanofibers with high porosity and large pore sizes. However, electrospun scaffolds often result in dense fiber accumulation, hindering uniform cell penetration and mechanical strength, thus impacting repair outcomes. Innovative strategies are necessary, as reconstructing the structure and composition may be required for restoring the functional integrity of the system.

Advanced 3D printing technology has found application in scaffolds due to its notable advantages in creating customized and intricately structured designs. Scaffolds produced through 3D printing exhibit a surface texture that better facilitates cell alignment and proliferation, mimicking the mechanical characteristics and anisotropy observed in native AF tissue. Some studies have employed 3D printing to create a laminar structure comprising polycaprolactone struts, adjusting the diameter and spacing between struts to achieve a more suitable morphological structure for AF repair.[221,222] While current 3D-printed scaffolds successfully capture the angular layer structure of the IVD, improvements are needed to better replicate the heterogeneity of native tissues due to limitations in printing materials and accuracy.[223] Additionally, challenges such as immediate post-implantation fixation, durability under repetitive motion, adverse microenvironments for resident cells, and the complexity of various factors, including cell type and source selection, must be addressed for the development of cell-based regenerative solutions.[186,224,225]

2.6 Culture model for IVD research

Dynamic loading with a certain magnitude, frequency and duration has been shown to maintain the matrix balance within the disc.[226–228] It can even provide a synergistic effect on the differentiation of stem cells towards the chondrocytic lineage under the influence of GFs.[229–234] A spinal compressive loading, comprising a diurnal dynamic loading variation in IVD pressure from low magnitude (~ 0.2 MPa) to high magnitude (~ 0.6 MPa) at a physiological frequency (0.2 – 1 Hz), is essential to maintain the health and function of the non-pathological IVD.[160] In addition to the compressive loading, hydrostatic pressure mediate on the matrix synthesis and matrix metalloproteinase expression in human IVD. Recent research indicated that a magnitude of 0.1 to 2.5 MPa, with a frequency of < 5 Hz and an 0.5 – 4 h of hydrostatic pressure loading per day are beneficial to isolated cells in 3D culture.[160] Other forms of loadings, such as torsion and bending are less investigated in IVD repair study.

IVD tissue culture is an important step to facilitate the translation of scientific findings into clinical use. Because human trials are time-consuming and expensive, it is critical to reproduce an in vitro condition recapitulating the IVD native environment to verify the hypotheses. Despite the fact that various combinations of cells and biomaterials have been explored for desc repair and regeneration, the effects of mechanical loading to cellular IVD implants are still convoluted. Bioreactors have been established for both human and animal models in the past decades.[156,235–238] The ex vivo organ culture model under simulated physiological conditions was developed. This enabled the culture of intact human or animal IVDs in a controlled dynamic environment. IVD bioreactors for long-term physiological organ culture of IVDs are developed to study the mechanisms of degeneration as well as IVD repair and regeneration.[237] Such bioreactors have been modified to apply dynamic mechanical loadings to agarose constructs that contain IVD cell-laden thermoreversible hyaluronan-based hydrogels. The results demonstrated the reliability of such platforms to evaluate the efficacy of tissue engineering therapy for IVD tissue repair and regeneration under biomimetic conditions before the clinical trials.

Chapter 3
Materials and Methods

This chapter outlines the materials and experimental methods used throughout the thesis. It is structured into seven sections. Firstly, it details the procedures involved in material synthesis, encompassing the nucleus pulposus (NP) glue and annulus fibrosus (AF) sealant. Subsequent sections elaborate on the mechanical characterizations conducted in this thesis. Following this, detailed methods for experiments involving cell culture and bioassays are provided. Then, the chapter presents the methods used for biomechanical testing on intervertebral disc (IVD), followed by an overview of the ex vivo evaluation methodology utilizing the human IVD bioreactor. Lastly, it covers the statistical analysis and presents the ethics statement.

3.1 Material synthesis

3.1.1 NP glue

Sodium alginate (Kimica Corporation) was used for all the experiments with NP glues and AF sealant. The purified alginate was obtained by sterile-filtered, frozen, and lyophilized. Calcium sulfate dihydrate was purchased from Sigma and sterilized by autoclaving the calcium sulfate dihydrate powder. The NP glue incorporated ionically crosslinked alginate hydrogel and adhesion primer. The coupling reagents, 1-ethyl-3-(3-dimethylaminopropyl) carbodiimide hydrochloride (EDC) (cat. #03450) and N-hydroxysulfosuccinimide (NHS) (cat. #130672), were purchased from Sigma-Aldrich.

The alginate hydrogel is synthesized by mixing sodium alginate solution with calcium sulfate solution. In brief, sodium alginate was dissolved in 2.25 mg L^{-1} glucose Dulbecco's Modified Eagle's medium (DMEM) at 3%, and calcium sulfate dihydrate was dissolved in calcium-free DMEM (Thermo Fisher Scientific, cat. #21068028) at 42 mM and stirred overnight. 2.25 mg L^{-1} glucose DMEM was prepared from the high glucose DEME (Thermo Fisher Scientific, cat. #11965092) and the no glucose DMEM (Thermo Fisher Scientific, cat. #11966025). Then mix the $CaSO_4$ slurries and alginate solution through syringe connectors with a volume ratio of 1/2 and ready for injection and application. The bridging polymers chitosan was dissolved into DI water at 2% w/v with 0.8 % v/v acetic acid overnight. The coupling reagents of EDC and NHS were dissolved in chitosan solution at a final concentration of 0 to 50 mg mL^{-1}. Then the mixture of the

chitosan and coupling reagents was applied to the target tissue surface (~ 0.25 μL mm^{-2}) before applying alginate hydrogel. Finally, the alginate hydrogel was injected on the primed surface immediately after mixing and applied compression before mechanical testing for 5-20 minutes.

3.1.2 AF sealant

Tough adhesives (TA) are deployed to seal the AF defect. They are synthesized and shaped in the form of a patch or plug following a previously reported protocol.[39] In essence, an alginate-polyacrylamide hydrogel was first formed and then received surface modification with a primer solution (chitosan, EDC and NHS) to bond with tissues via carbodiimide chemistry. For the alginate-polyacrylamide hydrogel, sodium alginate and acrylamide were first dissolved together in DI-water at 2% and 12%, respectively, and stirred overnight till a clear solution was obtained. This solution of 10 mL was then mixed with 36 μL of 2% covalent cross-linker MBAA (Sigma-Aldrich, cat. #M7279), 8 μL of accelerator TEMED (Sigma-Aldrich, cat. #T7024), 226 μL of 0.27 M initiator APS (Sigma-Aldrich, cat. #A3678), and 191 μL of 0.75 M ionic cross-linker CaSO4 slurries. For the AF sealant patch, the mixture was gelled inside a closed glass mold (1.5 mm thick) at room temperature overnight. Then a small piece of the hydrogel was punched out with a biopsy punch of 8 mm diameter (**Figure 3.1**). For the AF sealant plug, the gelation occurred in a petri dish to form an 8 mm thickness bulk gel, and then a cone-shaped hydrogel was punched out by a biopsy punch of 6 mm diameter. The adhesion primer, which is the same as used in the NP glue (30mg mL^{-1} of EDC/NHS in chitosan solution), was spread uniformly around the AF defect site. Subsequently, the defect site was covered with the sealant patch or inserted with the sealant plug, followed by gentle compression for 5-10 minutes manually.

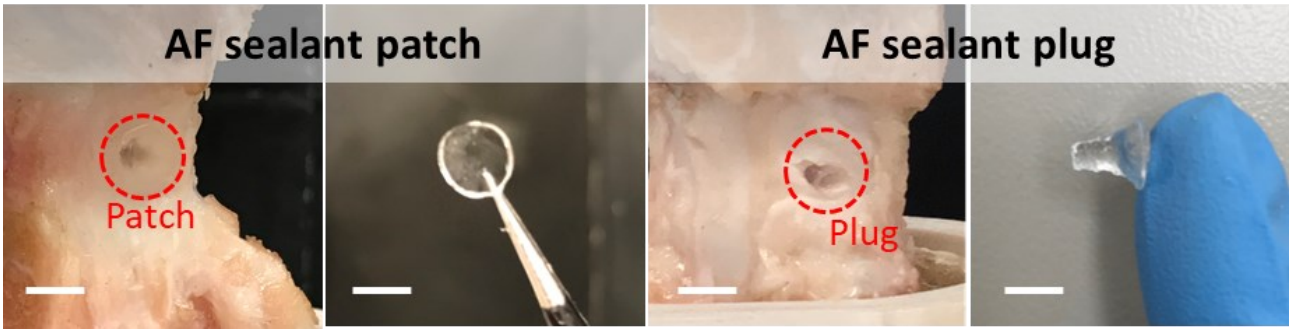

Figure 3.1 Images of annulus fibrosus sealant patch and plug. Scale bar = 5 mm.

3.1.3 Adhesion primer

Chitosan (Degree of deacetylation, DDA: 95%, medium and high MWs) was purchased from Lyphar Biotech and used for mechanical tests. For the cytocompatibility test, chitosan was dissolved in DI water with 0.8 % v/v acetic acid for 2 hours. The coupling reagents of EDC and NHS were dissolved in chitosan solution and then filtered through a 0.22 μm filter.

3.1.4 TPU composite hydrogel sealant

The thermoplastic polyurethane hydrogel (TPU-gel) was composed of alginate-polyacrylamide tough hydrogel and 3D-printed TPU mesh. The TPU mesh was 3D-printed using Creality Ender 3 V2 (Shenzhen Creality 3D Technology Co., Ltd.) into crossed layers with 40 mm in length, 5 mm in width, and 3 mm in thickness for tensile modulus test samples. The thickness of each layer of TPU mesh is 0.2 mm, and the width of the single-printed TPU fiber is 0.4 mm. Note that the TPU fiber angle between adjacent fibrous layers is 30°, matching with that of collagen fibers of AF respecting to the transversal plane of the spine (**Figure 3.2A**). In addition, each two adjacent layers of TPU mesh have offsets. The TPU mesh density is divided into 4 types according to the volume ratio of the TPU material: 20%, 30%, 40%. The filling volume was tuned by adjusting the distance between each fiber during printing. When preparing the flat TPU-gel patch, the alginate-polyacrylamide tough hydrogel was prepared as previously described and injected into the mold (40 mm in length, 5 mm in width, and 3 mm in thickness for tensile test), and the TPU was immediately pressed into the mold and covered with glass gelation at room temperature overnight (**Figure3.2B**). For the curved patches, a 3D-printed PLA mold was used in 1 mm thickness and 15 mm width, with an arc length of 20 mm and curvature radius of 13mm (**Figure 3.2C**). The partially filed TPU-gel patch was synthesized with a 5 mm punched TPU mesh placed in the middle of the mold and pulled with alginate-polyacrylamide tough hydrogel.

3.1.5 The congregation of rhodamine-B isothiocyanate to chitosan

To visualize the depth of chitosan, part of the adhesion primer, into the AF, Rhodamine-B isothiocyanate (Cayman Chemical, cat. #20653) was conjugated to chitosan polymeric chains with the following steps. Briefly, 1 wt% chitosan was first dissolved in 80 mM acetic acid and sterilized through 0.22 μm PES filters (Thermo Fisher Scientific, cat. #13100106). Anhydrous methanol (Thermo Fisher Scientific, cat. # A412-1) was added to the filtered chitosan solution with a volume ratio of 1:1. The mixture was stirred for 3 hours at room temperature and degassed before use. Rhodamine B was dissolved in methanol at 2 mg mL^{-1}. The staining solution was added to the

chitosan/methanol mixture drop-by-drop under stirring. The final concentration of fluorescent dyes in the reaction medium was controlled to give the label to D-glucosamine residue at a ratio of 1:50. The reaction lasted for 18 hours for rhodamine B-labeled chitosan in dark at room temperature. Then, 1 N NaOH solution (Sigma-Aldrich, cat. #S2770) was used to precipitate chitosan from the solution. The precipitates were collected and dialyzed with DI water until no fluorescent signal was detectable in the water. The precipitates were freeze-dried before use.

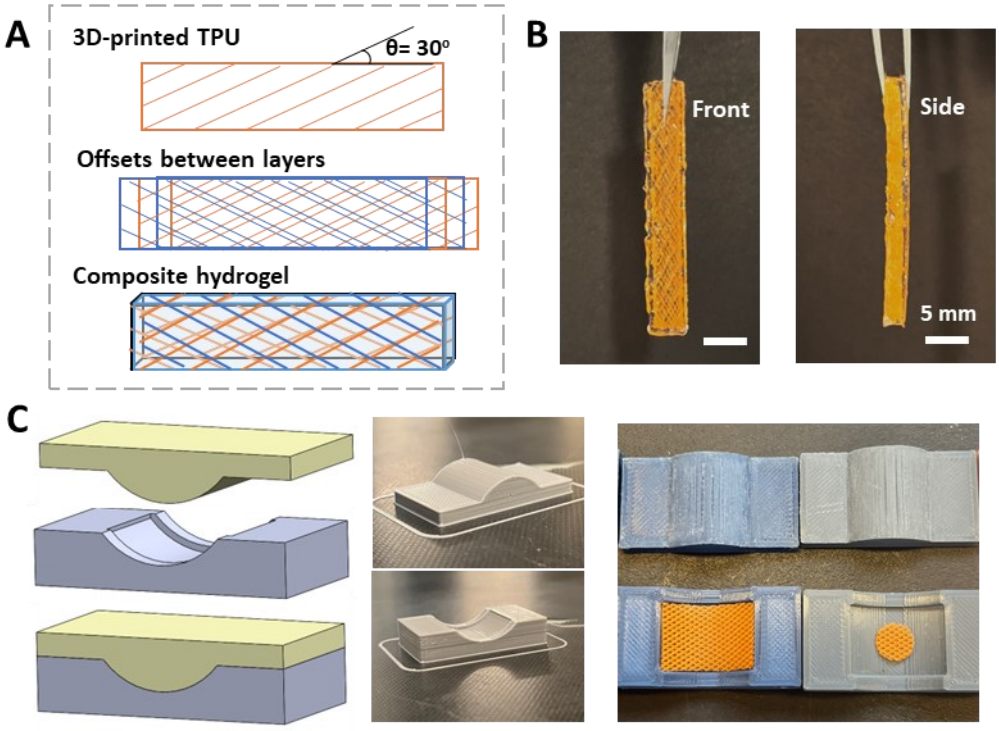

Figure 3.2 Representation of the mesh-reinforced composite sealant design and fabrication process. A. Illustration of TPU mesh design. B. Images of the composite hydrogel sample (20% volume fraction, 30°) for tensile test. C. The mold utilized in the synthesis of curved composite hydrogel sealant.

3.2 Mechanical characterization

3.2.1 Rheological measurement

Strain sweep tests were performed on human NP samples or the in-situ alginate hydrogels (20 mm in diameter and 1 mm in thickness) on the stage of rheometer (TA Instruments, Discovery HR-2). A 20-mm parallel plate was used, and a gap was set at ~1 mm. The strain swept from 0.05% to 50% under a constant angular rate of 10 rad/s. Time sweep tests characterized the gelation kinetics of the alginate hydrogel with an oscillation frequency of 1 Hz (~ 6.28 rad s^{-1}) and strain of 0.1% for 45 min. The viscoelasticity refers to the mechanical property of materials that exhibit both viscous

(fluid-like) and elastic (solid-like) behavior when subjected to deformation. The storage shear modulus and loss shear modulus provide a comprehensive characterization of the viscoelastic behavior of materials. Stress relaxation is a phenomenon observed in viscoelastic materials whereby the stress applied to the material decreases over time while the strain (deformation) remains constant. The storage modulus and shear modulus were recorded as a function of time. The stress relaxation profile was assessed under a step strain of 15%. The duration required to relax half of the initial stress defines the stress relaxation time, $t_{1/2}$.

3.2.2 Lap shear adhesion test

For the lap shear adhesion test of NP glue, NP glue adhesion imparted by the adhesion primer was quantified using a modified lap shear configuration. Before testing, lap-shear specimens were fabricated in an acrylic mold with 3 mm thickness, 10 mm width, and 20 mm length. First, 1.5 mm thick, 10 mm wide, and 20 mm length of tissues of NP, inner AF (IAF), or outer AF (OAF) were obtained from the bovine tail in coccygeal IVD levels of cc1/2, cc2/3, cc3/4, and cc4/5. Then the tissues were placed in the base of the acrylic mold. Then to apply the NP glue, the bridging adhesion primer was dropped on the top of the tissue, followed by an injection of the alginate hydrogel into the primed tissues. Next, it was covered by a glass sheet and kept in a 4°C refrigerator overnight. Negative control samples were without the application of adhesion primer. Before testing, the samples were placed at room temperature for 1 hour. For the adhesive failure strength measurement, specimens were taken out from the mold and glued to a custom acrylic backing by Super Glue and then fixed on a universal testing machine (model 596; Instron, Norwood, MA, USA) with a 10 N load cell (1/1000th of the force capacity to an accuracy of 0.5% of reading). Then, the specimen was loaded to failure at a constant loading rate of 5 mm per minute. The strain stress at failure and the type of failure were recorded. For the adhesive energy test, a 1-mm notch was created at the interface between hydrogel and tissues before loading, and the critical strain corresponding to the ultimate stress was recorded. All data were collected on Instron software and post-processed on MATLAB (MathWorks, Natick, MA, USA) code. The same method was used for characterizing the adhesion strength and adhesion energy of the TPU-gel patch on human AF tissue.

3.2.3 Tensile test of composite hydrogel sealant and human AF

To measure the tensile properties (elastic modulus and tensile strength), the strips (40 mm × 50 mm × 3 mm) of composite hydrogel were tested with a tensile test machine (1000 lb force load cell). The displacement rate was 100 mm min^{-1}. The nominal stress was obtained by dividing the force

by the area of the cross-section, and the nominal strain was obtained by dividing the change in length by the original length. The elastic modulus is extracted as the slope of the linearly fitted stress-strain curve at 5% strain. The tensile strength is defined by stress at highest strain. Non degenerated human AF tissue from four discs were used for the tests as well.

3.2.4 Pure shear test of composite hydrogel sealant

To measure the fracture toughness of the composite hydrogel sealant, the pure-shear test was performed according to previous studies.[239,240] Briefly, a pair of samples (width of 60 mm, thickness of 1.5 mm) were glued to rigid acrylic clamps for each test. One sample was unnotched, and the other one was edge-notched. The height (H) of the specimen (i.e., the distance between the two acrylic clamps) was 5 mm. The unnotched sample was pulled by an Instron machine (Model 5965) with a 1 kN load cell (1/1000th of the force capacity to an accuracy of 0.5% of reading) at a strain rate of 2 min^{-1} to measure the stress-stretch ($S - \lambda$) curve. For the notched sample, a notch length of 8 mm was introduced to the edge of the sample by a razor blade. The notched sample was pulled until rupture to obtain a critical stretch (λ_c). The fracture energy was calculated from $S - \lambda$ curve of the unnotched sample by $\Gamma = H \int_1^{\lambda_c} S \, d\lambda$.

3.2.5 3-point bending test of TPU-hydrogel patch and human AF tissue

The flexural modulus of TPU patch and AF tissue was measured by 3-point bending according to ASTM D790. A sample of rectangular cross-section rests on two supports (span length is 16 mm) and is loaded by means of a loading nose midway between the supports. The sample is 30 mm in length (L), 1.5 mm in thickness (d), and 3.5 mm in width (b). The specimen is deflected under loading at a strain rate of 0.10 mm s^{-1}. Deflection and load will be recorded. The flexural modulus is calculated by $E_B = L^3m/4bd^3$, where m is the slope of the tangent to the initial straight-line portion of the load-deflection curve.

3.2.6 In-situ peeling test of TPU-gel patch on bovine IVD segments

To assess the bond between the three types of composite sealant and IVD tissue, adhesion energy was measured using a described previously on bovine IVD segments.[241,242] Firstly, One end of a TPU-patch adhesive (10 mm × 1 mm × 12 mm) was bonded to the bovine IVD. In this experiment, the composite hydrogels were applied to seal the AF defects after injection of NP glue. The vertebrae were clamped in a plastic adapter attached to the test machine. Next the backing was secured to the load cell fixture above, and the force were recording. An acrylic backing was adhered on the

hydrogel with superglue. Then the free arm end (15 mm × 4 mm) was fixed by the clamp. The peeling test was conducted based on the 90-degree peeling device (**Figure 3.3**). Unidirectional tension was then applied to the patch, while the force and the extension were recorded. The loading rate was kept constant at 100 mm min^{-1}. Adhesion energy was calculated as the plateau value of the ratio of the force and the width of the hydrogel[243].

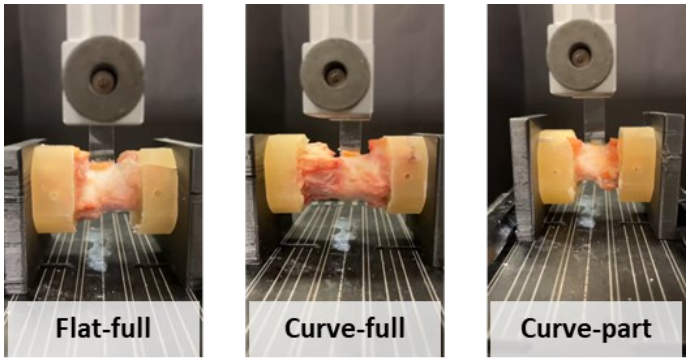

Figure 3.3 Images of the set-up of in-situ peeling test on IVD. Three types of composite hydrogel sealant are tested on the bovine IVD segments.

3.3 Cell culture and bioassays

3.3.1 Human IVD tissue and cell preparation

All the human IVD tissue and IVD cells in this study were provided by Spinal Tissue Biobank at McGill University. Details of the information can be found in **Table 2.1**. The isolation of human discs is followed established protocols from Spinal Tissue Biobank.[244] Briefly, after the removal of the muscles and ligament around the disc and vertebral, parallel axial cuts were made through the vertebral bodies close to the cartilage end plates using a handsaw. Discs isolated are rinsed in 1×PBS supplemented with 100 μg mL^{-1} gentamicin (Thermo Fisher Scientific, cat. #15710-072) and 0.5 μgmL^{-1} fungizone (amphotericin B; Thermo Fisher Scientific, cat. #15290018) for 5 minutes. Discs then received two 5 minutes of serial washes with Hank's Balanced Salt Solution (Sigma-Aldrich, cat. #H9394) supplemented with 100 μg mL^{-1} gentamicin and 0.5 μg mL^{-1} fungizone. Discs are cultured in tissue culture medium (2.25 g/L glucose DMEM, supplied with 0.5% gentamicin, 5% FBS (Sigma-Aldrich, cat. #12483020), 1% GlutaMAX (Thermo Fisher Scientific, cat. #35050-061), 50 μg mL^{-1} ascorbic acid) for pre-swelling for 48 hours. Then the fresh IVD were ready to use for the following tests. The NP or AF tissue is isolated separately for the 3D cytocompatibility test. The IVDs for ex vivo culture in bioreactor and MRI scanning, will be

processed as the same preparation before nucleotomy and repair. Besides, human cells were isolated from fresh non-degenerated IVD tissues from a human donor; around 1.07×10^6 NP cells were harvested from 1 g of NP tissue and used in passages 2-3.

Table 2.1 Summary of human IVD sample information

Experiment	Age	Sex at birth	Condition	Disc level	Isolated and used form	Frozen or fresh	Replicates n
2D cytocompatibility	56	Male	Non-degenerated	L2-4 & L5-S1	NP cell	Fresh	Technical replicates from one independent experiment of one donor
3D cytocompatibility	19	Male	Non-degenerated	T7-T9	NP tissue and AF tissue	Fresh	Technical replicates from one independent experiment of one donor
Rheology test of human NP	78	Male	Degenerated	L2-L3	NP tissue	Fresh	Technical replicates from one independent experiment of one donor
Ex vivo human IVD in bioreactor	53	Female	Degenerated	L2-L3	Whole IVD	Fresh	One preliminary experiment without replicates
MRI curvature calculation	53	Female	Degenerated	L4-L5	Whole IVD	Fresh	Replicates of five different IVDs of five independent experiments from two donors
	62	Female	Degenerated	T12-L1	Whole IVD	Fresh	
	62	Female	Degenerated	L1-L2	Whole IVD	Fresh	
	62	Female	Degenerated	L2-L3	Whole IVD	Fresh	
	53	Female	Degenerated	L2-L3	Whole IVD	Fresh	
TPU-gel tensile test	31	Male	Non-degenerated	L2-L3	AF tissue	Frozen	Replicates of four different IVDs of four independent experiments from four donors
	31	Male	Non-degenerated	L1-L2	AF tissue	Frozen	
	35	Male	Non-degenerated	L1-L2	AF tissue	Frozen	
	41	Male	Non-degenerated	L1-L2	AF tissue	Frozen	
TPU-gel lap shear test	31	Male	Non-degenerated	L1-L2	AF tissue	Frozen	Replicates of four different IVDs of four independent experiments from four donors
	35	Male	Non-degenerated	L1-L2	AF tissue	Frozen	
	41	Male	Non-degenerated	L1-L2	AF tissue	Frozen	
	61	Male	Degenerated	L1-L2	AF tissue	Frozen	
TPU-gel bending test	31	Male	Non-degenerated	L1-L2	AF tissue	Frozen	Replicates of five different IVDs of five independent experiments from five donors
	35	Male	Non-degenerated	L1-L2	AF tissue	Frozen	
	41	Male	Non-degenerated	L1-L2	AF tissue	Frozen	

	61	Male	Degenerated	L1-L2	AF tissue	Frozen	
	31	Male	Non-degenerated	T3-T4	AF tissue	Frozen	
Compressive cyclic loading test	61	Male	Degenerated	L3-L4	Whole IVD	Frozen	One preliminary experiment without replicates
	61	Male	Degenerated	L1-L2	Whole IVD	Frozen	

3.3.2 Cytocompatibility of NP glues

2D cytocompatibility. To measure the cytotoxicity of the NP glues to human primary NP cells, the monolayer culture of cells in the extracts medium of NP glues was performed following the standard protocols in International Organization for Standardization (IOS) 10993-5. Briefly, the extracts of NP glues were prepared with a 200 mg/mL concentration in 12-well cell culture-treated polystyrene microplates. A mass of 200 mg of NP glue was placed in the center of the well, and 1 mL of low glucose (2.25g L^{-1}) DMEM was added to cover the glue completely. The samples were incubated at 37ºC for 24 hours. The concentration of the EDC/NHS in the primer used for NP glue is in a gradient of 0, 20, 30, and 50 mg mL^{-1}. The extracts were prepared on the same day that human primary NP cells were seeded into 96-well microplates. After 24 hours of incubation, the extracts were collected into small vials and supplemented with 1% GlutaMAX, 0.5% gentamicin, and 10% FBS on the monolayer human primary NP cells. Cells were cultured in the normal complete DMEM medium for the negative control group. In the test, human primary NP monolayer cells cultured in the described extract medium for 24 hours were evaluated via Live/Dead assay. The negative control group was treated with 70% methanol for 30 minutes before the Live/Dead assay.

3D cytocompatibility. For 3D cytocompatibility of NP glue demonstration, human MSCs were encapsulated in the alginate hydrogel as described in ESI†. The cell-gel samples (8 mm in diameter and 2 mm in thickness) were mounted onto the primed living isolated human AF/NP tissue (8 mm in diameter and 2 mm in thickness) to form adhesion. After that, the specimens (i.e., cell-gel-tissue) were cultured in a tissue culture medium for five days, followed by a Live/Dead® assay and imaging using an inverted confocal laser scanning microscope (Zeiss LSM 800) to evaluate the viability of cells in NP glue and the tissues.

3.3.3 NP cell culture in NP glues

The NP cells were encapsulated in alginate hydrogels for in vitro experiments. Purified sodium alginate was dissolved in DMEM (2.25 g L^{-1} glucose) and mixed with NP cell suspension at a final density of 1 million cells per mL, matching the low cell density found in native human NP (4 million cells per cm^3). The cell-alginate mixture was then combined with calcium sulfate ($CaSO_4$) slurries.

This blend was promptly injected into a custom glass model with a 2 mm thickness and left to incubate at 37°C for 45 minutes for complete gelation. Subsequently, 6 mm diameter samples were punched out and placed in a 24-well plate for a 21-day culture period. Each well was supplemented with 600 μL of culture medium, which was refreshed every three days. The conditioned medium was collected at each time point.

Four formulations of alginate hydrogel NP glues were examined, denoted as 1 kPa-high-MW, 1 kPa-low-MW, 3 kPa-high-MW, and 3 kPa-low-MW, corresponding to calcium concentrations in the alginate hydrogels of 14 mM, 15 mM, 20 mM, and 23 mM, respectively. Here, "high" and "low" MWs refer to alginate molecular weights of 1500 kDa and 92 kDa, respectively.

3.3.4 Cell viability test of NP cells encapsulated in NP glues

For human primary NP cells encapsulated in the alginate hydrogel, on days 1, 3, 7, 14, and 21, the samples were put in a serum-free medium containing calcein AM and ethidium homodimer fluorescent dyes (Live/Dead®, Thermo Fisher Scientific, cat. #L3224), according to the manufacturer's instructions. Cell viability was evaluated using an EVOS M5000 microscope. Twenty consecutive 10 μm sections were imaged. The image stacks were merged and saved as a single-color JPEG file (red and green separate), and the labeled cells were quantified through Image J code. The viability of cells was calculated from the proportion of green and total cells.

3.3.5 Sulfated glycosaminoglycan quantification

The amount of sulfated glycosaminoglycan (sGAG) synthesized by NP cells encapsulated in alginate hydrogel for 21 days was evaluated by the 1,9-dimethylmethylene blue (DMMB) assay.[245] The hydrogels containing NP cells were removed from their culture medium on day 1 or day 21. The conditional medium was collected over the culture period. Chondroitin sulfate (Sigma-Aldrich, cat. #C9819) was used to make the standard curve, and 4 M guanidine hydrochloride ($CH_5N_3 \cdot HCl$) was added to standard curves when quantifying sulfated GAG content released in the hydrogel. Reagents are added to a 96-well plate, followed by reading under a microtiter plate reader (Tecan M200 Infinity Pro) using the absorbance at 530 nm. The dry mass of hydrogel was measured as the mass of the frozen and lyophilized constructs on day 1 and day 21. Samples without dilution were fit in the middle of the linear range of the standard curve, and results were expressed per mg of the dry weight of the gel sample.

3.3.6 Metabolic activity assay

Metabolic activity was measured in the NP cell-laden hydrogel samples on day 1, day 4 and day 7. Each of the sample in the 24 well-plate was incubated in 600 μL culture medium containing 10% (v/v) alamarBlue (Invitrogen, cat. #DAL1025) for 4 hours. 3 times 100 μL of each sample were transferred to black 96 well plates (Corning, cat. #3880) and fluorescence intensity was measured at excitation 540 nm, emission 585 nm (Tecan M200 Infinity Pro). 10% alamarBlue in culture medium was used as a blank value and was subtracted from all the sample values.

3.3.7 Immunostaining and imaging

For immunostaining, the hydrogel constructs were first fixed with 4% paraformaldehyde containing $BaCl_2$ (Sigma-Aldrich, cat. #342920) for 60 min and washed in 1×PBS. The gels were then processed using standard immunochemistry procedures. Briefly, gels were washed three times in Dulbecco's phosphate-buffered saline (DPBS), permeabilized with DPBS containing 0.5% Triton X-100 (Sigma), and then blocked with a blocking buffer that contained 1% bovine serum albumin (BSA, Sigma), 10% Goat serum (Invitrogen), 0.3 M glycine (Thermo Fisher Scientific) and 0.1% Triton X-100 in DPBS. The following antibodies/reagents were used for immunostaining: mouse monoclonal aggrecan antibody (Abcam, cat. #3778) (1:200), rabbit polyclonal type II collagen antibody (Abcam, cat. #34712) (1:200), Prolong Gold antifade reagent with 4′,6-diamidino-2-phenylindole (DAPI) (Invitrogen, Hoechst 33258) (1:1000), AF-488 Phalloidin (1:1000) to stain actin (Invitrogen), Goat anti-Rabbit IgG AF 647 (Invitrogen) (1:800) and Goat anti-Mouse IgG AF 555 (Invitrogen) (1:800). The samples were imaged using a Zeiss LSM 800 confocal microscope.

3.3.8 Confocal imaging for primer penetration depth

The adhesion primer, which was made by conjugated chitosan, was cast over an 8 mm diameter punch of bovine AF tissue for 2 min. Following incubation, the extra solution was aspirated off the AF and applied with alginate hydrogels for 15 min or 24 hours at 4 ^{o}C. Consequently, the specimens were embedded in Tissue-Teck O.C.T. Compound for cryosectioning to produce 12 μm thick sections mounted on charged slides (Thermo Fisher Scientific, cat. #22-037-246). Sections were then stained with a 1:1000 dilution of 1 μg mL^{-1} stock solution DAPI for 5 minutes to visualize AF cell nuclei. Slides were imaged on a Zeiss LSM 800 confocal microscope to visualize cross-sectional depth-of-penetration. The confocal images were imported into MATLAB, and the depth was analyzed.

3.4 Biomechanical test on IVD tissue

3.4.1 Bovine IVD tissue preparation

Bovine disc tissues used for the lap shear test were isolated from the bovine tail with 18 months provided by Oligo Medic. The bovine discs for ex vivo biomechanics tests are isolated from bovine tails with levels cc2/3, cc3/4, and cc4/5 from healthy and skeletally mature animals, purchased from a local grocery store.

3.4.2 Bovine IVD motion segment preparation for mechanical tests

Frozen bovine tails for biomechanical loading tests were purchased from a local grocery store. Spinal motion segments (i.e., vertebrae-disc-vertebrae) were isolated from the levels C2/C3, C3/4, and C4/C5. Facet joints, transverse processes, ligaments as well as musculature were carefully removed. The motion segments were potted in two Dragon Skin (Smooth-On) molds with an acrylic resin (DenPlus, Canada) on both ends of the segments. The cured potting materials were drilled to create holes for the fixture. Afterward, the potted motion segments were wrapped in PBS-soaked gauze and–stored at - 20^{o}C until further use. Before testing, the potted motion segments were submerged in 1×PBS with protease inhibitor at 4 ^{o}C to allow full hydration overnight. On the day of testing, the specimens were warmed in 1×PBS at room temperature for 2 hours.

All motion segments were randomly assigned to ‘Intact’, ‘Defect’, ‘Glue’, ‘Glue+Patch’, and ‘Glue+Plug’ groups. Except ‘Intact’, all the groups underwent nucleotomy following a standard clinical procedure. Specifically, a 3-mm biopsy punch (Integra LifeSciences) was inserted 7 mm deep into the posterolateral side of the AF, and the resulting plug of tissue was removed using a rongeur. Following the initial tissue removal, the NP was then disrupted with micro scissors, and ~ 200 mg of fragmented NP tissue (around ~25% of NP) was removed from the IVD. For the Glue condition, the injured IVD was treated with NP glue alone. To do so, the adhesion primer (Chitosan, EDC, and NHS) of ~150 μL was first injected slowly into the NP cavity using a 3-mL syringe and a 20G x 1-1/2” needle (BD PrecisionGlide™, NJ) to prime the inner tissue surface. After 2 minutes, the extra primer solution was aspirated, followed by injection of the mixture of alginate and calcium sulfate to in-situ form alginate hydrogels (~150 μL). The specimens were then covered by a parafilm and set for 15 minutes before mechanical testing. For the groups of Glue+Patch or Glue+Plug, after removal of the partial NP as mentioned for Glue groups, the AF defect was treated with the adhesion primer and sealed with the AF patch (Glue+Patch) or inserted with the AF plug (Glue+Plug). Gentle compression was applied on the AF sealant for 10 minutes to enable adhesion and covered by a parafilm until mechanical testing.

3.4.3 Biomechanical test of IVD bioadhesives in IVD motion segments

Cyclic loading tests: Changes in IVD motion segment biomechanical properties in the groups with/without repair after nucleotomy were characterized using axial tension-compression and stress relaxation tests on a testing device (model 596; Instron, Norwood, MA, USA). The test includes two phase steps (**Figure 3.4**). Specifically, in the first phase, specimens were loaded cyclically in force control at tensile 0.2 MPa and compressive 0.5 MPa loads for 20 cycles at 0.5 Hz.[246,247] In the second phase, after the same cyclic loading as the first phase, an additional stress relaxation tests were then performed with ramp displacement applied until the force equivalent of 0.15 MPa compression was achieved; after that, the constant displacement was held for 15 min. All biomechanical testing was performed at room temperature.

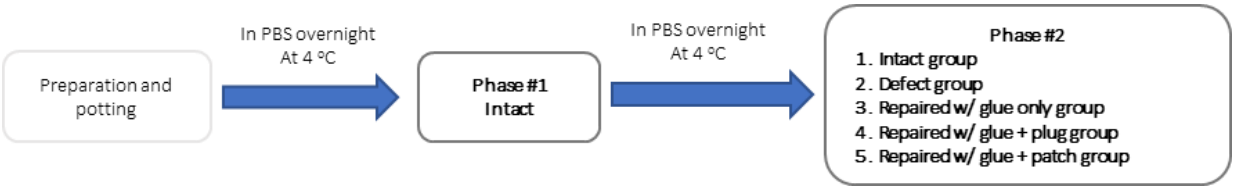

Figure 3.4 Workflow of the two-phase cyclic loading test process. Thawed bovine IVD segments are prepared, rehydrated, and subjected to initial cyclic loading. After treatments including nucleotomy with or without repairs, samples undergo a second phase of cyclic loading.

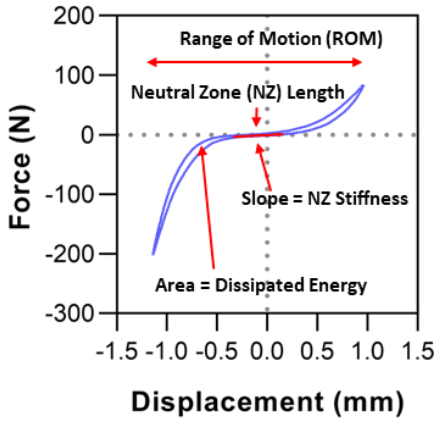

Figure 3.5 The representative force and displacement of one cycle from the biomechanical test. The biomechanical parameters are defined as indicated by red lines added to the force-displacement curve, including range of motion, neutral zone length and stiffness, and dissipated energy.

A MATLAB code was used to extract defined biomechanical parameters from raw force-displacement (**Figure 3.5**). The parameters were determined from the average value of the last 5 complete test cycles as described.[248] Compressive/tensile stiffness was defined as the slope of the force-displacement curve within 80% of the maximum/minimum displacement region. Range of motion (ROM) was the total displacement of the motion segment during a compression-tension cycle. Dissipated energy was defined as the area between loading and unloading curves in the force-displacement response. The neutral zone (NZ) length was defined as the distance between two points in the loading and unloading curves at which the load was zero and the slope of the force-displacement response in the NZ denoted the NZ stiffness. Preceding parameters were determined from the average value of the last 5 test cycles. In the stress relaxation test, the force-time was recorded, and the stress relaxation along with time was normalized to the initial stress.

Failure compression tests: To evaluate the herniation risks, we performed displacement-controlled (2 mm min^{-1}; ramp-to-failure) compressive failure tests on motion segments on a 5° inclined foundation to maximize stress at the repair site (**Figure 3.6**).[46,249] The tests were performed on a test instrument (ElectroPuls® E10000; Instron, Norwood, MA, USA). The stress was defined as the applied force normalized to IVD cross-sectional area. The load-displacement curves showed two types of failure mechanisms: endplate fracture or disc subsidence (a direct drop of force); NP extrusion (force perturbations). The extrusion failure can also be observed during the tests, which was defined as a 2 mm protrusion of NP or implant materials from the outer radius of the AF.[46] the failure strength for Intact groups was defined as the maximum stress at the point of endplate fracture; for the defect and repaired groups, the failure strength was defined the stress of NP extrusion point.

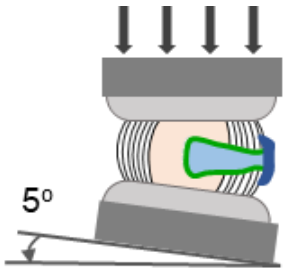

Figure 3.6 Illustration of compressive failure test conducted on bovine IVD segments. Ramp-to-failure tests are performed at a 5° incline to maximize stress at the repair site.

3.5 Bioadhesive evaluation on human IVD model

3.5.1 IVD Bioreactor experiments

To evaluate the adhesion of the bioadhesives under physiological conditions, we tested them on human IVD loaded with an IVD bioreactor for 28 days. The isolation of human disc and the design and operation of the IVD bioreactor were described in the previous studies.[244,250] Briefly, a living human lumbar IVD of level L2-L3 (from a donor, 53 years old, male) was isolated and then conditioned in a culture medium to reach equilibrium for 48 hours as described in section 3.3.1. Nucleotomy was performed by creating a 4 - 5 mm vertical linear incision with 3 mm depth in the AF at the post-lateral position of the disc with a scalpel (**Figure 3.7A**), followed by removal of 0.9248 g NP tissue with pituitary and curette (**Figure 3.7B**). After applying the MSC-laden NP glue (~1 mL) (**Figure 3.7C**) and the AF patch (**Figure 3.7D**), we assembled the bioreactor with the repaired IVD, and filled the culture chamber with the disc culture medium. After pre-loading of 0.1

MPa static compression for 48 hours to reach the equilibrium status, a physiologically relevant cyclic compressive loading was applied to the IVD for 26 days. The daily loading pattern contains 4 statuses: (1) 2 hours dynamic compressive loading from 0.1 – 0.6 MPa at 0.1 Hz; (2) 6 hours static compressive loading of 0.1 MPa; (3) 2 hours dynamic compressive loading from 0.1 – 0.6 MPa at 0.1 Hz; (4) 14 hours static compressive loading of 0.1MPa. The medium will be changed every 7 days. The displacement, force, and time of the mechanical data were recorded. The IVD height and diameters were recorded at the beginning and end of the culture.

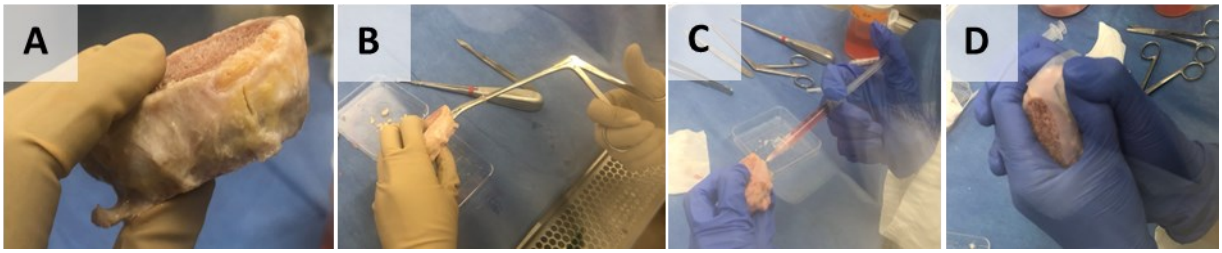

Figure 3.7 The procedure of nucleotomy and repair using bioadhesives on human IVD. Steps include human IVD nucleotomy (A, B), injection with NP glue (C), and repair with an AF patch (D).

3.5.2 MRI for human IVD

T1ρ-weighted MRI directly correlates with proteoglycan content in IVDs of intact human lumbar spine segments.[250] To determine the effect of cell-laden NP glue therapy on degenerate intact human lumbar discs, potential region of interest (ROI) in NP and AF areas were identified as previously described [251] and the average of the T1ρ values was calculated within the ROIs of the control and injected discs slices per image. Briefly, discs were sutured on one side (to mark for MRI positioning) and were allowed to equilibrate for 24 h in culture media pre injection. They were subjected to pre-T1ρ MRI scans and then cultured under dynamic loading for 28 days. Post-culture and after 24 h equilibration period, post-T1ρ MRI scans were acquired. All isolated human discs were scanned in sagittal and axial planes and images were obtained on a 7T Bruker BioSpec 70/30 USR (Bruker Biospin, Milton, ON, Canada) with the high-performance mini-imaging kit gradient upgrade AVIII electronics (Bruker) and a Bruker-issued T1ρ-RARE pulse sequence, as previously established.[250,251] Heat maps representing signal intensity were created using the MIPAV software (NIH Center for Information Technology, Bethesda, MD, USA). T1ρ values were calculated and quantified for all the axial slices using the MIPAV software. T1ρ values of ′before′ and ′after′ scans of each disc were normalized to the surrounding culture medium (strongest value) using editing features in MIPAV software. Specific regions of interest (ROIs) were drawn around regions

indicating NP region of the ′after′ images and superimposed onto the same region of the ′before′ image. This was performed in the axial plane of slices 3-7 (out of 8) for each sample. The T1ρ images were manually cropped by a single user (DHR) around the perimeter of the IVDs. The average of the T1ρ values was calculated within the ROIs for the hydrogel alone and the cell-seeded hydrogels from 3-7 slices per image in the axial plane. To determine the curvature of IVD, we used the ImageJ tool to draw and fit a curve consistent with the external AF profile at this location.

3.6 Statistical analysis

All experiments with statistical analysis contained at least three replicates per condition unless stated otherwise. Data distributions were assumed to be normal for all parametric tests but not formally tested. No statistical method was used to predetermine sample size. For the statistical analyses between two groups, statistical significance and p values were determined using a two-tailed Student's t-test with unequal variance. Statistical analyses were performed with Prism (GraphPad) using T-test, one-way ANOVA test or two-way ANOVA test. Data were presented as means ± SD and statistical significance as ****P < 0.0001, ***P < 0.001, **P < 0.01, *P ⩽0 .05, ns > 0.05.

3.7 Ethics statement

The human IVD tissue and cells were from Spinal Tissue Biobank (IRB A04-M53-08B) and the related tests were approved by Research Ethics Office of McGill University (A10-M113-13B).

Chapter 4

Tissue-mimetic Hybrid Bioadhesives for IVD Repair

In this chapter, a hybrid bioadhesive was reported that combines an injectable glue and a tough sealant to simultaneously repair and regenerate intervertebral disc (IVD) post-nucleotomy. The glue fills the nucleus pulposus (NP) cavity while the sealant seals the annulus fibrosus (AF) defect. Strong adhesion is formed with the IVD tissues and survives extreme disc loading. Further, the glue can match native mechanically, and support the viability and matrix deposition of encapsulated cells, serving as a suitable cell delivery vehicle to promote NP regeneration. Besides, biomechanical tests with bovine IVD motion segments demonstrate the capacity of the hybrid bioadhesives to restore the biomechanics of bovine discs under cyclic loading and to prevent permanent herniation under extreme loading. This work highlights the synergy of bioadhesive and tissue-engineering approaches.

4.1 Design principles of IVD-mimetic hybrid bioadhesives

An ideal bioadhesive to treat IVD post-nucleotomy should fill the NP cavity and seal the AF defect concurrently. These requirements are difficult to satisfy with a single bioadhesive, since the NP differs from the AF mechanically, biochemically, and structurally. The heterogeneous nature of IVD thus necessitates a hybrid strategy to repair different parts of IVD. The hybrid strategy is manifested with the developed hybrid bioadhesives, which comprise two different yet integral components: AF sealant and NP glue (**Figure 4.1**). For the AF sealant, which was repurposed and customized bioinspired tough adhesives, consisting of tough alginate-polyacrylamide hydrogels and surface adhesion primer (Chitosan/EDC/NHS).[39] As reported previously, such bioadhesives achieve unprecedented wet adhesion performance on diverse biological tissues, including skin,[252] cartilage[253], and tendon.[33] This work aims to study their applicability to the IVD environment and the form factor (flat patch versus plug) for sealing the AF defect. While the plug design has been proposed to seal AF defects,[254] the patch design is hypothesized to be easier to implement and resistant to extrusion. Their performance will be tested given the shape and size of the AF defect and the loading of IVD.

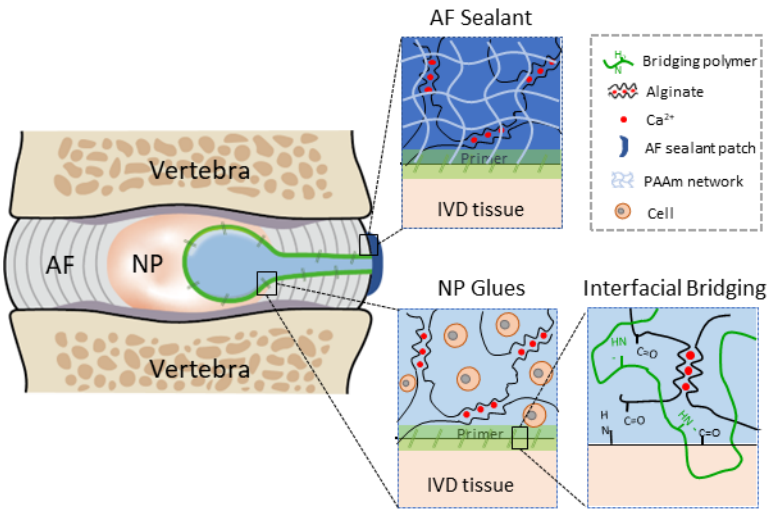

Figure 4.1 Design and working principle of IVD hybrid bioadhesives. Annulus fibrosus (AF) defect is sealed using the AF sealant, while the nucleus pulposus (NP) cavity after nucleotomy is filled with NP glue.

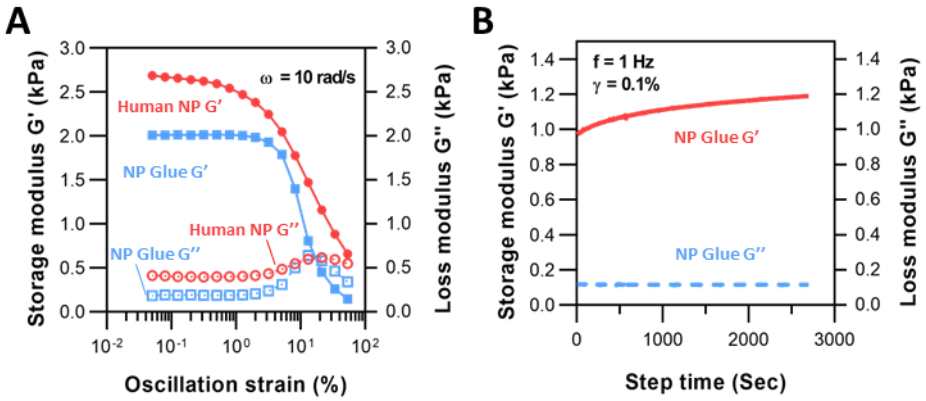

Figure 4.2 Rheology test on NP glue and human NP tissue. A. Shear moduli of the NP glue (blue) and human NP (red) as a function of oscillation strain (*G'* solid dots; *G"* empty dots). B. Instantaneous gelation of NP glue.

To resemble and adhere to the native NP, the NP glue comprises the same surface adhesion primer (Chitosan/EDC/NHS) but a viscoelastic alginate hydrogel as the matrix. The alginate hydrogel has been proposed to fill the NP cavity but lacks bioadhesion with IVD tissues.[32,255] Thus the bioadhesive agents were deployed to prime the surface of the NP cavity before the injection of alginate hydrogel. After removing the excess primer solution, a mixture of calcium sulfate and alginate precursors will be injected, which exhibits shear-thinning behavior (**Figure 4.2A**). The NP glue is formed nearly instantaneously, as evidenced by the overwhelming *G'* over *G"* from the very beginning (**Figure 4.2B**). The residues of chitosan and EDC/NHS facilitate the bonding between the alginate matrix and the surrounding tissue. The alginate hydrogel acts as a cell carrier designed

to deliver and support exogenous cells for regeneration purposes. Moreover, by adjusting the calcium concentration, we approximated the shear storage and loss moduli of the NP glue with those of human NP (**Figure 4.2A**). The values are within the range of non-degenerated human NP reported in previous studies.[68,256] Together, the resulting NP glue is bioadhesive, injectable, and viscoelastic.

Combining the NP glue and the AF sealant, the hybrid bioadhesives are proposed to repair and regenerate IVD post-nucleotomy. Mechanically, the bioadhesives can fill NP cavities and seal AF defects, as well as restore IVD biomechanics and arrest herniation concurrently. Biologically, the NP glue can not only deliver exogenous cells but also instruct them to deposit matrix for regeneration. As a result, the IVD after nucleotomy could be repaired and regenerated with our hybrid bioadhesives (**Figure 4.3**).

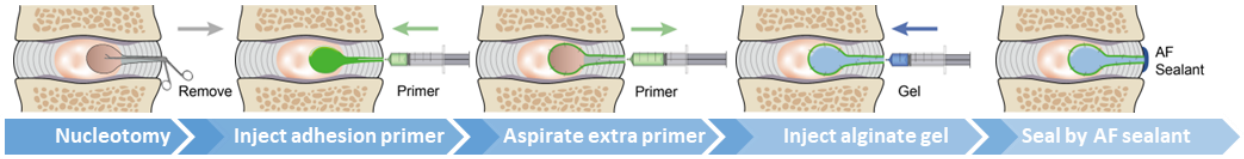

Figure 4.3 Hybrid bioadhesive application procedure post-nucleotomy. The nucleotomy is performed with NP removal through the AF defect, then the adhesion primer is injected into the NP cavity. After excess primer removal, cell-laden glue is injected into the cavity, followed by the application of AF sealant on the outer AF to seal the defect.

4.2 Strong adhesion to IVD tissues

The modified lap-shear tests were performed to quantify the adhesion performance of the NP glue and the AF sealant on IVD tissues (**Figure 4.4**). Such tests have been widely applied to specimens, with and without pre-cracks introduced at the tissue-bioadhesive interface, to measure adhesion energy and adhesion strength, respectively. Bovine discs were used as a model system, given their accessibility and extensive use for IVD research, as well as recognized similarity with their human counterpart.[215,244,246,257] Besides the whole disc, we dissected bovine discs into NP, inner AF (IAF), and outer AF (OAF) in an attempt to delineate the tissue-mimetic adhesiveness. Note that the mechanics and biochemistry vary substantially from NP to OAF.[258] For instance, the content of sGAG, part of aggrecan,[259] decreases sharply from IAF to OAF.[260]

It is hypothesized that the adhesion primer could enable the adhesion of hybrid bioadhesives on individual IVD substructures. The chitosan chains carrying amine groups can penetrate the IVD tissue and form covalent amide bonds via carbodiimide reactions with carboxylate groups of

proteins (IVD tissues) and alginate (the NP glue and the AF sealant). In addition, the neutralization of the diffusing chitosan results in a chitosan network bridging between the hydrogel and the tissue, contributing to bioadhesion. To visualize the interfacial processes, rhodamine-labeled chitosan[81] was developed and imaged to show how the adhesion primer penetrates the AF tissue over time (**Figure 4.5**). The penetration depth was measured at ~30 μm after 15-minute incubation and varied negligibly when the incubation time was prolonged up to 24 hours. The finding agrees well with our previous measurements, indicating that the primer agents are spatially confined at the interface, and thus unlikely to impact deeper tissues.

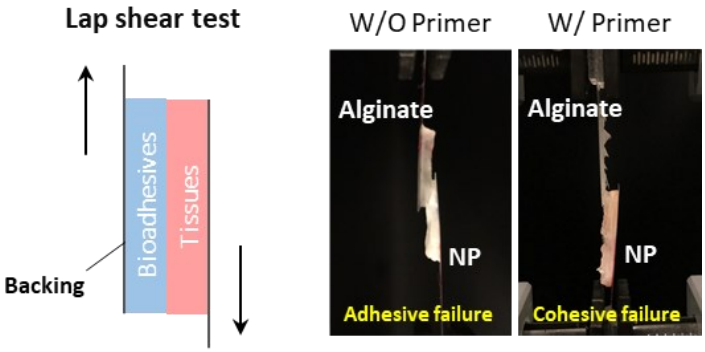

Figure 4.4 Characterization of adhesion properties of NP glue via modified lap shear test. Variances in failure modes are observed between groups with and without primer application.

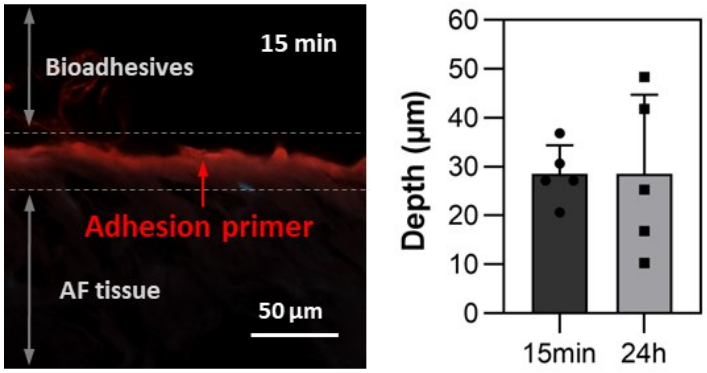

Figure 4.5 The adhesion primer penetration after applying the NP glue. The observed penetration thickness of the adhesion primer within the interface measures approximately 30 μm, with no significant difference noted between 15 minutes and 24 hours.

To study the effect of the adhesion primer on IVD adhesion, the NP glue and substructures of bovine IVD (NP, IAF, and OAF) were tested. When examining the interfacial fracture behavior, we observed the cohesive failure of the NP glue, indicating a stronger interface than the hydrogel

matrix. The cohesion was evidenced by the pre-crack kinking into the glue matrix, leaving a rough fracture surface (**Figure 4.4**). In contrast, without the adhesion primer, the alginate hydrogel alone detached readily from the tissue, leading to an adhesive failure and a smooth fracture surface. **Figure 4.6A** shows the stress-displacement curves of modified lap-shear tests. The maximum stress (i.e., adhesion strength) is significantly improved (P_Alg/NP = 0.013, P_Alg/IAF = 0.0001, P_Alg/OAF = 0.0159 by two-way ANOVA tests) with the aid of the primer (**Figure 4.6B**). The same conclusion is drawn by comparing the adhesion energy (i.e., the energy needed to detach the adhesive from the tissue) with and without the primer (P_Alg/NP < 0.0001, P_Alg/IAF = 0.0864, P_Alg/OAF < 0.0001 by two-way ANOVA tests) (**Figure 4.6C**). The results demonstrate the effectiveness of adhesion primer for IVD-mimetic adhesion.

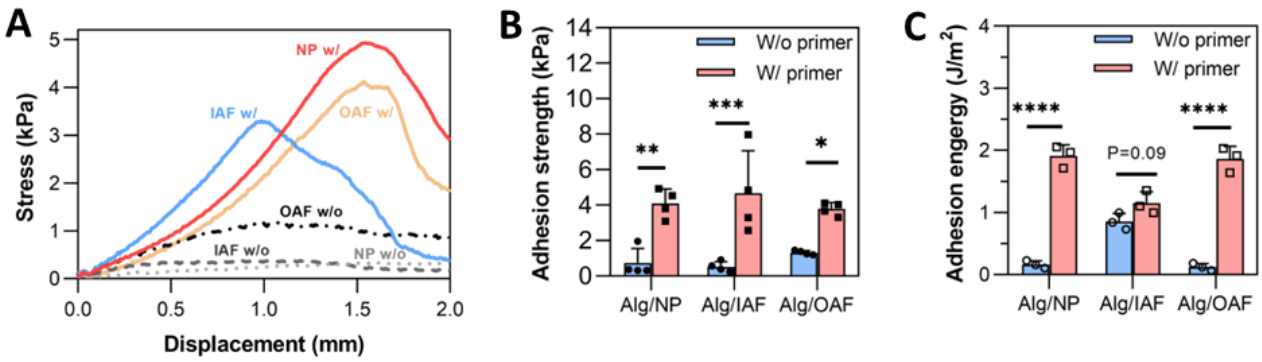

Figure 4.6 Lap-shear test of NP glue on sub-tissue of bovine IVD. A. Stress and displacement from lap-shear tests. The alginate hydrogel plus adhesion primer presents significantly higher adhesion strength (B) and adhesion energy (C) to bovine IVD tissues than no-primer groups (****P < 0.0001, ***P < 0.001, **P < 0.01 and *P < 0.05 by two-way ANOVA tests)

Next, the adhesion performance on the transverse surface of the whole IVD was characterized. The adhesion between the NP glue and the AF sealant was also characterized to examine the cohesion between the two components of hybrid bioadhesives. **Figure 4.7A** confirms the formation of adhesion in all three conditions. The sealant-IVD adhesion sustains considerable stress and strain due to the tough and stretchable matrix of the AF sealant (**Figure 4.7A-B**). The adhesion energy between the sealant and the IVD was measured at ~159 J m^{-2} (**Figure 4.7C**), exceeding the values measured between commercially available bioadhesives and biological tissues.[39,253]

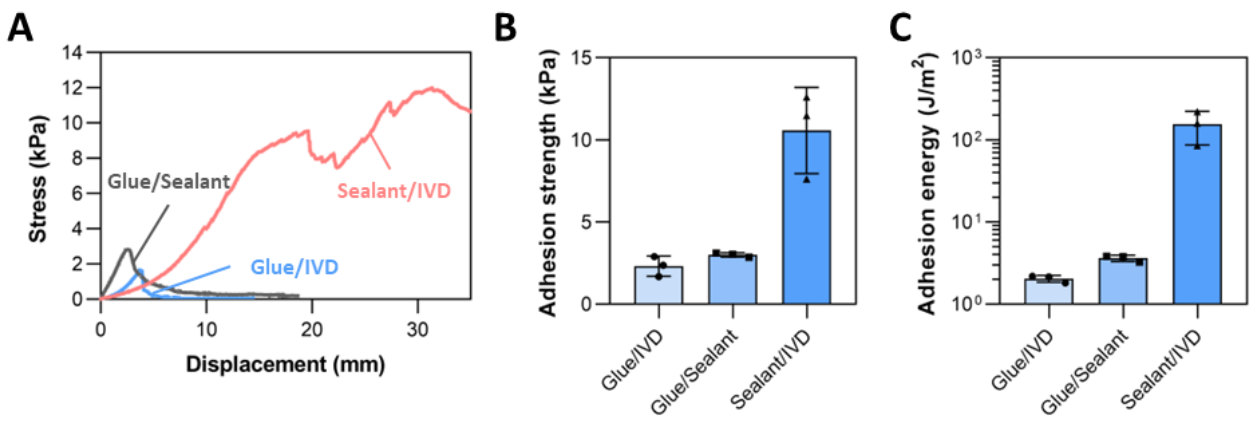

Figure 4.7 Lap-shear test of NP glue and AF sealant whole bovine IVD. A. Representative curves of stress and displacement for the glue and sealant adherent on whole IVD, as well as the glue/sealant adhesion. (B) and (C) show the corresponding adhesion strength and adhesion energy.

4.3 Biomechanical performance under physiological cyclic loading

After confirming the strong adhesion of hybrid bioadhesives within the IVD niche, effects on the biomechanics of IVD under physiological cyclic loading conditions were studied. An *ex vivo* model of bovine disc motion segments was used, receiving nucleotomy representative of standard clinical treatment. The specimens contain endplates and parts of vertebrates to recapitulate the physiological stress distribution in the disc. A two-phase cyclic loading protocol[248] was adopted, accounting for variances of disc samples and physiological relevance; as such, this *ex vivo* model was chosen over *in vivo* animal models because the loading pattern of human discs is different from those of animals.[261] Specifically, an initially intact specimen was preloaded and loaded cyclically between tensile (0.2 MPa) and compressive (0.5 MPa) stresses for 20 cycles at 0.5 Hz (1st phase); the same specimen, after receiving the nucleotomy and treatment,[26] was loaded again with the same loading profile (2nd phase) (**Figure 4.8**).[248] The compressive stress represents the stress magnitudes during physiological loading on the human spine when relaxed standing (0.5 MPa).[262–264] The first few loading cycles preconditioned the disc, eliminating potential effects of cycle number and load history.[265] A comparison between the two phases of the same specimen, intact and repaired, informs the repair outcome of a specific treatment condition.

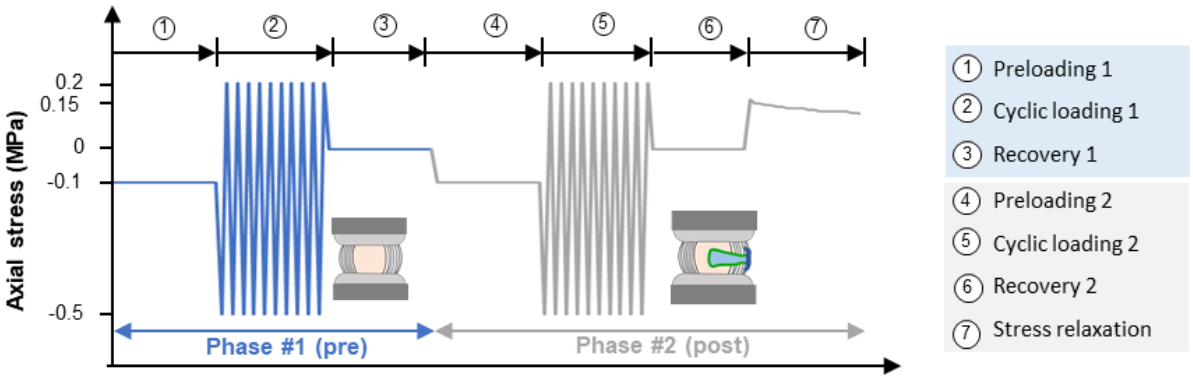

Figure 4.8 Loading pattern of two-phase cyclic loading for biomechanical evaluation. Nucleotomy and repair are performed between two phases on the disc.

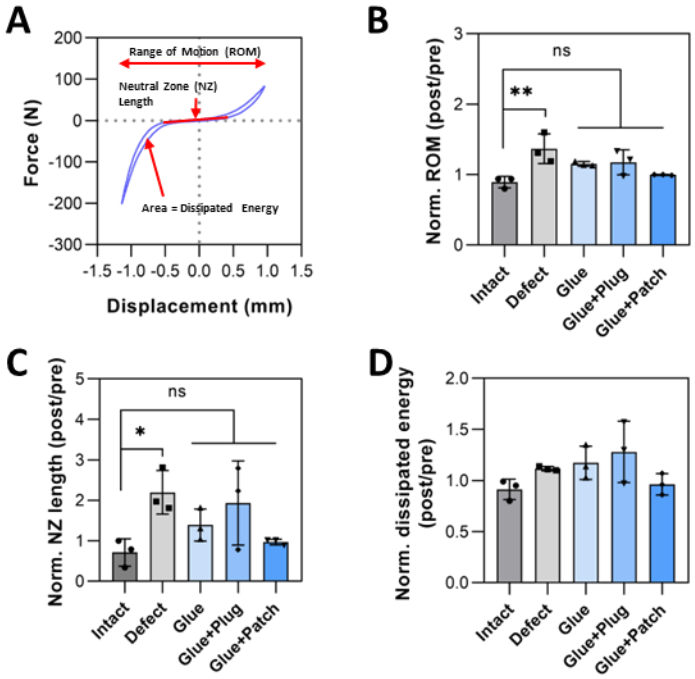

Figure 4.9 The biomechanical parameter of bovine IVD repaired with hybrid bioadhesives. Representative force-displacement curve (A) of the last five loading cycles of Phase #2, informing ROM (B), NZ length (C), and dissipated energy (D), normalized with the corresponding data from Phase #1. ($p > 0.05$ for ns, $^{***}P < 0.001$, $^{**}P < 0.01$ and $^{*}P < 0.05$ compared with values of Intact group by one-way ANOVA tests).

Five conditions were evaluated: the glue alone (Glue), the glue plus the sealant plug (Glue+Plug), and the glue plus the sealant patch (Glue+Patch), along with intact and defect (non-repaired) samples for comparison. **Figure 4.9A** illustrates a representative force-displacement curve in the last cycle of the group (Glue+Patch), where key biomechanical readouts such as ROM, NZ length, and dissipated energy are extracted. It was confirmed that the defect samples after partial

nucleotomy increase significantly in ROM and NZ length ($p = 0.0040$ for ROM and $p = 0.0312$ for NZ length by one-way ANOVA tests) in a good agreement with prior works, validating the developed model and testing methods.[262] The results showed the repaired specimens better resemble the intact conditions (**Figure 4.9B-D**). When examining the discs under loading, it was found that the extrusion of NP and glue in the defect and glue alone conditions, but not in the conditions in relation with the AF sealant. These results indicate that hybrid bioadhesives can help restore the biomechanics of disc motion segments and mitigate disc re-herniation under physiological cyclic loading.

Next, the viscoelastic properties of the segments by performing stress relaxation tests at the end of the 2nd phase were evaluated (**Figure 4.8**). The viscoelastic behavior, associated with the hydration level and swelling pressure in NP, plays a vital role in the load-bearing mechanism.[266] The stress relaxation curves show the defect disc relaxes considerably less stress, indicating compromised viscoelasticity (**Figure 4.10A**). In comparison, the disc repaired with Glue+Patch is found to relax more stress, a good indication of restored viscoelasticity (**Figure 4.10B**). By combing NP glue and AF patch, our hybrid strategy outperforms other treatments in restoring the disc biomechanics.

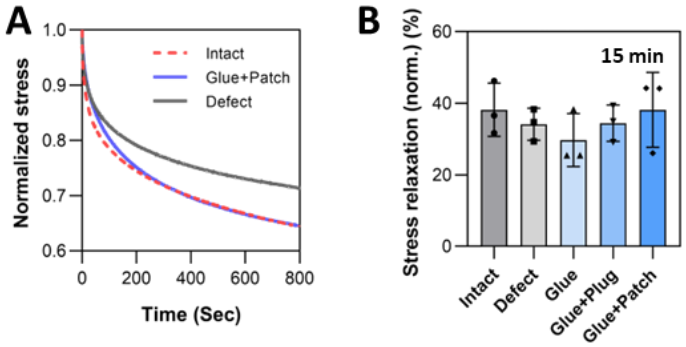

Figure 4.10 Stress relaxation behaviour of the bovine IVD repaired with hybrid bioadhesives. A. Representative stress relaxation curves. B. Normalized stress relaxation.

4.4 Capacity to improve failure strength and prevent re-herniation

To assess the response of repaired discs under extreme loading, ramp-to-failure tests were performed, that is, compression loading with a constant speed until the specimens to the failure point. The bottom of motion segment specimens is inclined by an angle of 5° at the post-lateral site to promote herniation specifically. It is worth noting that the combination of heavy loads and

inclination represents an extreme scenario to probe the failure behavior of our hybrid bioadhesives. Representative force-displacement curves of Glue+Patch (blue curve) and Intact (grey curve) groups are plotted in **Figure 4.11A**, showing two modes of motion segment failure - extrusion and subsidence. The failure events are further examined with video screenshot (**Figure 4.11B**), confirming that intact specimens fail only by subsidence, whereas all post-nucleotomy specimens exhibit both failure modes. Since the specimens after nucleotomy are predisposed to extrusion, the failure strengths (stress to extrusion) of the defect and repair cohort are below that of the intact specimen (**Figure 4.11C-D**), indicating the need of future optimization. Nevertheless, the failure strength of the Glue+Patch condition (8.2 ± 4.7 MPa) is closer to that of intact control (22.2 ± 4.8 MPa), compared to the defect control (3.2 ± 1.7 MPa), indicating enhanced repair outcomes. Noteworthy, the obtained failure strength is well above the physiological upper bound of intradiscal pressure (2.3 MPa).[263]

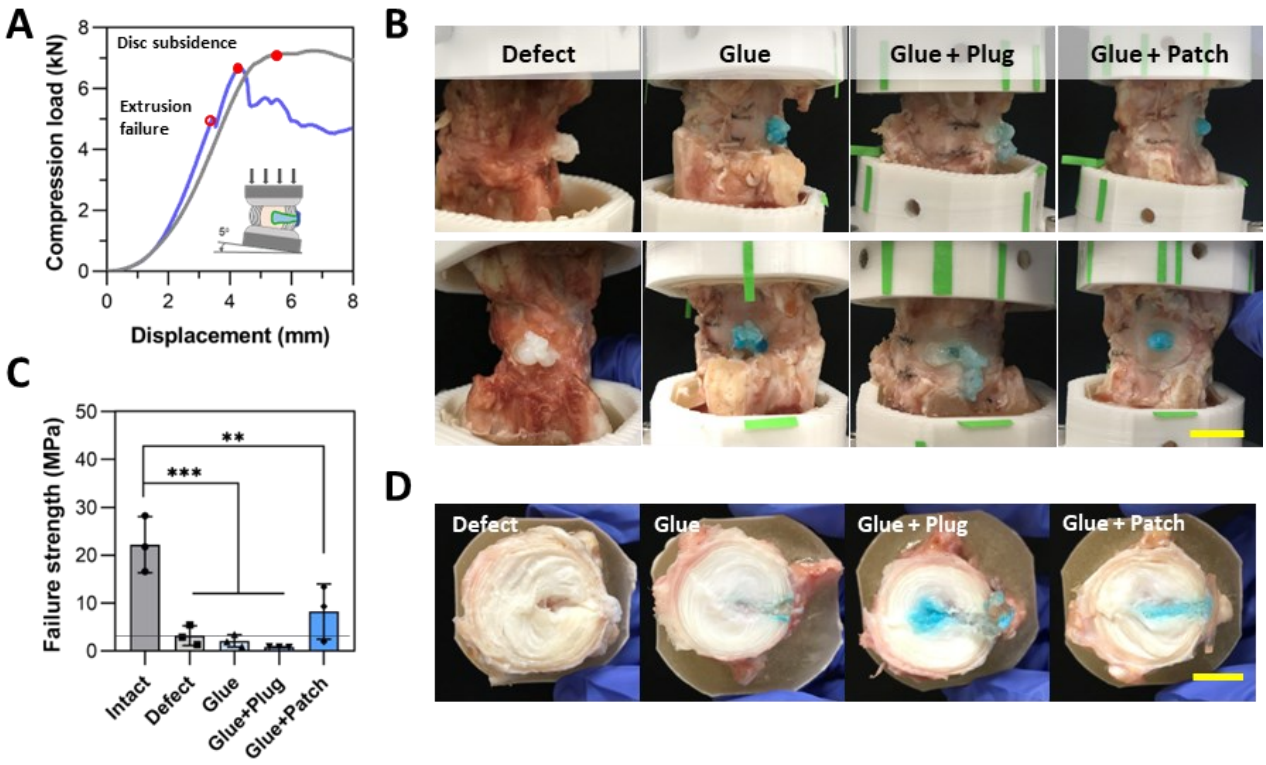

Figure 4.11 The compressive failure test on bovine IVD repaired with hybrid bioadhesives. A. Representative load-displacement curves of the conditions of Defect (grey) and Glue+Patch (blue). B. Images of bovine IVD after extreme loading. C. Comparison of failure strength in all conditions. D**.** Images

of the cross-sections of IVD after the failure test. Scale bar = 10 mm. ***P < 0.001 and **P < 0.01 compared with values of Intact group by one-way ANOVA tests).

Another advantage of the treatment with glue and patch is found by examining the extruded substance. Similar to the NP of the defect specimen extruding out of the disc, the NP glue and AF plug are displaced and extruded due to the extreme loading. The phenomenon is accompanied by the debonding of the AF plug from the AF defect. To this end, the form factor of the AF sealant is critical, as the sealant patch withstands the extreme loading and remains adherent to the AF. Thanks to the robust adhesion, the extruded substance can be held by the sealant patch and, remarkably, pushed back with slight pressure applied manually (**Figure 4.12A**). The pressure present in the disc space from the surrounding muscle and ligament might serve the same purpose.[267,268]

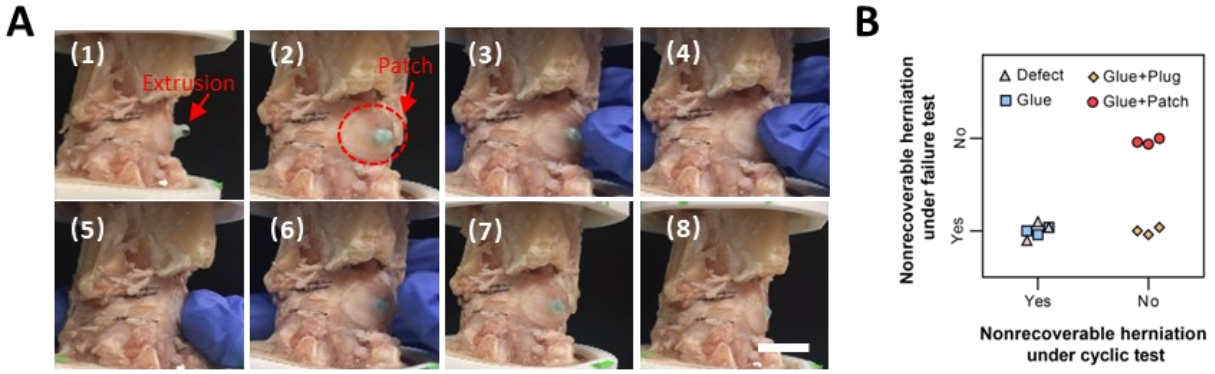

Figure 4.12 Herniation recovery with the Glue+Patch treatment. A. The AF patch holds the NP glue after extreme compressive failure test and the herniation can be recovered by gently pressing the extrusion part back to the disc (scale bar = 10 mm). B. Nonrecoverable herniation under cyclic and extreme loading shows that the treatment with Glue + Patch can prevent permanent extrusion.

Unlike extreme loading data in **Figure 4.11A**, the biomechanical data of low-strain cyclic loadings shows smooth and undisturbed curves of displacement-time and force-time (**Figure 4.13**). This further indicates that there was no NP extrusion or failure throughout the test. The incidences of nonrecoverable extrusion of tested conditions under cyclic and extreme loading are summarized in **Figure 4.12B**. The difference between the patch and plug designs can be attributed to the different stress fields of the sealant: the plug-AF interface is subjected to Poisson's effect and much larger shear stress than that experienced by the AF patch. Together with the preceding results, it can be concluded that the treatment with the combination of the glue and the sealant patch is optimal for IVD repair.

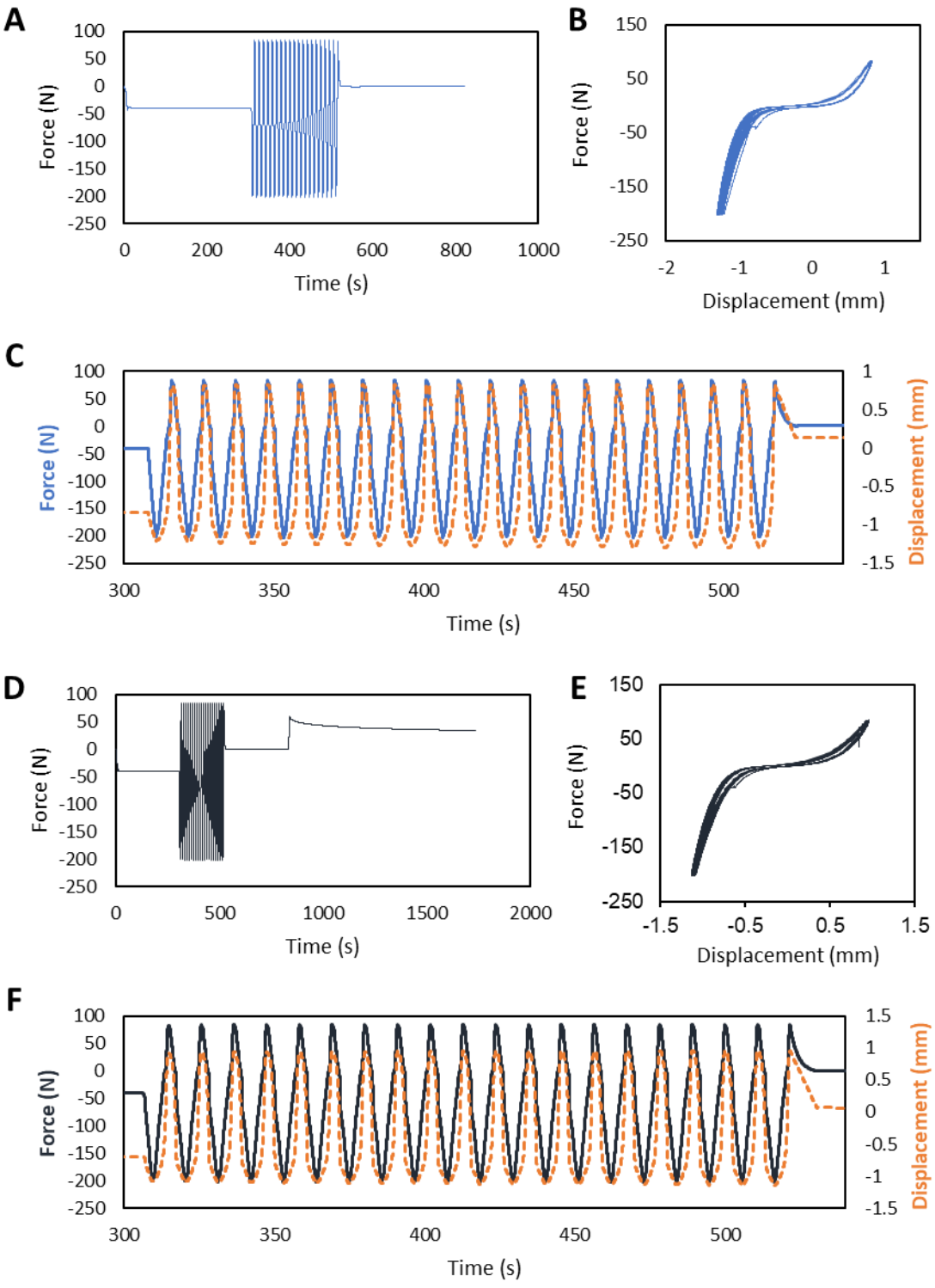

Figure 4.13 Representative raw data of the complete cyclic loading pattern for Glue+Patch sample. A-C: Phase #1 is for pre-repair. D-F: Phase #2 is for post-repair.

4.5 Compatibility with native and delivered cells

After proving the repair capacity of hybrid bioadhesives, biocompatibility and regenerative capacity were studied. To demonstrate their cytocompatibility with human primary NP cells, the conditioned culture medium with the NP glue (alginate hydrogel + adhesion primer) was then used to culture monolayer human primary NP cells for 24 hours (**Figure 4.14A**). On average, the viability is 98% for all groups with ingredient concentrations of EDC/NHS (0-50 mg mL^{-1}) (**Figure 4.14B-C**). The result supports that the NP glue is cytocompatible at or below their working concentrations (30 mg mL^{-1} of EDC/NHS in 2% chitosan).

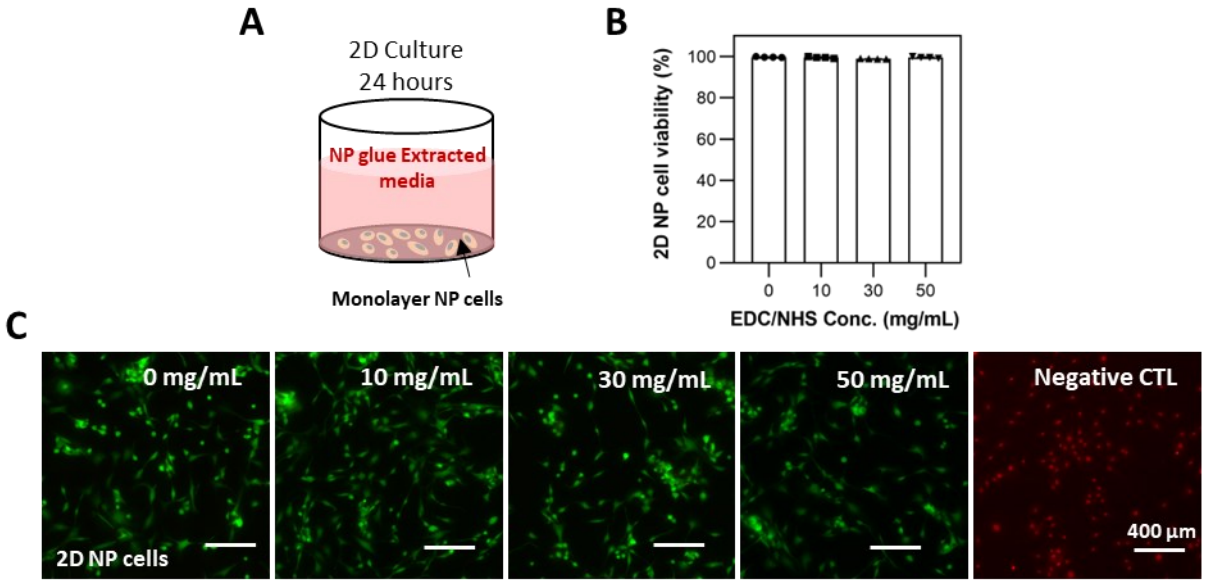

Figure 4.14 2D cytocompatibility test of NP glue. A. Evaluation of cytotoxicity of NP glues in 2D culture. B. The NP cell viability is up to 98% over all concentrations of EDC/NHS. C. Fluorescence images of Live/Dead assay on 2D cells.

To further test the biocompatibility at tissue levels, a 3D culture model with human disc tissues was developed, where the NP glue was applied to human NP and AF tissues separately (**Figure 4.15A**). Meanwhile, to test the feasibility of cell delivery, MSCs were encapsulated with NP glue. The MSC is proposed for IVD regeneration because of its accessibility and differentiation toward NP-like cells. The cell-laden NP glue and the IVD tissues were cultured with tissue culture mediums for five days. Examination of the native cells within IVD tissues reveals high viability and no discernible effect of the adhesion primer (**Figure 4.15B**). The viability of cells in the tissue from its surface (0 µm) to its 20 µm and 40 µm depths are all comparable and not significantly

different from the control groups (tissue only, without NP glues). Also, comparable viability was found with MSCs encapsulated within NP glues applied to the tissue. The viability of MSCs in the NP glue from the interface to the depth of 40 μm is not significantly different from the control groups (without primer), further assuring the cytocompatibility of the adhesion primer (**Figure 4.15C**). As a result, it is concluded that the cytocompatibility of NP glue is in part attributed to the small amount and spatial confinement of the adhesion primer presented at ~20 μm depth in the tissues.

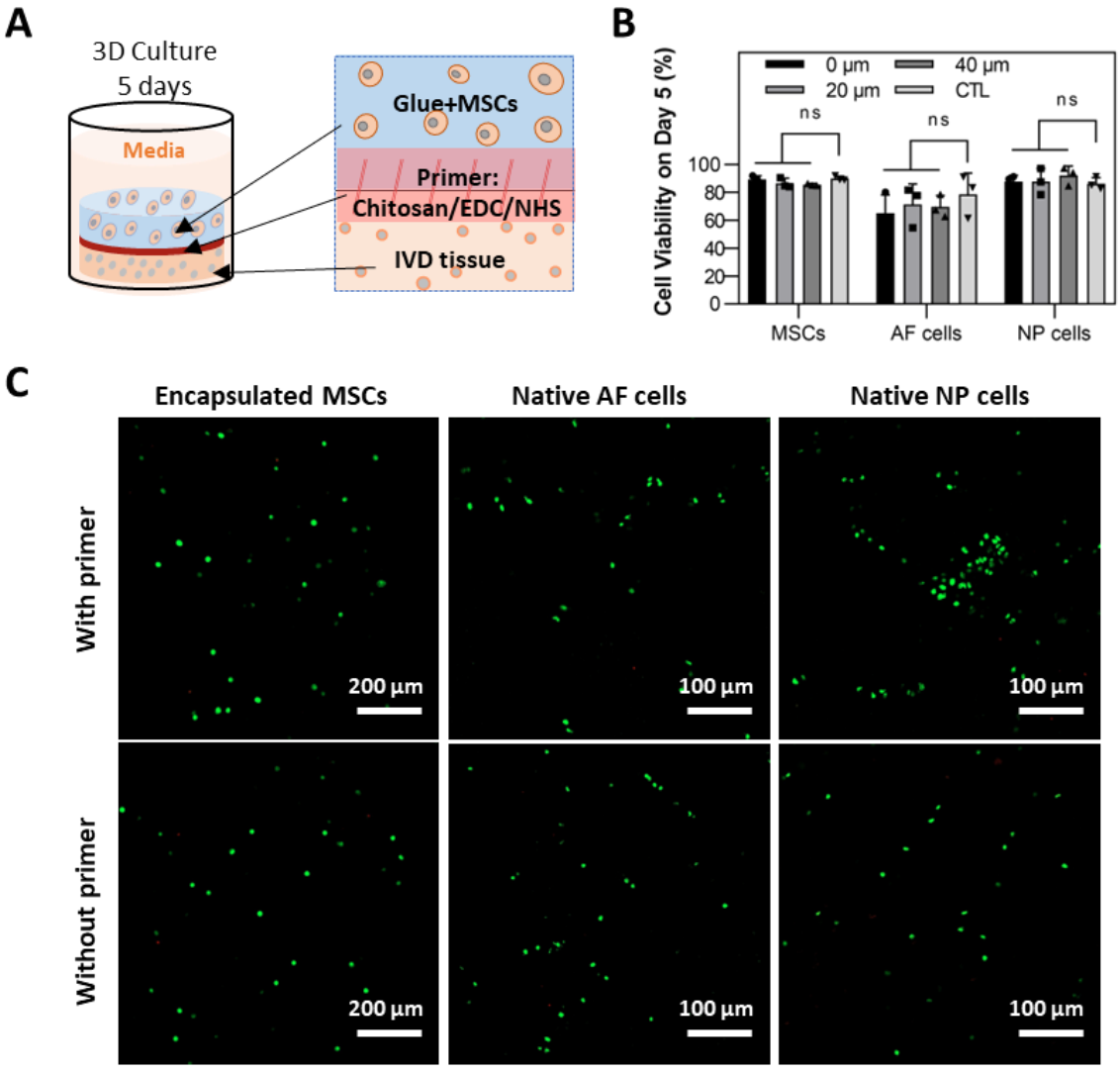

Figure 4.15 3D cytocompatibility test of NP glue. A. 3D culture of cell-laden glues on human IVD tissues. B. Viability of MSCs encapsulated in the glue or IVD cells in native tissues on day 5. C. Confocal imaging

of Live/Dead assay of MSCs in NP glue. $P > 0.05$ for ns by one-way ANOVA tests compared with control (CTL)CTL group.

4.6 Regenerative capacity with delivered cells

To further demonstrate the regenerative capacity of our bioadhesives, the mechanics of the NP glue were fine-tuned to promote the activities of encapsulated cells. The feasibility of this approach is attributed to the design of the NP glue, decoupling the hydrogel matrix, and the adhesion primer spatially confined at the interface. To this end, the focus was the viscoelasticity of the NP glue, motivated by the recent works showing a viscoelastic matrix upregulates the matrix deposition of chondrocytes.[52,269] Given the viscoelasticity of the native NP, it was hypothesized that engineering the viscoelastic properties of NP glue could promote the activities and function of NP cells.

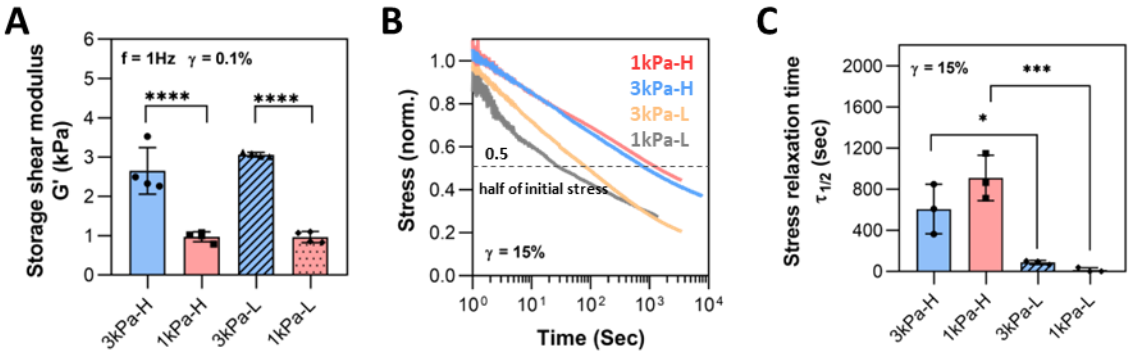

Figure 4.16 Viscoelasticity of NP glue is characterized by rheology tests. The storage shear modulus, stress relaxation pattern, and the stress relaxation time are shown in (A), (B), and (C). ($n \geq 3$, ****$P < 0.0001$, *** $P < 0.001$, and *$P < 0.05$ by one-way ANOVA tests).

To vary the viscoelasticity of the hydrogel, the MW of alginate and the input of calcium crosslinkers were both tuned. Two levels of storage modulus at 1 kPa and 3 kPa were obtained and which were measured with rheological tests (**Figure 4.16A**). Note that the stiffness is within the range of non-degenerated human NP.[68] For the same storage modulus, the deployment of low-Mw alginate can substantially expedite the stress relaxation (**Figure 4.16B**). The time to relax half of the peak stress, $t_{1/2}$, reflects the viscoelastic property of the matrix (**Figure 4.16C**). Compared to the high Mw condition (~900 s), the stress relaxation time (~10 s) of the NP glue containing low Mw alginate is closer to that of human NP tissues (~1 s).[68,270] To further reduce the relaxation time to match with NP tissues, reported strategies include conjugating alginate with PEG.[52] The series of hydrogels were used to culture human primary NP cells for 21 days.

Viability assays confirmed high viability of the primary NP cells within the hydrogels with different viscoelastic properties throughout the extended culture period (**Figure 4.17A-B**). To further reveal the activity and function of encapsulated NP cells, their metabolic activity and matrix deposition were characterized as a function of the viscoelastic properties of the NP glue. As collagen type II and aggrecan are the characteristic components of the NP environment, their production by the encapsulated cells is the key indicator of the regenerative potential of the hybrid bioadhesives. These results imply that the viscoelasticity (stress relaxing property) prevails the shear modulus in upregulating the metabolism and matrix deposition. This effect is significant on Day 7, when the metabolic levels of the Low-Mw conditions exceed those of High-Mw conditions (**Figure 4.17C**).

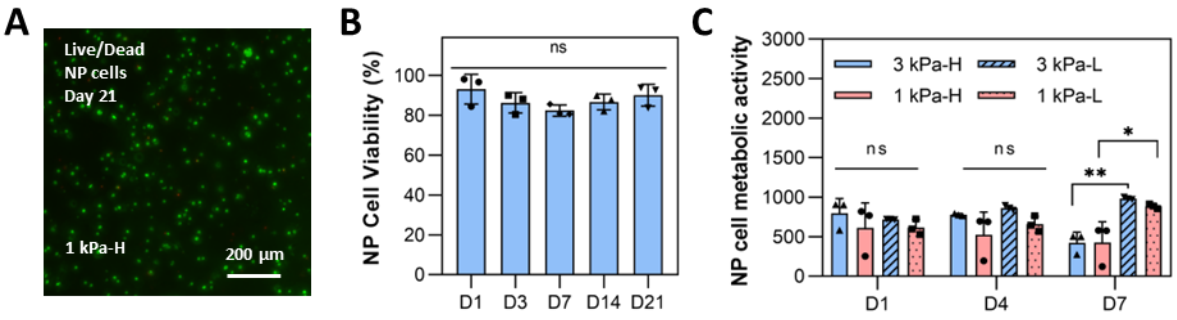

Figure 4.17 Viability and metabolic activity evaluation of NP glue. NP glues were shown to fully support the viability (A and B) and metabolic activity (C) of human primary NP cells ($P > 0.05$ for ns, $^{**}P < 0.01$, and $^{*}P < 0.05$ by two-way ANOVA tests).

Confocal imaging reveals the deposition of collagen type II and aggrecan by the encapsulated cells on Day 21 (**Figure 4.18A**). The cells within the NP glue remain circular, similar to the native NP cells. To quantify the aggrecan production, the DMMB assay was performed to measure sGAG, the main subcomponent of aggrecan in NP,[259] present within the glue and in the culture medium (**Figure 4.18B**). Interestingly, under at Low-Mw conditions (1kPa or 3kPa), the most of sGAGs were detected from the culture medium but not in the hydrogel. This may be because the lower-Mw alginate builds up a relatively loose polymer network with large meshes; so that the sGAG secreted from cells leaks through the network into the medium. The ECM release to the medium is attributed to the in vitro culture (no constraint) and possibly the fact that the sGAG is smaller than the mesh of the hydrogel network. The retention of sGAG is favored in NP cavity due to the containment of the surrounding tissues in vivo, the limited mass exchange,[271,272] and the electrostatic interaction between the chitosan-based adhesion primer and the negatively charged

sGAG.[273] After considering the total sGAG amounts from both the NP glue and the culture medium, it was found that the fast-relaxing NP glues (1 kPa or 3 kPa hydrogel composed of lower Mw alginate) led to more sGAG production than the slow-relaxing counterparts (**Figure 4.18B**). The finding is consistent with the prior work with chondrocytes.[52,269] This study showcases the feasibility and efficacy of finely tuning the hydrogel mechanics, decoupled from the bioadhesion consideration, to promote cellular activities for IVD regeneration.

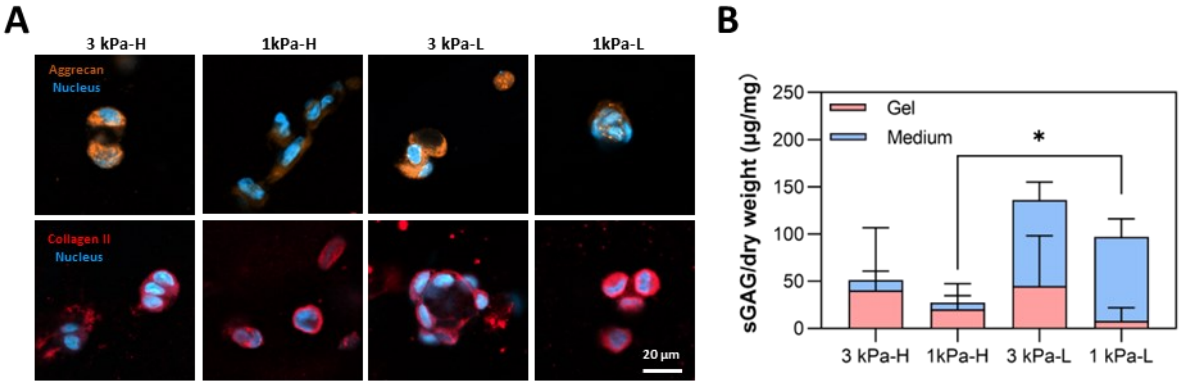

Figure 4.18 Matrix deposition of primary NP cells in NP glue. The matrix deposition in 21 days is detected by the immunostaining images (A) and the sGAG content in gel or in the media is quantified using DMMB assay (B) (*P < 0.05 by T-tests).

4.7 Preliminary ex vivo validation on human disc model under bioreactor

Further study with ex vivo whole human disc culture with bioreactors deserves exploration to fully recapitulate the biomechanical loading characteristic of humans for further clinical translation purposes.[244,274,275] Based on this purpose, a preliminary experiment of *ex vivo* culture of living human IVD model was included. The IVD repaired with the hybrid bioadhesives was cultured in a bioreactor that had been previously developed.[274,275] Previous experiments were conducted on bovine IVDs. Before starting the bioreactor culture, a preliminary mechanical loading on frozen human IVD with nucleotomy and repaired was conducted to confirm that the hybrid bioadhesives are capable of preventing herniation under physiological cyclic compressive loading range (0.1MPa – 0.5MPa, 0.1Hz, 20 cycles). The mechanical loading results show that the repaired group sustained the physiological loading without NP/implant extrusion, while the NP tissue was extruded out from the AF defect of the non-repaired group in the first loading cycle (**Figure 4.19A**). The raw data of force and displacement also indicated that the non-repaired group was extruded, reflected by the disturbing the curve in the first cycle (**Figure 4.19B**).

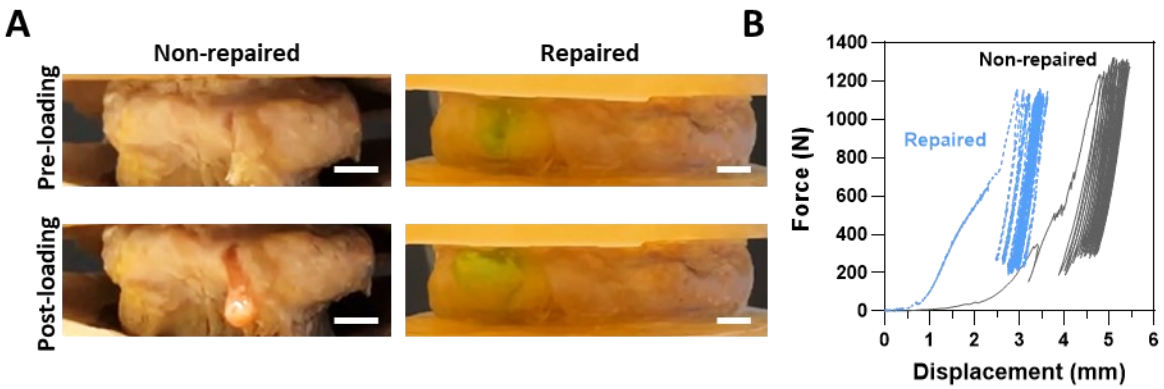

Figure 4.19 Compressive cyclic loading test on human IVD repaired with hybrid bioadhesives. Digital images of repaired and non-repaired human IVDs under compressive loading (A) (scale bar = 5 mm) and the raw data of force-displacement curve (B).

Next, a preliminary experiment of *ex vivo* culture of living human IVD model was included. The IVD repaired with the hybrid bioadhesives was cultured in a bioreactor that had been previously developed.[274,275] After nucleotomy on the IVD, The IVD sample was repaired with Glue+Patch bioadhesives before loaded on the bioreactor (**Figure 4.20A**). **Figure 4.20B** shows the setup of the culture chamber in the bioreactor with culture medium. At the end point of the culture, the medium was removed from the culture chamber (**Figure 4.20C**). After culture for 28 days in the bioreactor under physiological compressive loadings, no herniation was detected, and the AF patch still adhered to the defect sites (**Figure 4.20D**).

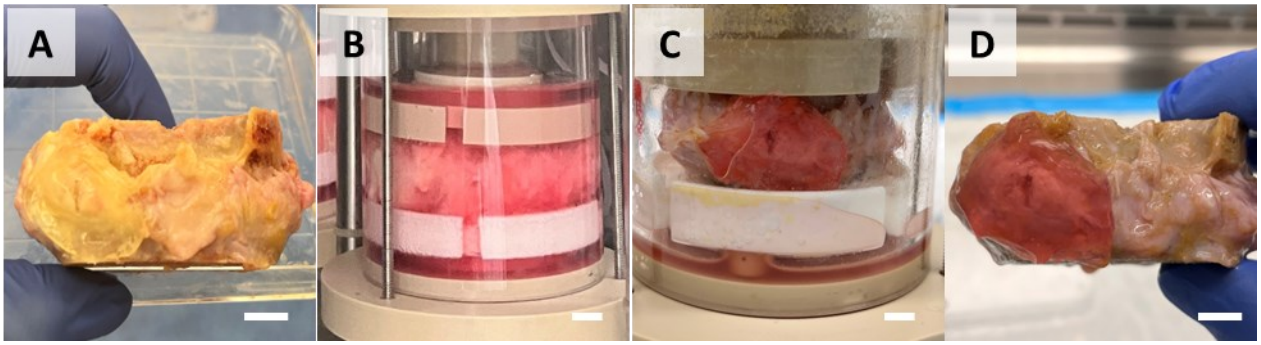

Figure 4.20 Digital images of the bioreactor setup for evaluating bioadhesives on human IVD. The process involved initial repair of the disc using hybrid bioadhesives post-nucleotomy (A), followed by a four-week culture in the bioreactor under cyclic compressive loading simulating physiological conditions (B-C). Notably, no glue extrusion or patch detachment occurred at the conclusion of the culture period (D).

The loading data was recorded, and the representative loading pattern of stress and displacement was shown in **Figure 4.21A-B**. During the ex vivo culture, no extrusion or detachment

of bioadhesives was observed in the purifying medium and dynamic loading environment. The biomechanical parameters of the stiffness (**Figure 4.21C**), range of motion (**Figure 4.21D**), and dissipated energy (**Figure 4.21E**) were extracted from the dynamic loading for each day. These values indicate that the repaired IVD can withstand a load that simulates human physiological conditions for 4 weeks and maintains relatively stable mechanical properties.

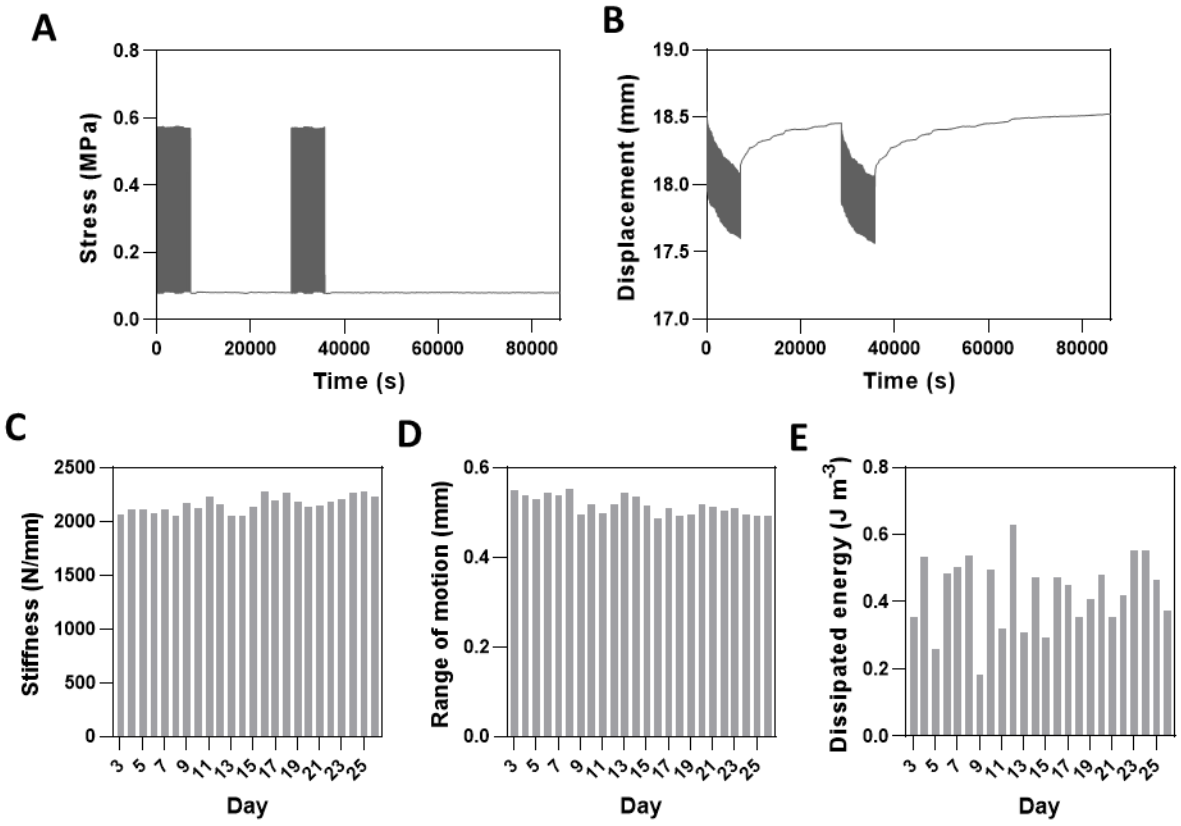

Figure 4.21 Biomechanical evaluation of bioadhesives on human IVD ex vivo model in bioreactor. Representative loading pattern of stress (A) and displacement (B). Biomechanical parameters of the stiffness (C), range of motion (D), and dissipated energy (E) are extracted from the dynamic loading for each day.

To evaluate tissue regeneration ability, pre- and post-culture MRI imaging was performed. Normalized T1ρ intensity, an indicator of regeneration in terms of hydration and proteoglycan content, in the NP region was increased by 1.58-fold following the culture in the repaired discs compared with their respective pre-culture data (**Figure 4.22**). The results from the ex vivo human IVD model proved the excellent efficacy of our bioadhesive system for IVD repair and regeneration. Further validation using other pre-clinical models and clinical trials is underway. We envision the

proposed material system will synergize the bioadhesive and tissue-engineering approaches to better repair IVD and can motivate the design of implants for repairing a broader range of tissues.

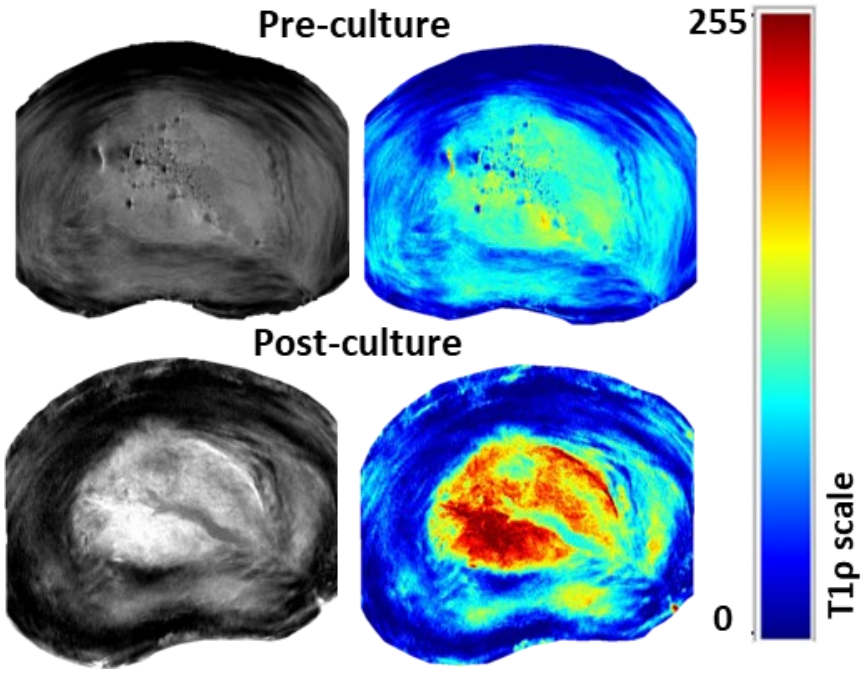

Figure 4.22 MRI imaging of disc pre- and post- culture. The T1ρ scale represent the level of hydration which indicate the regeneration.

To sum up, I developed a hybrid bioadhesive for IVD repair and regeneration and examined their adhesion to IVD tissue and subsequent biomechanical properties. Modified lap-shear tests evaluated the adhesion of the bioadhesives to different IVD substrates and showed a significant increase in adhesion with the use of an adhesion primer. The adhesive primer enhanced the adhesion strength and energy. Biomechanical testing under physiologic loading confirmed that the repaired discs were similar to intact discs, mitigated re-herniation and restored viscoelastic properties. Failure compression testing showed that the bioadhesive-treated discs had enhanced failure strengths that approached intact levels. Notably, the AF sealant successfully prevented permanent extrusion under extreme loading, contributing to herniation recovery. Besides, this study demonstrated the cytocompatibility and regenerative potential of the bioadhesive, demonstrating its ability to support cell viability, metabolic activity, and matrix deposition. The preliminary experiments on human IVD bioreactor demonstrated the potential of clinical transformation of these strategy for repair and regeneration IVD tissues. The reported material exemplifies the synergy of bioadhesive and tissue-engineering strategies and the potential of tissue-mimetic bioadhesives. This

work is expected to open new possibilities in bioadhesives, regenerative medicine, mechanobiology, cartilage repair, wound management, and beyond.

Chapter 5
Composite Hydrogel Sealant for AF Repair

Despite the validated efficacy of the hybrid bioadhesive strategy in preventing post-nucleotomy disc protrusion under physiological compression, bulging of the annulus fibrosus (AF) patch was observed during cyclic loading and compressive failure tests though remained adhered to the disc. Although the extent of the deformation was far below the stretch limit of the hydrogels, it still posed risk to unexpected disc protrusion under extreme compressions. This large deformation of the AF patch was hypothesized to stem from the low modulus of the hydrogel implemented in the current strategy compared to native AF tissues. To this end, this chapter aims to further improve the bioadhesive strategy with emphasis on enhancing the mechanical performances of the AF patches. A composite design featuring a thermoplastic polyurethane (TPU) mesh-reinforced hydrogel patch is developed to enhance the mechanical robustness of the bioadhesive sealant. Attributes pertaining to the fiber angle and volume fraction of the TPU mesh design is tailored to match the mechanical performances of native AF. To validate the design, tensile modulus, flexural modulus, and fracture toughness of the TPU mesh-reinforced AF patch are characterized. To ensure secure sealing of the optimized composite bioadhesive, the adhesion performance of the composite sealant to AF tissues is evaluated. With the established TPU mesh design and validated adhesion performance, we innovate the bulk geometrical design of the composite bioadhesive sealant is innovated, and their adhesion performance and biomechanical recovery behavior in-situ within an IVD model are investigated.

5.1 Composite hydrogel sealant design

Hydrogel AF sealant require further refinement to mimic the tissue specific structure and match the mechanical properties of natural AF tissue. Native AF has a complex structure and is a layered fibrocartilaginous tissue composed of 15 – 25 concentric rings or layers with a pattern of highly oriented, parallel type I collagen fiber bundles oriented 30° – 45° to the vertical axis angular arrangement, and the angles of fiber bundles in successive layers are opposite (**Figure 5.1A**).[276] This unique structure allows the AF to withstand greater loads under physiological loads.

In order to achieve the design principle of recapturing the special hierarchical angle-ply structure of AF tissue, we propose to introduce 3D-printed multilayer mesh material to simulate the directional fiber in AF, compositing hydrogel bioadhesives as mesh-reinforced AF sealant. 3D-printed mesh is designed with the same angle as the native AF fiber, that is, 30° from the disc axis (**Figure 5.1B**). 60° mesh will be used as a control in the subsequent mechanical validation. Here, TPU has been selected as the meshing material integrated into the current composite bioadhesive design, due to its elasticity, adjustable physicochemical properties, and compatibility with polymer.[277,278]

Another design principle is to match the mechanical properties of the AF tissue. Theoretically, the composite's stiffness increases with a higher volume fraction of TPU. Hence, the optimization of volume fraction (V_{TPU}) of TPU will be performed to achieve the desired modulus (**Figure 5.1C**). Importantly, the anisotropy of the AF tissue can result in different tensile behaviours observed from different angles when performing tensile tests. Study indicates that the moduli for human AF tissue along the radial, axial, and circumferential directions were reported to be 0.14 ± 0.05 MPa, 0.42 ± 0.11 MPa, and 2.70 ± 2.33 MPa, respectively.[279] The TPU mesh design specifically incorporates TPU fibers aligned at 30°, mimicking the collagen fiber configuration present in the circumferential direction of AF tissue. Therefore, the benchmark for mechanical properties relies on the AF tensile modulus tested specifically along the circumferential direction.

In this design, the 3D-printed multilayer TPU mesh with the original alginate-polyacrylamide hydrogel is investigated. Several key outcomes are anticipated: (1) Structurally, the multilayer mesh with directional alignment aims to replicate the complex architecture of natural AF. (2) Mechanically, the mesh-reinforced sealant enhances the modulus, and the optimization of TPU fraction is expected to achieve the desired mechanical properties, including tensile modulus, flexural modulus, and fracture toughness. (3) The presence of the hydrogel fraction is intended to maintain strong adhesion at the tissue interface. This biomimetic mesh-reinforced composite sealant could potentially mitigate implant deformation and address re-herniation issues associated with post-nucleotomy.

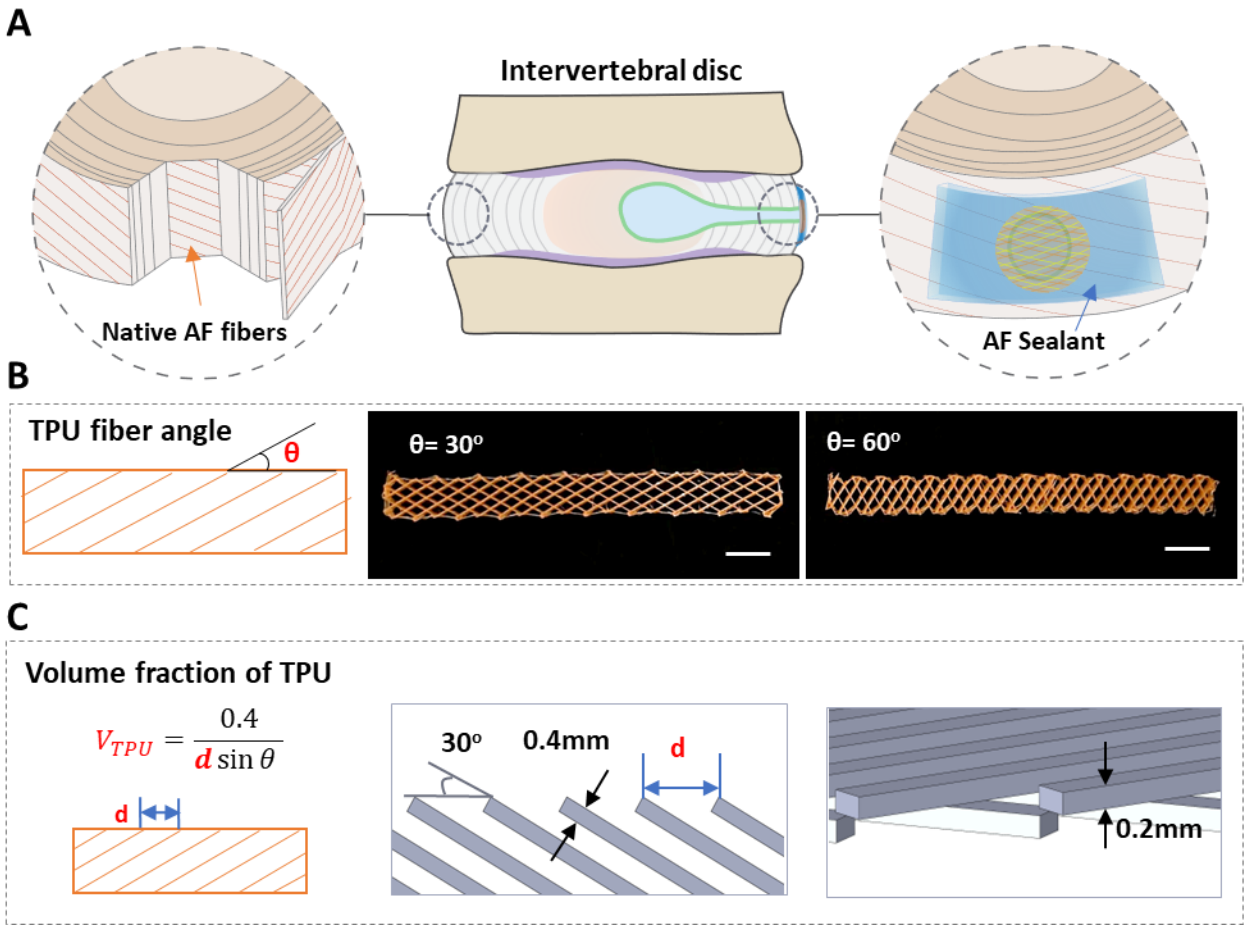

Figure 5.1 Schematic of composite hydrogel bioadhesive application and design. A. Illustration of the composite hydrogel bioadhesive for repair AF defects shows a fiber angle-layer structure similar to native AF. B. TPU fiber angle design and the representative 3D-printed TPU mesh (scale bar = 10 mm). C. Illustration of the TPU volume fraction design shows the TPU fiber dimensions design of 40% volume fraction from CAD drawing.

5.2 TPU mesh optimization

The optimization process for the TPU mesh of the composite sealant drew inspiration from the collagen fiber alignment of the AF, specifically focusing on a 30° angle in the circumferential direction. To validate the impact of this angle on enhancing the tensile modulus of the composite sealant, a control group featuring a 60° TPU alignment was established, mimicking the axial direction of the AF's fiber structure and standing perpendicular to the circumferential orientation. The evaluation of the tensile response involved pure TPU samples corresponding to both 30° and 60° alignments, with a TPU volume fraction set at 100%. **Figure 5.2A** illustrates the representative tissue-strain curves of 30°-100% and 60°-100% groups. The findings reveal a substantial difference

in the tested tensile modulus, indicating a significantly higher modulus for the 100% TPU sample aligned at 30° compared to its 60° counterpart (**Figure 5.2B**). This confirms that not only does the 30° TPU mesh replicate the AF's structure, but it also augments the material's modulus. Further exploration involved testing composite hydrogel sealants, with one set having 20% volume fraction with alignment at 30° and another 23% volume fraction with alignment at 60°. The data obtained show a significant difference in modulus, with the former being significantly higher than the latter. This demonstrates that even with a smaller TPU volume fraction, the 30° TPU composite sealant surpasses its 60° counterpart in terms of modulus. This reaffirms that the 30° alignment stands as the optimal angle, elevating the modulus of the composite hydrogel sealant design. In addition, the results for tensile strength do not differ significantly between the 30° and 60° groups (**Figure 5.2C**). This implies that the angle of the TPU has no significant effect on tensile strength of composite sealant.

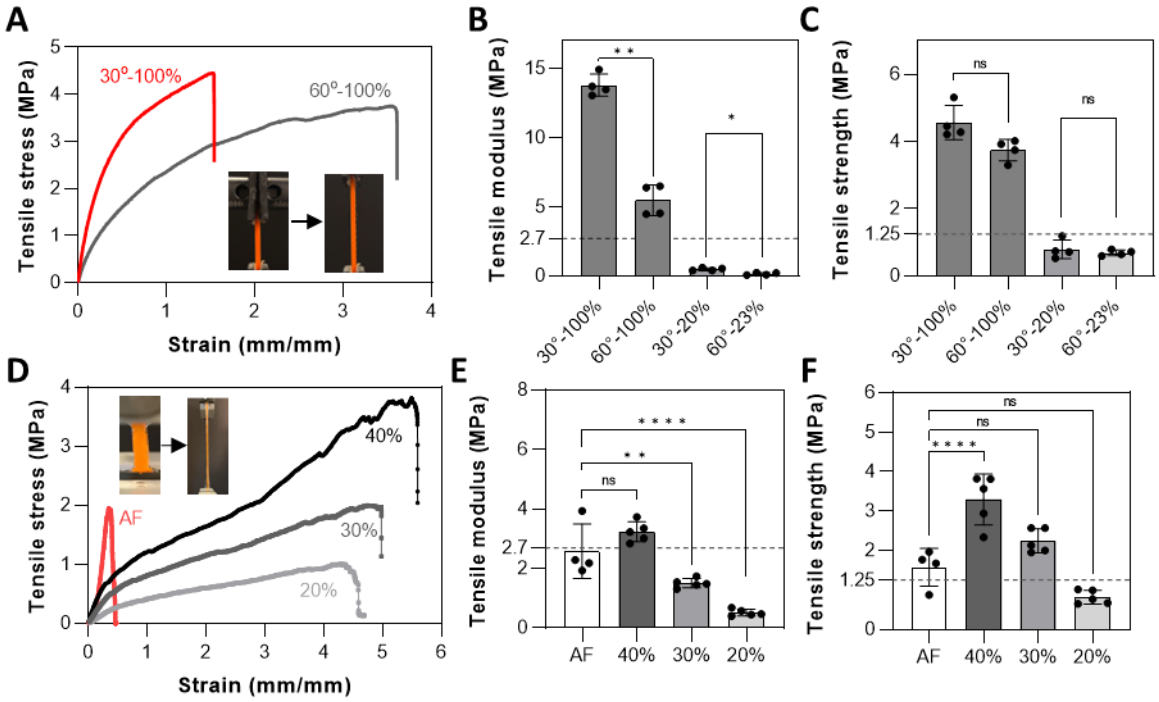

Figure 5.2 Tensile test of composite hydrogel with TPU angle and volume fraction optimization. A. Representative stress-strain curve of composite hydrogel with 30° and 60° TPU. The tensile modulus (B) and strength (C) of the TPU-composite hydrogel with different angles (n = 4, ** $P < 0.01$, *$P < 0.05$, and $P > 0.05$ for ns by T-tests). D. Representative stress-strain curve of human AF tissue in circumferential direction and the 30-degree TPU composite hydrogel with volume fraction of 20%, 30%, and 40%. The tensile

modulus (E) and strength (F) of the AF tissue and composite hydrogel with different volume fraction ($n \geqslant 4$, ****$P < 0.0001$, **$P < 0.01$, and $P > 0.05$ for ns, compared to AF group by one-way ANOVA tests).

Furthermore, to match the tensile behaviour of native human AF tissue, the tensile modulus and strength of composite hydrogels with TPU volume fractions of 20%, 30%, and 40% were measured via a tensile test. The tensile test of human AF tissue in circumferential of disc was also included as a benchmark for comparison. **Figure 5.2D** shows representative stress-strain curves for composite hydrogel sealant and human AF. The results showed that all composite hydrogels were able to withstand strains much higher than the target tissue. Examining the small-strain responses, we found the 30 ^{o} TPU composite hydrogel at 40% volume (3.24 ± 0.35 MPa) nearly matches the AF tissue (2.59 ± 0.92 MPa) in terms of tensile modulus (**Figure 5.2E**). The composite hydrogel became more compliant with decreasing TPU volume fraction, with the modulus of 1.51 ± 0.16 MPa for 30% and 0.52 ± 0.12 MPa for 20%. A similar trend was also observed in tensile strength measurements (**Figure 5.2F**). Notably, the 40% TPU volume exhibits the highest failure strength (3.29 ± 0.65 MPa) among the tested groups, surpassing even the strength of AF tissue (1.57 ± 0.49 MPa). The AF tensile modulus and the tensile strength measured in these experiments are close to the data reported in the previous literature, thus verifying the accuracy of these experiments. The dashed lines in **Figure 5.2E** and **Figure 5.2F** represent the tensile modulus (2.7 MPa) and strength (1.25 MPa) of circumferential AF reported in the literature.[279,280]

The overall tensile test results show that the composite hydrogel of TPU with 30^{o} and 40% volume fraction can meet the requirements of modulus and strength at the same time. Therefore, this TPU mesh configuration will be used for subsequent mechanical testing and further geometric optimization.

5.3 Flexural modulus

Aside from tension, AF is subjected to other complex mechanical loadings. Under physiological disc loading conditions, the NP tissue is enclosed by and exerts hydrostatic pressures on the AF tissue, leading to a resultant bending load on the AF tissue. Similar loading is also expected by the composite hydrogel sealant after repair. To evaluate the resilience to such loadings, it is important to assess the flexural modulus of the composite hydrogel and compare it with native AF tissues. To assess the flexural modulus, 3-point bending tests were performed on both the composite hydrogel (30^{o} and 40%) and AF tissues for comparison (**Figure 5.3A**). As the tensile modulus of composite

hydrogel is close to that of AF, we also expect a good agreement in flexural modulus. Indeed, the flexural modulus of the composite hydrogel (1.97 ± 0.35 MPa) and human AF tissue (2.09 ± 1.38 MPa) demonstrated no significant differences, as shown in **Figure 5.3B**. The close match in flexural moduli suggests a mechanical equivalence in their bending behavior, assuring the mechanical robustness of the mesh-reinforced composite hydrogel design and the resemblance to recapitulate the native biomechanical function of AF. Notably, this work is the first to identify the significance of flexural modulus as a mechanical property index in the assessment of AF and AF repair materials. The measured values serve as a benchmark for future investigations on the mechanical response of AF tissues as well as designs and improvements of bioadhesives in disc repair.

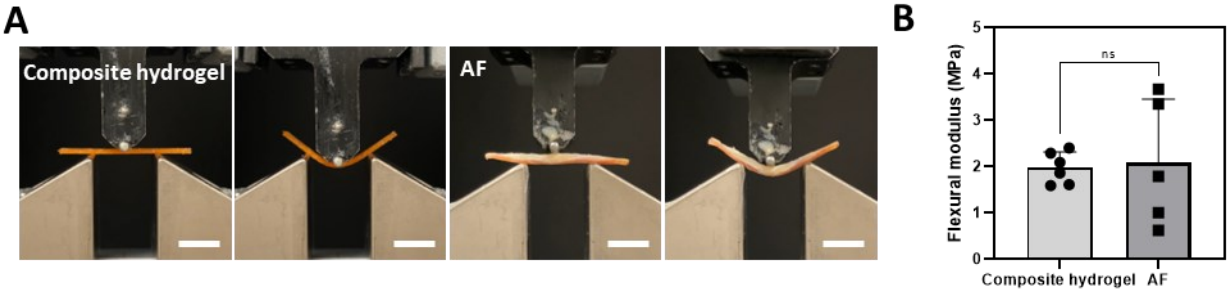

Figure 5.3 Flexural modulus assessment of composite hydrogel and AF via 3-point bending test. A. Visual representation of the 3-point bending test conducted on composite hydrogel and native human AF tissue (scale bar = 10 mm). B. Comparable flexural modulus values between composite hydrogel and AF tissue. ($n \geqslant 4$, $P > 0.05$ for ns by T-tests).

5.4 Fracture toughness

Degeneration of the IVD deteriorates the mechanical performances of the bulk AF tissues and creates fissures in them. The combination of these two factors undermines the load-bearing capability of AF against the exerted complex loadings and increases the risks of AF tearing. Tearing of AF aggravates the biomechanical function of the IVD and may lead to further complications such as disc herniation, spinal stenosis, and spondylolisthesis.[281] Therefore, to effectively repair damaged IVDs, it is crucial to design sealant that possess high resistance to crack extension, which can be quantified by fracture toughness.

Here, pure shear tests were performed to characterize the fracture toughness of the composite hydrogel. TPU meshes with optimized volume fraction of 40% with fiber orientation at 30° were implemented. As shown in **Figure 5.4A**, both notched and unnotched samples can be

stretched to more than 8.5 and 3.5 times their original length. During stretch, no delamination was observed between the stiff TPU mesh and the soft tough hydrogel matrix, underlining the successful merging of the two material constitutes. The high stretchability of the composite hydrogel far exceeds the deformation expected in native AF tissues under either physiological or pathological conditions, signifying the mechanical robustness of our composite hydrogel strategy. Thanks to the tough hydrogel matrix and TPU mesh design, the notched hydrogel composite sample successfully blunted the induced crack and exhibited extensive energy dissipation capability. To quantify this, **Figure 5.4B** displayed the stress-stretch characteristics of both the notched and the unnotched sample, and the fracture toughness was obtained. Remarkably, the composite hydrogel showed a high fracture toughness of 47.90 ± 1.60 kJ m^{-2}, demonstrating a 3-time enhancement compared to the tough hydrogel sealant in our previous design (~16 kJ m^{-2}).[282] Although no studies have reported the fracture toughness of human AF, to the best of the author's knowledge, some reported the fracture toughness of ovine AF tissue, ranging from 10 to 90 kJ m^{-2}.[283] The agreement of our results to the literature suggests the resemblance of fracture toughness of the hydrogel composite to that of AF tissue.

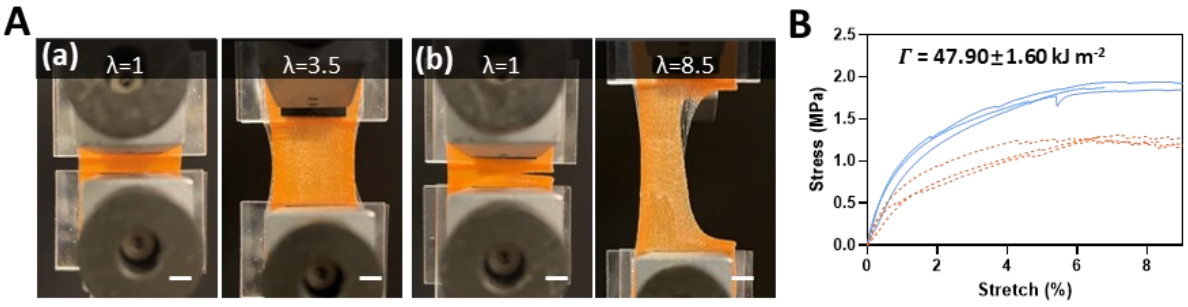

Figure 5.4 Fracture toughness evaluation in composite hydrogel via pure shear testing. A. Visual representation of the pure shear test conducted on unnotched (a) and notched (b) composite hydrogel samples (scale bar = 5 mm). B. Stress and stretch data from the pure shear test, yielding a fracture toughness value of 47.90±1.60 kJ m^{-2}. The solid blue line and dotted orange line represent the unnotched and notched sample respectively.

5.5 Adhesion performance

Although the adhesion surfaces of the improved hydrogel sealant remain unchanged, stiffening of the bulk material might undermine the adhesion performances of the sealants to the AF tissues. Modified lap shear tests were conducted on both composite hydrogel and non-composite hydrogel sealant to assess the adhesion performances (**Figure 5.5A**). As expected, the composite adhesive

exhibited lower adhesion strength (37.79 ± 4.04 kPa), compared to the non-composite counterpart (62.78 ± 18.24 kPa) (**Figure 5.5B**). However, as both sealants displayed cohesive failure in the tough hydrogel matrix, the adhesion energy was found to be comparable, with values of 0.92 ± 0.13 kJ m^{-2} for the composite hydrogel sealant and 1.0 ± 0.18 kJ m^{-2} for the non-composite group (**Figure 5.5C**). The results confirmed the adverse effect of a stiffened adhesive matrix on the adhesion strength performances. Due to the relatively low interfacial toughness between the stiff TPU mesh and the soft hydrogel matrix, the capacity of energy dissipation at the interface of the composite sealant and the AF tissues was dominated by the hydrogel matrix. As such, the resulting adhesion energy was independent of the inclusion of the TPU mesh, whereas the adhesion energy, showed similar values between the composite and non-composite groups. Nevertheless, the adhesion performances of the composite hydrogel were still high enough to ensure secure bonding of it to the AF tissues during repair.

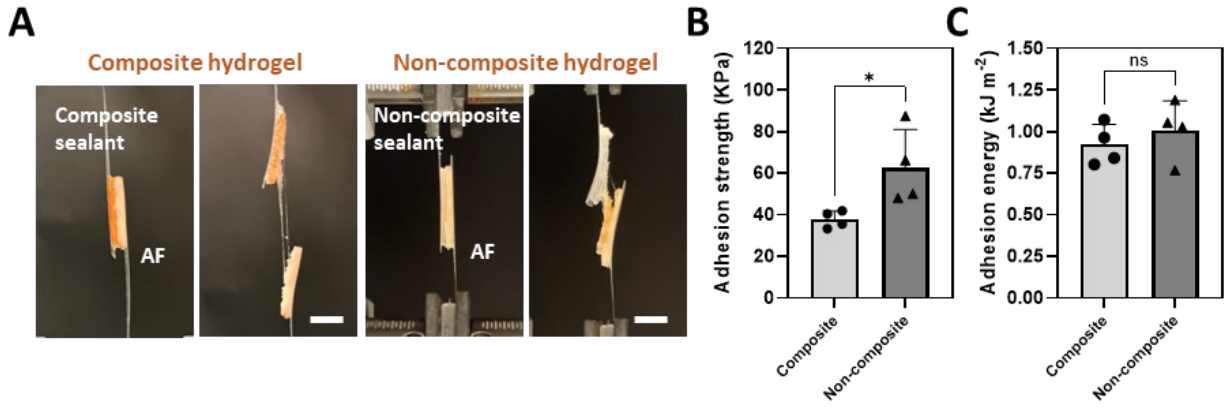

Figure 5.5 Adhesion tests of the composite hydrogel sealant. A. Lap-shear test images of composite or non-composite hydrogel sealant applied on human AF tissue (Scale bar = 10 mm). (B) and (C) show the adhesion strength and energy between both sealants on AF respectively (n ⩾ 4, *$p < 0.05$ and ns > 0.05, by T-tests).

5.6 Geometric design

Previous sections focus on optimizations of the material properties of the composite hydrogel by tailoring the TPU mesh designs. In this section, the composite sealant was further improved by through geometric design. Two design parameters were considered: the curvature of the bulk composite hydrogel and the shape of the embedded TPU mesh.

The curvature of the bulk composite hydrogel sealant was first modified. The overall cylindrical shape of the IVDs renders the curved outer AF surfaces. Adhesion of flat sealants to curved AF surfaces require application of excessive compression and pose risks for detachment due to the generated residual stress. The situation is more critical given the high flexural stiffness of TPU composite sealant compared to pure hydrogel sealants. Creating curved sealants with curvatures matching that of the AF could ease the adhesive placement process and minimize the residue stress at the interface afterwards. The curvature information of the human IVDs was obtained from MRI scanning, as presented in **Figure 5.6A**. Curvature of the posterolateral position in the IVDs was specifically chosen and measured due to its ubiquity for acute herniation [284]. Analysis of five human disc samples yielded an average radius of curvature of 12.74 ± 1.46 mm (Table 5.1). To this end, the curved composite hydrogel sealants were designed with a 13 mm radius of curvature.

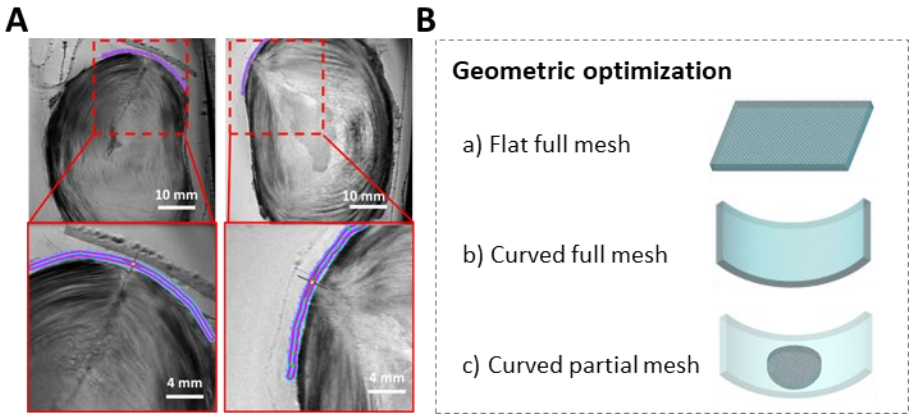

Figure 5.6 Geometric optimization of composite hydrogel bioadhesive. A. Human IVD curvature measurement from MRI scanning. B. Three designs of the composite hydrogel patch: a) flat with fully TPU filled; b) curved with fully TPU filled; c) curved with partially TPU filled.

Next, the overall size and shape of the embedded TPU mesh in the composite hydrogel sealant were refined. As studied in previous sections, despite the stiffness augmentation effect, the TPU mesh inevitably attenuated the adhesion strength of the composite hydrogel sealant to the AF tissues. It is hypothesized that a partial TPU mesh sealant could effectively enhance the stiffness at the targeted defect site while minimally diminish the adhesion performances. A design with a circular TPU mesh of 5-mm-diameter embedded at the center of the composite hydrogel sealant was embodied. The partial TPU mesh will be positioned to overlap and cover the AF defect created by the 3-mm-diameter biopsy punch. This “band-aid” design combines a portion of the TPU mesh

material to precisely match the size and shape of the AF defect, preventing the injected NP glue from causing excessive deformation on the sealant. In the meantime, the substantially reduced TPU mesh size renders the bulk composite hydrogel low stiffness that is comparable to the non-composite hydrogels, making it easy to apply on curved AF tissue and restoring tough and strong adhesions. With the established two design considerations, three patch designs results: a flat full-TPU-meshed patch, a curved full-TPU-meshed patch, and a curved partial-TPU-meshed patch (**Figure 5.6B**).

Table 5.1 Radius of curvature of the lateral-postural site of human IVD

Sample	Donor – level	Radius of curvature from MRI (mm)
1	Donor 1 L2L3	15.17
2	Donor 1 L4L5	13.48
3	Donor 2 T12L1	10.97
4	Donor 2 L1L2	11.97
5	Donor 2 L2L3	12.09

5.7 In-situ peeling adhesion evaluation

Next, an in-site peeling test was performed aiming at evaluating the adhesion performance of sealants with different design geometries on curved bovine IVD segments. The in-situ peeling setup recapitulated the adhesion scenario of the composite hydrogel sealant and took geometric factors of the adherends into consideration. The experiment results showed that the mean adhesion energy values for the three types of sealants were 274 ± 92 J m^{-2}, 161 ± 49 J m^{-2}, and 220 ± 70 J m^{-2} for the flat-full, curve-full, and curve-partial groups, respectively (**Figure 5.7B**). There was no statistically significant difference between the three groups, indicating that the geometry has less influence on the in-situ adhesion performance. The result could be attributed to the large variation among biomaterials, leading to the wide range of variation. In addition, due to the small number of samples tested, the results of statistical analysis did not present significant differences. A previous study using the same method tested in-situ peeling between non-composite hydrogel sealants and bovine IVDs, which resulted in the adhesion energy of 239 ± 49 J m^{-2}.[242] This is similar to the results of this thesis, especially for the curved partial sealant group, suggesting that all three designs are

capable of achieving high adhesion energies, thus ensuring the formation of secure AF repair on curved IVD surface.

To validate the geometric design, the adhesion performances of the proposed composite sealant on curved IVD tissue surfaces were investigated. To assess this, we performed an in-situ peeling test on bovine IVD segments. There was no significant difference in in-situ disc adhesion among the three groups, which was comparable to the results previously reported, indicating that the TPU-enhanced patch was still able to form a strong adhesion in-situ to the disc. This can be reasonably explained by the fact that the adhesion properties are mainly dependent on the covalent bonds formed between the hydrogel and the tissue surface, and the TPU does not have a dominant effect on the in-situ adhesion property.

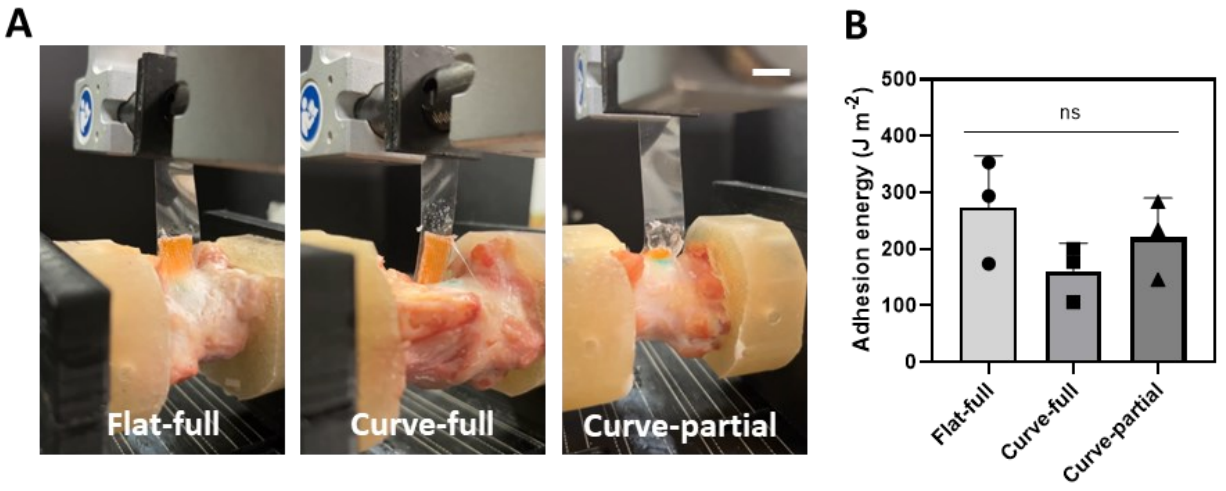

Figure 5.7 In-situ peeling test for assessing the adhesion of composite hydrogel sealants. A. Images depicting the in-situ peeling test assessing the adhesion of TPU-gel patches on bovine IVD tissue. B. The tested adhesion energy results. Scale bar = 10 mm. n = 3, P > 0.05 for ns by one-way ANOVA tests.

5.8 Biomechanical recovery assessment

To further evaluate the efficacy of the geometric design of the composite hydrogel sealants, axial cyclic loading tests were performed on bovine IVD motion segments after repair using the same method as described in Chapter 4 (**Figure 4.8**). Biomechanical parameters, such as ROM, NZ length, and NZ stiffness were extracted from the force and displacement data and used to assess the performances of the sealants (**Figure 5.8A**). Firstly, the ROM result showed that three repaired groups had no significant difference with intact control, while the defect control (negative control) had significant difference with intact control (**Figure 5.8B**). This suggests that the repaired strategy

with the composite hydrogel sealants is better at restoring the ROM of the disc compared to the defect group. Next, similar results can be found in the NZ length (**Figure 5.8C**), where three repaired groups showed comparable with the intact group. Within these three repaired groups, the curve-part-TPU sealant group notably stands out, displaying significant differences compared to the defect control. This result suggests an improvement can be achieved with the curved and partially TPU-designed approach. Lastly, the NZ stiffness of the flat-full-TPU sealant and curve-part-TPU sealant are compared to intact group indicating the recovery in these two types of designs (**Figure 5.8D**). However, the curve-full group did not restore the NZ stiffness and showed a significant difference compared to the intact control.

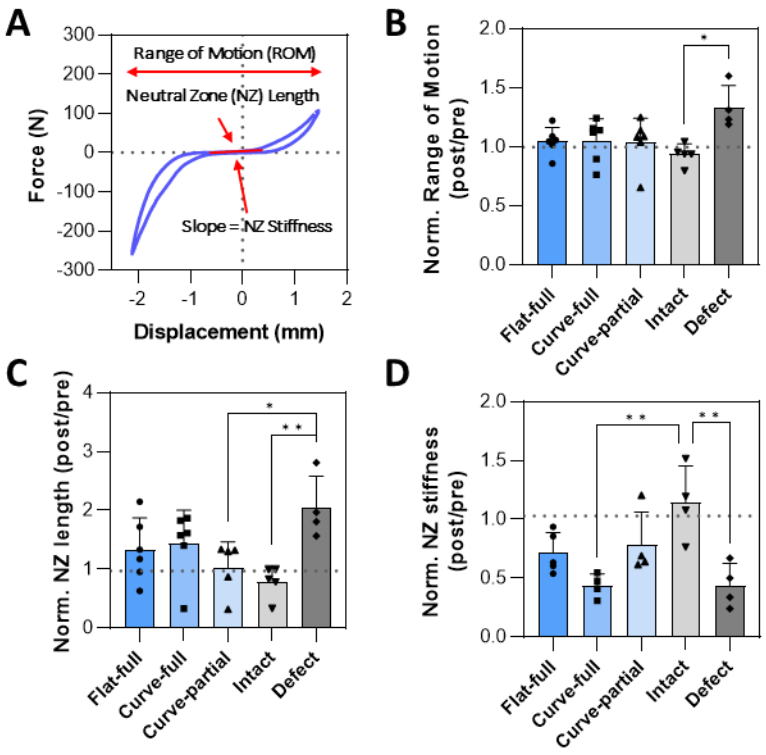

Figure 5.8 Biomechanical assessment on bovine IVD after repaired with composite hydrogel sealant. Biomechanical assessment on bovine IVD after repaired with patches were performed and the parameters were extracted from the cyclic loading curves (A), including range of motion (B), NZ length (C) and stiffness (D). The dashed lines are the results of the non-composite hydrogel patch group from Chapter 4, are 1.03, 0.97, and 0.99 respectively. n ≥ 4, **P < 0.01, *P < 0.05, and P > 0.05 for ns by one-way ANOVA tests.

Capacity to improve failure strength and prevent re-herniation was evaluated through the ramp-to-failure compressive loading test as described previously.[285] Representative curves of load and displacement were shown in **Figure 5.9A**, and the failure strength was recorded among the

groups (**Figure 5.9B**). Notably, the failure strength in the curve-partial group (9.80 ± 6.58 MPa) is the highest among the repaired groups with flat-full sealant (6.03 ± 5.59 MPa) and curve-full sealant (4.92 ± 4.36 MPa) and also far larger than the defect control (3.23 ± 2.07 MPa). Moreover, the curve-partial group does not show statistically difference from the intact control (22.19 ± 5.86 MPa). Images after the failure test show that the NP glue (blue color) was still present in the injected disc. The composite hydrogel AF sealant remained tightly adhered to the tissue, although in some area there was debonding leading to failure, as indicated by the red arrows in **Figure 5.9C**.

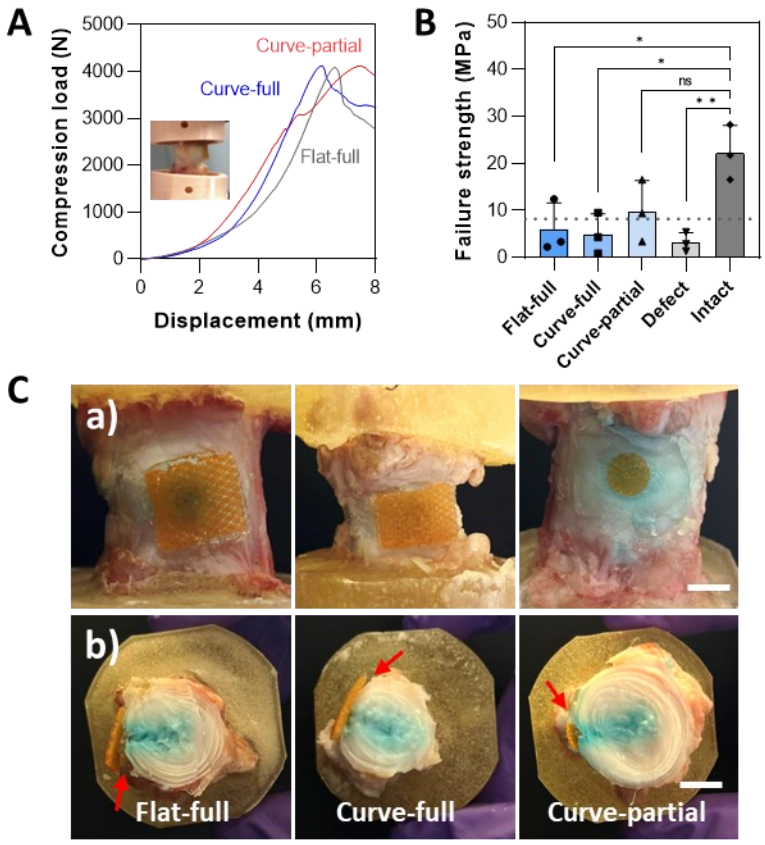

Figure 5.9 Failure strength of the bovine disc motion segments with repair of composite sealant under compressive loading. A. the representative raw data of load and displacement of 3 types of composite sealants. The curve-part design of the composite sealant presents higher failure strength than other groups (B). The curved-part group exceeds the failure strength of the non-composite hydrogel sealant (8.23 MPa). C. Images of the bovine disc after failure loading tests in the front view and the transversely cutting views (Scale bar = 5 mm). n ⩾ 4, **P < 0.01, *P < 0.05, and ns P > 0.05 by one-way ANOVA tests.

In summary, this work presents the development of composite hydrogel sealants for AF repair, focusing on their design refinement, TPU mesh optimization, mechanical properties, adhesion properties, geometrical enhancement, in-situ adhesion assessment, and biomechanical

recovery assessment. Through careful tuning of the TPU volume fraction and fiber angle, this study yielded a composite hydrogel sealant that closely resembles the natural AF structurally and mechanically, showing excellent fracture toughness and promising flexural modulus alignment. Despite a slight reduction in bond strength due to hardening, the composite exhibits comparable adhesive energy, ensuring a strong bond during the repair process. Geometric design innovations, including curved sealant and partial TPU mesh configurations, revealed the potential effectiveness of high adhesion energy and biomechanical restoration, addressing previous limitations and paving the way for more robust AF repair bioadhesive strategies.

Chapter 6
Discussions

This thesis proposed hydrogel bioadhesives strategies for intervertebral disc (IVD) repair. The strategies enable strong adhesion formation, recover biomechanical functions, deliver cells, and prevent re-herniation. They have expanded the material repertoire for IVD treatments and suggested the potential of clinical translation in the biomedical applications associated with load-bearing biological tissues. However, there remain a few limitations of the proposed technologies, which demand further optimization and improvement. These issues are discussed herein in the following categories: the development of tissue-mimetic hybrid bioadhesives, adhesion performance within IVD niche, biomechanical recovery performance, cytocompatibility and cell-delivery capacity, ex vivo validation for clinical translation, mesh-reinforced composite hydrogel sealant, and future works. This thesis provides essential proof of concept data supporting the use of regenerative bioadhesives with cell therapy for disc regeneration and repair.

6.1 Development of tissue-mimetic hybrid bioadhesives

This study developed and validated tissue-mimetic hybrid bioadhesives, which were customized for the repair and regeneration of IVD after nucleotomy. The hybrid bioadhesive consisted of an injectable alginate hydrogel for filling the nucleus pulposus (NP) and an alginate-polyacrylamide double network hydrogel for sealing the annulus fibrosus (AF). In previous studies, alginate hydrogels have been developed for NP repair by delivery of cells,[255,286] but in this thesis, this is the first time that the effect of viscoelasticity on encapsulated human NP cells has been investigated. These results offer a possibility to further enhance the regenerative capacity by fine-tuning the viscosity of hydrogel. Alginate-polyacrylamide double network hydrogels are known for their tough tissue adhesion and have been used for tendon and skin repair.[39,253] In this study, this material was used for the first time to repair IVD tissue, specifically targeting AF tissue. This adaptation extends the application of bioadhesives to IVD repair, expanding their potential in different medical fields. Different from previously reported bioadhesives, the developed material combines an injectable and cell-compatible NP glue and a pre-formed mechanically tough AF sealant. The former resembles the NP mechanically and biologically, allowing for delivering exogenous cells to fill and regenerate the NP cavity. The latter serves as a mechanically optimized barrier to seal the AF defects and secure

the NP glue in place, even under the stress of extreme mechanical loadings on the IVD. The synergy of the two components renders the hybrid bioadhesives with excellent biomechanical performance.

When studying the form factor of AF sealant, we found that the debonding and extrusion associated with the plug design, but not with the patch design. The phenomena can be attributed to the Poisson's effect under compression, that is, a substantial expansion in the transverse direction. In this regard, the patch attached to the AF wall is parallel with the loading direction and thus experiences much less mechanical loading (or energy release rate) to drive debonding between the bioadhesives and the IVD. Previous adhesive designs overlooked the heterogeneity of native AF and NP tissues, which resulted in inadequate recovery in biomechanical properties despite formation of relatively strong adhesion between the tissue and material.

This work exemplifies tissue-mimetic bioadhesives, accounting for the unique mechanics and repair needs for the IVD niche after nucleotomy. Specifically, this work is the first to demonstrate the applicability of the adhesion primer and hydrogels to different substructures of the IVD and benchmark the adhesion and sealing performance of these materials under physiological and extreme loading conditions relevant to IVD. The IVD-mimetic bioadhesive distinct from other bioadhesive systems designed for general surgical procedures and wound management. According to the unique structure of IVD, the needs for NP filling and AF sealing is decoupled. Essentially, the NP glue resembles the NP in viscoelasticity and cell compatibility; the AF sealant excels in adhesion and toughness. As such, the hybrid strategy simultaneously satisfies the requirements of repair and regeneration.

6.2 Adhesion performance within IVD niche

Regarding adhesion performance, hybrid bioadhesives function as designed within the IVD niche. The combination of NP glue plus AF sealant patch achieved the best repair outcomes in restoring biomechanics and avoiding re-herniation post-nucleotomy. The modified lap-shear tests using samples with and without pre-cracks characterized the adhesion strength and adhesion energy of NP glue and AF sealant on different regions of IVD, including NP, inner and outer AF. The comprehensive adhesion characterizations confirmed the effectiveness of the adhesion primer. The implementation of primer significantly enhanced adhesion performance of the NP glue (~ 4 kPa, Figure 4.6) compared to pristine alginate hydrogels in prior works and achieved strong adhesion of the hydrogel AF sealant with the AF (~ 62.78 kPa, Figure 5.5). Comparing these results with other

studies using bioadhesive hydrogels for AF repair, this approach yielded higher lap-shear adhesion strengths than riboflavin-crosslinked collagen,[287] FibGen,[288] and oxidized-methacrylate-modified GAG.[46] Although the modest adhesion energy of the NP glue is bound by the toughness of the alginate hydrogel matrix, the biomechanics studies and post-test examination confirmed the retention of NP glue within the NP cavity with the aid of the AF sealant. Since NP glue can carry cells into the NP cavity to promote regeneration, fixing NP glue at the injection site is of great significance for precise repair and resident cells of the target tissue. From this point of view, the adhesion achieved in this work can not only structurally repair the tissue, but also improve the therapeutic accuracy of delivered cells. It is worth noting that the full enclosure of the glue by the AF and the sealant mitigates the need to further toughen the NP glue for even higher mechanical performance; also, toughening the alginate hydrogel often involves toxic reagents and harsh reaction conditions. This is in accordance with the design principle of tissue-mimetic bioadhesives, considering the specific tissue environment.

6.3 Biomechanical performance

The repair outcome of hybrid bioadhesives was successfully validated with an ex vivo model using bovine spinal motion segments. Considering the accessibility and costs of collecting the human discs, we primarily used bovine discs to assess the repair performance of the hybrid bioadhesives strategy under physiological loading and extreme loading conditions. The ex vivo model demonstrated that the hybrid bioadhesive prevented re-herniation under axial cyclic loadings and partially restored the biomechanical parameters in the bovine disc model. Specifically, in the biomechanical evaluation results in section 4.3 (Figure 4.9B, C), the ROM and NZ length in the repair group reached values closer to those in the intact group (positive control). ROM represents the flexibility of the motion segment, describing the normal range of the motion segments. NZ length represents the region of displacement or deformation where the IVD exhibits a more elastic response, it also indicates the stability of the discs under loading. The recovery of those two key parameters implies that the applied adhesive repair fills the cavity and is anchored in the tissue through adhesive bonding compared to the defect group. Thus, the preservation of IVD integrity facilitates the restoration of typical motion behavior. This result highlights the critical role of AF sealant and its design in restoring IVD biomechanics.

The compression failure test showed that the Glue+Patch condition excelled among three repair conditions in terms of failure strength and herniation inhabitation. The other two conditions were found to have the NP (for Glue) and the AF sealant (for Glue+Plug) extruded from the AF defect, a phenomenon also reported in recent works.[46,289,290] Previous studies have proposed a two-part approach using biomaterials to repair AF after removal of the NP. An injectable interpenetrating network hydrogel and modified glycosaminoglycans were used to bond the hydrogel to the AF tissue. While this cell-compatible method showed improved tissue adhesion, testing on bovine discs with nucleotomy showed lower repair strength (~ 4 MPa) than the non-repaired group (~ 5 MPa),[46] suggesting its inferior effectiveness compared to current clinical standards. In this thesis, the repair of a bovine disc with the Glue+Patch strategy demonstrated compressive failure strength of 8.2 ± 4.7 MPa, exceeding previously reported values and was almost 3 times higher than that of the defect control group (3.2 ± 1.7 MPa). This is a significant advance in herniation prevention. However, although the Glue+Patch group was significantly better than the other repaired groups, its strength was still lower than intact IVD (22.2 ± 4.8 MPa). Addressing this challenge requires further studies in the future, such as further increasing the adhesion properties of materials and tissues.

6.4 Cytocompatibility and cell-delivery capacity

Regarding the cytocompatibility and cell-delivery capacity, the hybrid bioadhesives were shown to be biocompatible and bio-instructive via mechanotransduction. The 2D cell culture and 3D tissue were combined to demonstrate that the NP glue induced no cytotoxicity against native cells (NP and AF cells), as well as exogenous cells (NP cells and MSCs). Also, our study demonstrated that the encapsulated NP cells exhibited high viability and metabolic activities while depositing collagen (type II) and aggrecan. Importantly, we showed, for the first time, that the NP-mimetic viscoelastic condition (soft and fast stress relaxation) promoted the matrix deposition of encapsulated NP cells. These results substantiate the potential of cell-laden NP glue in regenerating NP tissues. To further augment ECM synthesis, one could leverage the delivery of GFs and other therapeutics, as well as functionalization with ligand proteins to regulate the phenotype of encapsulated NP cells or stem cells. For example, laminin ligands have been shown to promote the sGAG production of human NP cells.[291,292] For stem cells, other factors such as GFs and wnt5a mimetic ligands could be included in the NP glue to promote ECM production and to guide the differentiation toward NP phenotype.[293] The stem cell delivery capacity is an important attribute, as MSCs have been proven to mediate IVD repair and functional recovery in degenerate ovine IVDs.[294,295] Further combined

with scaffold, cell delivery MSCs-hydrogel delivery therapy has been widely studied in cartilage tissue repair.[296–298] Notably, the developed tissue-mimetic bioadhesives not only show the stem cell delivery capacity, but the strong local adhesion to the tissue surface also provides improved cell retention, which distinguishes from existing hydrogel scaffolds in the demanding environment of the IVD. This innovation can potentially improve IVD tissue engineering efficacy.

6.5 Ex vivo validation for clinical translation potential

Discs from large animal models have been widely used in ex vivo studies for investigating the biomechanics of NP/AF implants.[289,290] In this study, a bovine IVD ex vivo model was used to simulate a standard nucleotomy by forming a 3-mm biopsy punch in the AF and removing approximately 20% of the NP, similar to what had been observed clinically in severe herniation and aggressive nucleotomy.[247,299] The biomechanical damage formed in this model represented an AF defect, and the performance of the hybrid bioadhesive in this model highlighted its superior adhesive and biomechanical repair performances. However, animal models cannot fully mimic the biomechanical conditions of human lumbar IVD[261] due to their intrinsic discrepancies in disc size, geometry, biomechanical properties, composition, metabolism, and cells.[257,300,301] Therefore, it is worth exploring the use of bioreactors for the study of isolated whole human IVD cultures to fully mimic the biomechanical loading characteristics of humans for further use for clinical translational purposes.[244,274,275] With this purpose in mind, Section 5.8 incorporated preliminary experiments with ex vivo culture of living human IVD models. IVDs repaired with hybrid bioadhesives were cultured in a previously developed bioreactor. After 28 days of incubation under physiologic compressive loading, no protrusion was observed, and the AF patch remained adherent to the defect site. In addition, MRI evaluation showed an increase in T1ρ intensity in the NP region, suggesting a trend toward regeneration of the NP after repair with NP adhesive during incubation.

To develop hydrogel therapy, previous studies used injections of hydrogel and cells through a small needle.[302] The injected hydrogel filled cracks and fissures in the human IVD. Subsequent incubation in a bioreactor was observed to restore disc height and MRI results showed disc regeneration. However, these studies have a limited reflection of the nucleotomy situation because pinhole injections only create small AF defects with a low risk of reherniation. In contrast, standard treatment of severe degeneration actually leads to the formation of cavities within the disc, increasing the risk of reherniation. Thus, to fully simulate the situation of AF defects, our study is

the first to use an ex vivo model of human IVD nucleotomy. Over the 28-day incubation period, no significant fluctuations in the biomechanical properties of the ROM (~0.5 mm) and stiffness (~2000 N/mm) of the repaired disc segment were observed (Figure 4.21), demonstrating the high stability of the bioadhesive. In addition, the results were comparable to previously reported values of ROM (0.2 – 0.6 mm) and stiffness (1500 – 2000 N/mm) of human intact IVD under the same loading and incubation conditions.[302] The agreements of the biomechanical properties of the repaired and native discs further suggested the potential of the hybrid bioadhesive to repair the discs to their normal state.

6.6 Mesh-reinforced composite hydrogel sealant

Composite scaffolds have been used for AF repair in the literature. A previous study developed a composite scaffold resembling the AF structure, combining HA-based hydrogel and Poly (L-lactic acid) (PLLA) fibers via electrospinning. While promising for mimicking AF and aiding cell growth, its mechanical properties and adhesion performance remain unexplored for assessing AF repair.[303] Another study explored various approaches like FibGen, poly (trimethylene carbonate) (PTMC) scaffolds for cell delivery, and polyurethane membranes to prevent herniation. However, combining scaffolds with FibGen only partially restored biomechanics, and even reinforced with polyurethane membranes, it struggled to prevent herniation effectively.[246]

In Chapter 5, we developed a 3D-printed TPU-reinforced composite hydrogel sealant that not only achieved natural AF mechanical properties but also demonstrated superior adhesion performance and herniation prevention compared to previous composite repair strategies. The composite design differed from our initial design of the bioadhesive with pure hydrogel Glue+Patch. The enhanced composite sealants exhibit higher stiffness and strength, as also demonstrated in other applications of tissue-engineered biomaterials.[221,304] By incorporating a hydrogel with a 3D-printed scaffold mesh, the modulus of the composite material was significantly enhanced (3.24 ± 0.35 MPa), aligning closely with that of the AF tissue (2.59 ± 0.92 MPa). In the case of disc repairs, the enhanced patch demonstrated reduced deformation when subjected to pressure, reducing the risks of compressing the peripheral nerves and causing pain. Moreover, apart from the modulus improvement, the mesh-reinforced composite sealant exhibits a high fracture toughness (47.90 ± 1.60 kJ m^{-2}), surpassing that of the previous hydrogel sealant (~16 kJ m^{-2}) by 3 times.[282] Additionally, this fracture toughness aligns with values of AF reported in existing literature (10 to

90 kJ m^{-2}),[283] indicating that the developed composite sealant effectively attains a comparable level of fracture toughness to that of AF tissue.

The overall geometry of the composite hydrogel sealant played a significant role in the materials design. One main consideration was the curvature of the AF, since strong adhesion of the sealant necessitate conformal contact with the outer AF tissue, where the defect site resides. Additionally, the TPU-mesh distribution was also considered because the mesh-reinforced stiffer patch compromised adhesion properties. Therefore, a curved partial-TPU-mesh design was proposed in the study. Interestingly, the compression failure test showed promising results: curve-partial group achieving the highest levels of failure strength (9.80 ± 6.58 MPa) among others, a level statistically comparable to that of the intact group (22.19 ± 5.86 MPa). This is attributed to the strong adhesion maintained between the original hydrogel and the tissue in the surrounding part of the sealant patch, while the TPU reinforcement in the centre part provides sufficient stiffness support. This result shows that curved partial-TPU sealant can be a promising AF repair design that further improves the repair outcomes. A previous study using the same method tested in-situ peeling between non-composite hydrogel sealants and bovine IVDs, which resulted in the adhesion energy of 239 ± 49 J m^{-2}.[242] This is similar to the results of this thesis, especially for the curved partial sealant group (220 ± 70 J m^{-2}), suggesting that all three designs are capable of achieving high adhesion strengths, thus ensuring the formation of secure AF repair on curved IVD surface.

6.7 Limitations and future works

The regenerative bioadhesives developed in this study have demonstrated advances in restoring biomechanical function, preventing re-herniation, and supporting stem cell-driven regeneration. However, despite these encouraging outcomes, several limitations exist in the current work, prompting avenues for future research.

First the interactions between the NP glue and native cells remain unexplored. While the cytocompatibility study offered insights into cellular behavior, it fell short in elucidating endogenous cell recruitment and tissue remodeling processes. Addressing this gap necessitates focused research on mechanotransduction pathway study between these cells and the NP glue to facilitate a comprehensive understanding of their interplay. Second, a potential modification for the NP glue involves incorporating a macroporous structure. The current alginate hydrogel used for cell encapsulation has a polymer network with an average mesh size of less than 100 nm,[286] hindering cell growth and reducing tissue

formation. Introducing macropores (100 μm - 300 μm) within the hydrogel could alleviate these limitations by facilitating improved mass transport of nutrients and waste products, providing space for cell proliferation and migration, enabling ECM deposition, and enhancing cell attachment. Various methods have been developed to control structure/pore size and morphology in hydrogel scaffolds, including salt templating, gas forming, bicontinuous emulsion templating, cryogelation, electrospinning, and 3D printing.[80] To further refine the NP, another critical focus lies in studying its degradation kinetics to synchronize with tissue regeneration. It is pivotal to achieve an ideal degradation rate that can align with the formation of newly deposited ECM. Understanding and controlling this degradation-regeneration interplay will optimize the efficacy of NP glue in supporting integrated tissue regeneration.

Regarding the design of the mesh-reinforced composite hydrogel sealant, its limited TPU mesh pattern design and the evaluation using only 40% of the TPU volume ratio underscore areas for enhancement. Future research should explore diverse configurations for the 3D-printed mesh, including varying angles, shape, gap sizes, and diverse layouts. Employing finite element method studies can provide an in-depth understanding of the impact of TPU mesh variations on adhesion strength and the modulus of the composite sealant, allowing for optimization while maintaining optimal adhesion properties. Furthermore, the current design of the composite sealant overlooked regenerative functions. Subsequent investigations will focus on studying the effects of the composite hydrogel sealant on native cell behaviors and inflammatory response. The results would broaden understanding of how the patch interacts with and influences native cellular processes, thereby uncovering its regenerative potential.

The anatomical variations between human and bovine IVD segments are noteworthy, encompassing differences in size, shape, composition, as well as the distribution and density of cells, and collagen fiber arrangement, all impacting biomechanical properties and functional behavior. Additionally, functional dissimilarities arise from variations in biomechanical loading conditions and environmental factors. Human IVDs undergo unique mechanical stresses and loading patterns associated with upright posture and bipedal locomotion, contrasting with the loading conditions experienced by quadrupedal bovines, which can affect tissue adaptation, degenerative processes, and treatment responses. Consequently, when translating research findings between species, it is essential to recognize the limitations and challenges involved in extrapolating results from bovine IVD models to human conditions, despite the advantages such as availability, cost-effectiveness, and similarity in basic anatomy that bovine models offer.

Moving towards broader applications, future directions involve evaluating the performance of the bioadhesive strategy in more complex environments by utilizing animal models and human IVD ex vivo

cultures. In vivo studies with large animal models are crucial for understanding immune responses, degradation rates, regenerative potential, and herniation inhibition associated with the hybrid bioadhesives. Validating the integration of the developed NP glue and AF patch with neighboring tissues within these models stands significant. Although the use of rat tail IVD models presents a convenient and efficient starting point for implantation and analysis due to their accessibility,[221,303] more comprehensive studies using larger animal models such as ovine are still necessary.[216] These larger animals offer advantages in studying the size and loading conditions. Additionally, evaluating the long-term resilience of the developed bioadhesives against complex mechanical loading post-implantation is imperative for clinical translation. Furthermore, the expension of studies on a larger number of human IVDs in the bioreactor is critical for increasing confidence in conclusions drawn from human IVD culture experiments. This expansion will lead to more statistically validated observations, thus enhancing the reliability of clinical translation and potential application of the findings.

Chapter 7
Concluding Remarks

The research objectives outlined in this study have been successfully achieved. The outcome of this thesis advances the development and validation of regenerative bioadhesives for intervertebral disc (IVD) repair. Through meticulous material engineering and comprehensive functional validation, this study addressed critical challenges in developing biomaterials for enhanced IVD repair and regeneration.

The first objective of this thesis aimed to develop viscoelastic hydrogels specifically for nucleus pulposus (NP) regeneration. Fine-tuning of the alginate hydrogel successfully replicated the viscoelastic properties inherent in native NP tissue. Rheological characterization of these hydrogels revealed a notable decoupling between modulus and stress relaxation time. This critical distinction facilitated the creation of hydrogels that displayed stress relaxation behavior more closely resembling that of the native NP tissue. Encapsulation of human primary NP cells within these engineered hydrogel systems for 3D in vitro culture yielded promising results. Hydrogels exhibiting faster relaxation behavior showcased substantially higher metabolic activity. Additionally, immuno-staining and imaging techniques confirmed the secretion of key ECM components, specifically aggrecan and collagen II, within these hydrogels. Moreover, the engineered viscoelasticity of the NP glue significantly upregulated the deposition of sGAG, a vital marker for enhanced matrix production, thereby laying a solid foundation for improved NP regeneration. These outcomes underscore the intricate interplay between hydrogel viscoelasticity and cellular behavior, showcasing their pivotal role in enhancing the regenerative capacity of the NP tissue.

The second research objective was to develop a biomimetic adhesive strategy for AF repair. A composite hydrogel sealant featuring TPU meshes and the alginate-polyacrylamide tough hydrogel was developed. This work focused on optimizing the TPU mesh, enhancing mechanical and adhesion properties, and addressing AF defect through geometric innovations. Fine-tuning of the mesh volume fraction and fiber angles resulted in a composite hydrogel sealant with structural and mechanical properties that closely resembled those of natural AF. The mesh mimicked the angle-ply laminate structure of natural AF while matching the tensile modulus of AF tissue. The optimized composite hydrogel sealant exhibited fracture toughness and flexural modulus that was

comparable to those of AF. In addition, careful geometric designs, including curved sealant and partial TPU mesh configurations, revealed the potential effectiveness for higher adhesion energy and better biomechanical restoration. Our design addressed previous limitations and enlightened the design paths for more robust AF repair bioadhesive strategies.

The third objective focused on evaluating the efficacy of the hybrid bioadhesive strategy combining the developed NP glue and AF sealant. By filling the disc cavity with NP glue and sealing the defect with AF sealant, the hybrid bioadhesive could simultaneously repair and regenerate the disc. Biomechanical testing of bovine IVD motion segments showed that the hybrid bioadhesive achieved a significant enhancement in the ability to withstand loads compared to unrepaired specimens and successfully prevented extrusion of NP under physiologic stress. The efficacy of this hybrid bioadhesive strategy was further validated with a ex vivo organ culture study by incubating human IVD for 28 days under a dynamic loading bioreactor. The repaired disc was able to withstand physiologic loading for more than four weeks without herniation, as verified by the resulting stiffness, range of motion, and dissipated energy parameters. Furthermore, we validated the potential of the bioadhesion system in promoting disc regeneration through normalized T1ρ intensity analysis of MRI of the disc. These results confirm the effectiveness of our hybrid bioadhesive system in disc repair and regeneration.

The findings of this thesis advanced IVD repair and hold promises for translation into the clinic. The outcomes are expected to open new frontiers for the use of regenerative bioadhesives in enhancing IVD repair, provide a solid foundation for future research and innovation, and make broader impacts in regenerative medicine and tissue engineering.

Bibliography

[1] J. Hartvigsen, M. J. Hancock, A. Kongsted, Q. Louw, M. L. Ferreira, S. Genevay, D. Hoy, J. Karppinen, G. Pransky, J. Sieper, R. J. Smeets, M. Underwood, R. Buchbinder, D. Cherkin, N. E. Foster, C. G. Maher, M. van Tulder, J. R. Anema, R. Chou, S. P. Cohen, L. Menezes Costa, P. Croft, P. H. Ferreira, J. M. Fritz, D. P. Gross, B. W. Koes, B. Öberg, W. C. Peul, M. Schoene, J. A. Turner, A. Woolf, *The Lancet* **2018**, *391*, 2356.

[2] A. Wu, W. Dong, S. Liu, J. P. Y. Cheung, K. Y. H. Kwan, X. Zeng, K. Zhang, Z. Sun, X. Wang, K. M. C. Cheung, M. Zhou, J. Zhao, *Pain* **2019**, *160*, 237.

[3] Walker B, *J. Spinal Disord.* **2000**, *13*, 205.

[4] D. Schopflocher, P. Taenzer, R. Jovey, *Pain Res. Manag.* **2011**, *16*, 445.

[5] A. Maetzel, L. Li, *Best Pract. Res. Clin. Rheumatol.* **2002**, *16*, 23.

[6] I. A. Steenstra, J. H. Verbeek, M. W. Heymans, P. M. Bongers, *Occup. Environ. Med.* **2005**, *62*, 851.

[7] P. M. Kent, J. L. Keating, *Chiropr. Osteopat.* **2005**, *13*, 1.

[8] D. Hoy, C. Bain, G. Williams, L. March, P. Brooks, F. Blyth, A. Woolf, T. Vos, R. Buchbinder, *Arthritis Rheum.* **2012**, *64*, 2028.

[9] GBD 2015 Diseases and Injuries Collaborators. *The Lancet* **2016**, *388*, 1545.

[10] K. Luoma, H. Riihimäki, R. Luukkonen, R. Raininko, E. Viikari-Juntura, A. Lamminen, *Spine* **2000**, *25*, 487.

[11] C. Q. Zhao, L. M. Wang, L. S. Jiang, L. Y. Dai, *Ageing Res. Rev.* **2007**, *6*, 247.

[12] S. M. Richardson, A. Mobasheri, A. J. Freemont, J. A. Hoyland, *Histol. Histopathol.* **2007**, *22*, 1033.

[13] N. V. Vo, R. A. Hartman, P. R. Patil, M. V. Risbud, D. Kletsas, J. C. Iatridis, J. A. Hoyland, C. L. Le Maitre, G. A. Sowa, J. D. Kang, *J. Orthop. Res.* **2016**, *34*, 1289.

[14] R. Freynhagen, R. Baron, *Curr. Pain Headache Rep.* **2009**, *13*, 185.

[15] M. A. Adams, P. J. Roughley, *Spine* **2006**, *31*, 2151.

[16] M. A. Adams, P. Dolan, *J. Anat.* **2012**, *221*, 497.

[17] S. Roberts, H. Evans, J. Trivedi, J. Menage, *J. Bone Jt. Surg. - Ser. A* **2006**, *88*, 10.

[18] K. M. C. Cheung, J. Karppinen, D. Chan, D. W. H. Ho, Y. Q. Song, P. Sham, K. S. E. Cheah, J. C. Y. Leong, K. D. K. Luk, *Spine* **2009**, *34*, 934.

[19] G. Lyons, S. M. Eisenstein, M. B. E. Sweet, *BBA - Gen. Subj.* **1981**, *673*, 443.

[20] M. A. Adams, P. J. Roughley, *Spine* **2006**, *31*, 2151.

[21] M. A. Adams, B. J. C. Freeman, H. P. Morrison, I. W. Nelson, P. Dolan, *Spine* **2000**, *25*, 1625.

[22] S. Rajasekaran, J. N. Babu, R. Arun, B. R. W. Armstrong, A. P. Shetty, S. Murugan, *Spine* **2004**, *29*, 2654.

[23] J. Karppinen, F. H. Shen, K. D. K. Luk, G. B. J. Andersson, K. M. C. Cheung, D. Samartzis, *Orthop. Clin. North Am.* **2011**, *42*, 513.

[24] A. E. Bussières, G. Stewart, F. Al-Zoubi, P. Decina, M. Descarreaux, D. Haskett, C. Hincapié, I. Pagé, S. Passmore, J. Srbely, M. Stupar, J. Weisberg, J. Ornelas, *J. Manipulative Physiol. Ther.* **2018**, *41*, 265.

[25] C. Schizas, G. Kulik, V. Kosmopoulos, *Eur. Cell. Mater.* **2010**, *20*, 306.

[26] M. Putzier, S. V. Schneider, J. F. Funk, S. W. Tohtz, C. Perka, *Spine* **2005**, *30*, E109.

[27] B. Farrugia, S. M. Smith, C. C. Shu, J. Melrose, *Cartilage* **2020**, *11*, 234.

[28] J. Melrose, S. Smith, C. B. Little, J. Kitson, S.-Y. Hwa, P. Ghosh, *Spine* **2002**, *27*, 1756.

[29] E. S. Fuller, C. Shu, M. M. Smith, C. B. Little, J. Melrose, *J. Tissue Eng. Regen. Med.* **2018**, *12*, e216.

[30] W. R. Sears, I. G. Sergides, N. Kazemi, M. Smith, G. J. White, B. Osburg, *Spine J.* **2011**, *11*, 11.
[31] S. L. Parker, G. Grahovac, D. Vukas, M. Vilendecic, D. Ledic, M. J. McGirt, E. J. Carragee, *Clin. Spine Surg.* **2016**, *29*, 454.
[32] R. D. Bowles, L. A. Setton, *Biomaterials* **2017**, *129*, 54.
[33] Z. Ma, G. Bao, J. Li, *Adv. Mater.* **2021**, *33*, 2007663.
[34] G. Bao, R. Huo, Z. Ma, M. Strong, A. Valiei, S. Jiang, S. Liu, L. Mongeau, J. Li, *ACS Appl. Mater. Interfaces* **2021**, *13*, 37849.
[35] S. Tarafder, G. Y. Park, J. Felix, C. H. Lee, *Acta Biomater.* **2020**, *117*, 77.
[36] G. Bao, Q. Gao, M. Cau, N. Ali-Mohamad, M. Strong, S. Jiang, Z. Yang, A. Valiei, Z. Ma, M. Amabili, Z.-H. Gao, L. Mongeau, C. Kastrup, J. Li, *Nat. Commun.* **2022**, *13*, 5035.
[37] Z. Ma, C. Bourquard, Q. Gao, S. Jiang, T. De Iure-Grimmel, R. Huo, X. Li, Z. He, Z. Yang, G. Yang, Y. Wang, E. Lam, Z. Gao, O. Supponen, J. Li, *Science* **2022**, *377*, 751.
[38] X. Su, Y. Luo, Z. Tian, Z. Yuan, Y. Han, R. Dong, L. Xu, Y. Feng, X. Liu, J. Huang, *Mater. Horiz.* **2020**, *7*, 2651.
[39] J. Li, A. D. Celiz, J. Yang, Q. Yang, I. Wamala, W. Whyte, B. R. Seo, N. V. Vasilyev, J. J. Vlassak, Z. Suo, *Science* **2017**, *357*, 378.
[40] M. A. Adams, in *Mech. Prop. Aging Soft Tissues* (Eds.: B. Derby, R. Akhtar), Springer International Publishing, Cham, **2015**, pp. 7–35.
[41] P. P. Raj, *Pain Pract.* **2008**, *8*, 18.
[42] J. L. Bron, M. N. Helder, H.-J. Meisel, B. J. Van Royen, T. H. Smit, *Eur. Spine J.* **2009**, *18*, 301.
[43] J. P. Urban, S. Roberts, *Arthritis Res Ther* **2003**, *5*, 120.
[44] N. L. Nerurkar, D. M. Elliott, R. L. Mauck, *J. Biomech.* **2010**, *43*, 1017.
[45] M. D'Este, D. Eglin, M. Alini, *Acta Biomater.* **2018**, *78*, 13.
[46] T. J. DiStefano, J. O. Shmukler, G. Danias, T. D. P. von Treuheim, W. W. Hom, D. A. Goldberg, D. M. Laudier, P. R. Nasser, A. C. Hecht, S. B. Nicoll, J. C. Iatridis, *Biomaterials* **2020**, *258*, 120309.
[47] J. Z. Young, P. B. Medawar, *The Lancet* **1940**, *236*, 126.
[48] Y. Xiong, X. Zhang, X. Ma, W. Wang, F. Yan, X. Zhao, X. Chu, W. Xu, C. Sun, *Polym. Chem.* **2021**, *12*, 3721.
[49] W. Zhu, Y. J. Chuah, D.-A. Wang, *Acta Biomater.* **2018**, *74*, 1.
[50] X. Li, Y. Liu, S. Liu, N. Y. K. Li-Jessen, L. Haglund, B. Huang, J. Li, *Adv. Ther.* **2023**, *n/a*, 2300139.
[51] C. F. Guimarães, L. Gasperini, A. P. Marques, R. L. Reis, *Nat. Rev. Mater.* **2020**, *5*, 351.
[52] O. Chaudhuri, L. Gu, D. Klumpers, M. Darnell, S. A. Bencherif, J. C. Weaver, N. Huebsch, H. Lee, E. Lippens, G. N. Duda, D. J. Mooney, *Nat. Mater.* **2016**, *15*, 326.
[53] B. V. Fearing, P. A. Hernandez, L. A. Setton, N. O. Chahine, *JOR SPINE* **2018**, *1*, e1026.
[54] P. T. Coburn, X. Li, J. Li, Y. Kishimoto, N. Y. K. Li-Jessen, *Adv. NanoBiomed Res.* **2022**, *2*, 2100119.
[55] F. Burla, Y. Mulla, B. E. Vos, A. Aufderhorst-Roberts, G. H. Koenderink, *Nat. Rev. Phys.* **2019**, *1*, 249.
[56] Z. Tong, L. Jin, J. M. Oliveira, R. L. Reis, Q. Zhong, Z. Mao, C. Gao, *Bioact. Mater.* **2021**, *6*, 1375.
[57] I. L. Kim, S. Khetan, B. M. Baker, C. S. Chen, J. A. Burdick, *Biomaterials* **2013**, *34*, 5571.
[58] S. O. Blacklow, J. Li, B. R. Freedman, M. Zeidi, C. Chen, D. J. Mooney, *Sci. Adv.* **2019**, *5*, eaaw3963.

[59] R. Langer, J. P. Vacanti, *Science* **1993**, *260*, 920.
[60] F. Baumgart, J. Cordey, *Injury* **2000**, *31*, B14.
[61] W. D. Callister, D. G. Rethwisch, *Materials Science and Engineering: An Introduction*, Wiley New York, **2018**.
[62] A. Arani, M. C. Murphy, K. J. Glaser, A. Manduca, D. S. Lake, S. A. Kruse, C. R. Jack, R. L. Ehman, J. Huston, *NeuroImage* **2015**, *111*, 59.
[63] B. C. W. Kot, Z. J. Zhang, A. W. C. Lee, V. Y. F. Leung, S. N. Fu, *PLOS ONE* **2012**, *7*, e44348.
[64] D. L. Robinson, M. E. Kersh, N. C. Walsh, D. C. Ackland, R. N. de Steiger, M. G. Pandy, *J. Mech. Behav. Biomed. Mater.* **2016**, *61*, 96.
[65] J. Y. Rho, R. B. Ashman, C. H. Turner, *J. Biomech.* **1993**, *26*, 111.
[66] J. H. Wen, L. G. Vincent, A. Fuhrmann, Y. S. Choi, K. C. Hribar, H. Taylor-Weiner, S. Chen, A. J. Engler, *Nat. Mater.* **2014**, *13*, 979.
[67] O. Chaudhuri, J. Cooper-White, P. A. Janmey, D. J. Mooney, V. B. Shenoy, *Nature* **2020**, *584*, 535.
[68] J. C. Iatridis, L. A. Setton, M. Weidenbaum, V. C. Mow, *J. Biomech.* **1997**, *30*, 1005.
[69] C.-Y. Huang, V. C. Mow, G. A. Ateshian, *J. Biomech. Eng.* **2001**, *123*, 410.
[70] Y. Hu, Z. Suo, *Acta Mech. Solida Sin.* **2012**, *25*, 441.
[71] D. Huang, Y. Huang, Y. Xiao, X. Yang, H. Lin, G. Feng, X. Zhu, X. Zhang, *Acta Biomater.* **2019**, *97*, 74.
[72] D. D. McKinnon, D. W. Domaille, J. N. Cha, K. S. Anseth, *Adv. Mater. Deerfield Beach Fla* **2014**, *26*, 865.
[73] X. Zhao, N. Huebsch, D. J. Mooney, Z. Suo, *J. Appl. Phys.* **2010**, *107*, 063509.
[74] Andrew. R. Cameron, Jessica. E. Frith, Justin. J. Cooper-White, *Biomaterials* **2011**, *32*, 5979.
[75] H. Tavakoli Nia, L. Han, I. Soltani Bozchalooi, P. Roughley, K. Youcef-Toumi, A. J. Grodzinsky, C. Ortiz, *ACS Nano* **2015**, *9*, 2614.
[76] Q.-M. Wang, A. C. Mohan, M. L. Oyen, X.-H. Zhao, *Acta Mech. Sin.* **2014**, *30*, 20.
[77] L. Su, M. Wang, J. Yin, F. Ti, J. Yang, C. Ma, S. Liu, T. J. Lu, *Acta Biomater.* **2023**, *155*, 423.
[78] G. Han, C. Hess, M. Eriten, C. R. Henak, *J. Mech. Behav. Biomed. Mater.* **2018**, *84*, 28.
[79] G. Bao, in *Racing Surf. Antimicrob. Interface Tissue Eng.* (Eds.: B. Li, T. F. Moriarty, T. Webster, M. Xing), Springer International Publishing, Cham, **2020**, pp. 289–312.
[80] K. J. De France, F. Xu, T. Hoare, *Adv. Healthc. Mater.* **2018**, *7*, 1700927.
[81] G. Bao, T. Jiang, H. Ravanbakhsh, A. Reyes, Z. Ma, M. Strong, H. Wang, J. M. Kinsella, J. Li, L. Mongeau, *Mater. Horiz.* **2020**, *7*, 2336.
[82] D. R. Griffin, W. M. Weaver, P. O. Scumpia, D. Di Carlo, T. Segura, *Nat. Mater.* **2015**, *14*, 737.
[83] X. Long, X. Xu, D. Sun, Y. Hong, C. Wen, Y. Xie, B. Yan, H. Zhang, Q. Ge, W. Li, L. Duan, H. Ouyang, D. Wang, *Appl. Mater. Today* **2022**, *27*, 101442.
[84] J. p. Gong, Y. Katsuyama, T. Kurokawa, Y. Osada, *Adv. Mater.* **2003**, *15*, 1155.
[85] Y. Okumura, K. Ito, *Adv. Mater.* **2001**, *13*, 485.
[86] J. D. Bobyn, G. J. Wilson, D. C. MacGregor, R. M. Pilliar, G. C. Weatherly, *J. Biomed. Mater. Res.* **1982**, *16*, 571.
[87] D. Taylor, N. O'Mara, E. Ryan, M. Takaza, C. Simms, *J. Mech. Behav. Biomed. Mater.* **2012**, *6*, 139.
[88] S. Brandstaeter, S. L. Fuchs, R. C. Aydin, C. J. Cyron, *GAMM-Mitteilungen* **2019**, *42*, e201900001.
[89] J. Liu, S. Lin, X. Liu, Z. Qin, Y. Yang, J. Zang, X. Zhao, *Nat. Commun.* **2020**, *11*, 1071.
[90] X. Li, J. P. Gong, *Proc. Natl. Acad. Sci.* **2022**, *119*, e2200678119.

[91] X. Chen, J. Zhang, G. Chen, Y. Xue, J. Zhang, X. Liang, I. M. Lei, J. Lin, B. B. Xu, J. Liu, *Adv. Funct. Mater.* **2022**, *32*, 2202285.
[92] J. He, Z. Zhang, Y. Yang, F. Ren, J. Li, S. Zhu, F. Ma, R. Wu, Y. Lv, G. He, B. Guo, D. Chu, *Nano-Micro Lett.* **2021**, *13*, 80.
[93] Z. Wang, X. Zheng, T. Ouchi, T. B. Kouznetsova, H. K. Beech, S. Av-Ron, T. Matsuda, B. H. Bowser, S. Wang, J. A. Johnson, J. A. Kalow, B. D. Olsen, J. P. Gong, M. Rubinstein, S. L. Craig, *Science* **2021**, *374*, 193.
[94] W. Wang, Z. Zeng, L. Xiang, C. Liu, D. Diaz-Dussan, Z. Du, A. B. Asha, W. Yang, Y.-Y. Peng, M. Pan, R. Narain, J. Liu, H. Zeng, *ACS Nano* **2021**, *15*, 9913.
[95] J. Hu, T. Wei, H. Zhao, M. Chen, Y. Tan, Z. Ji, Q. Jin, J. Shen, Y. Han, N. Yang, L. Chen, Z. Xiao, H. Zhang, Z. Liu, Q. Chen, *Matter* **2021**, *4*, 2985.
[96] S. Nam, B. R. Seo, A. J. Najibi, S. L. McNamara, D. J. Mooney, *Nat. Mater.* **2023**, *22*, 249.
[97] R. Elbaum, L. Zaltzman, I. Burgert, P. Fratzl, *Science* **2007**, *316*, 884.
[98] Y. Kuang, C. Chen, J. Cheng, G. Pastel, T. Li, J. Song, F. Jiang, Y. Li, Y. Zhang, S.-H. Jang, G. Chen, T. Li, L. Hu, *Extreme Mech. Lett.* **2019**, *29*, 100463.
[99] H. M. El-Husseiny, E. A. Mady, L. Hamabe, A. Abugomaa, K. Shimada, T. Yoshida, T. Tanaka, A. Yokoi, M. Elbadawy, R. Tanaka, *Mater. Today Bio* **2022**, *13*, 100186.
[100] X. Le, W. Lu, J. Zhang, T. Chen, *Adv. Sci.* **2019**, *6*, 1801584.
[101] A. Zolfagharian, A. Z. Kouzani, S. Y. Khoo, B. Nasri-Nasrabadi, A. Kaynak, *Sens. Actuators Phys.* **2017**, *265*, 94.
[102] M. L. O'Grady, P. Kuo, K. K. Parker, *ACS Appl. Mater. Interfaces* **2010**, *2*, 343.
[103] X. Kong, Y. Li, W. Xu, H. Liang, Z. Xue, Y. Niu, M. Pang, C. Ren, *Macromol. Rapid Commun.* **2021**, *42*, 2100416.
[104] J. Li, D. J. Mooney, *Nat. Rev. Mater.* **2016**, *1*, 1.
[105] X. Guan, M. Avci-Adali, E. Alarçin, H. Cheng, S. S. Kashaf, Y. Li, A. Chawla, H. L. Jang, A. Khademhosseini, *Biotechnol. J.* **2017**, *12*, 1600394.
[106] J. A. Burdick, W. L. Murphy, *Nat. Commun.* **2012**, *3*, 1269.
[107] G. Chen, Y. Yu, X. Wu, G. Wang, J. Ren, Y. Zhao, *Adv. Funct. Mater.* **2018**, *28*, 1801386.
[108] L. Teng, Y. Chen, Y.-G. Jia, L. Ren, *J. Mater. Chem. B* **2019**, *7*, 6705.
[109] S. Hou, X. Wang, S. Park, X. Jin, P. X. Ma, *Adv. Healthc. Mater.* **2015**, *4*, 1491.
[110] L. M. Caballero Aguilar, S. M. Silva, S. E. Moulton, *J. Controlled Release* **2019**, *306*, 40.
[111]K. F. Bruggeman, R. J. Williams, D. R. Nisbet, *Adv. Healthc. Mater.* **2018**, *7*, 1700836.
[112] C. Borrelli, C. T. Buckley, *Acta Biomater.* **2020**, *117*, 142.
[113] J. Hwang, M. O. Sullivan, K. L. Kiick, *Front. Bioeng. Biotechnol.* **2020**, *8*.
[114] M. Brown, J. Li, C. Moraes, M. Tabrizian, N. Y. K. Li-Jessen, *Biomaterials* **2022**, *289*, 121786.
[115] H. J. Yan, T. Casalini, G. Hulsart-Billström, S. Wang, O. P. Oommen, M. Salvalaglio, S. Larsson, J. Hilborn, O. P. Varghese, *Biomaterials* **2018**, *161*, 190.
[116] M. G. McCoy, B. R. Seo, S. Choi, C. Fischbach, *Acta Biomater.* **2016**, *44*, 200.
[117] R. Ravichandran, C. Astrand, H. K. Patra, A. P. F. Turner, V. Chotteau, J. Phopase, *RSC Adv.* **2017**, *7*, 21068.
[118] M. Goktas, G. Cinar, I. Orujalipoor, S. Ide, A. B. Tekinay, M. O. Guler, *Biomacromolecules* **2015**, *16*, 1247.
[119] N. Chen, Z. Zhang, B. Soontornworajit, J. Zhou, Y. Wang, *Biomaterials* **2012**, *33*, 1353.
[120] L. Bacakova, E. Filova, M. Parizek, T. Ruml, V. Svorcik, *Biotechnol. Adv.* **2011**, *29*, 739.
[121] M. M. Hasani-Sadrabadi, P. Sarrion, S. Pouraghaei, Y. Chau, S. Ansari, S. Li, T. Aghaloo, A. Moshaverinia, *Sci. Transl. Med.* **2020**, *12*, eaay6853.

[122] A. Abdal Dayem, S. B. Lee, K. M. Lim, A. Kim, H. J. Shin, B. Vellingiri, Y. B. Kim, S.-G. Cho, *Biomed. Pharmacother.* **2023**, *160*, 114376.
[123] C. R. Nuttelman, M. C. Tripodi, K. S. Anseth, *Matrix Biol.* **2005**, *24*, 208.
[124] S. Nam, R. Stowers, J. Lou, Y. Xia, O. Chaudhuri, *Biomaterials* **2019**, *200*, 15.
[125] L. D. Amer, S. J. Bryant, *Ann. Biomed. Eng.* **2016**, *44*, 1959.
[126] A. Lueckgen, D. S. Garske, A. Ellinghaus, D. J. Mooney, G. N. Duda, A. Cipitria, *Biomaterials* **2019**, *217*, 119294.
[127] S. C. Skaalure, S. Chu, S. J. Bryant, *Adv. Healthc. Mater.* **2015**, *4*, 420.
[128] L. L. Palmese, M. Fan, R. A. Scott, H. Tan, K. L. Kiick, *J. Biomater. Sci. Polym. Ed.* **2021**, *32*, 635.
[129] J. L. Holloway, H. Ma, R. Rai, K. D. Hankenson, J. A. Burdick, *Macromol. Biosci.* **2015**, *15*, 1218.
[130] D. F. Evans, G. Pye, R. Bramley, A. G. Clark, T. J. Dyson, J. D. Hardcastle, *Gut* **1988**, *29*, 1035.
[131] L. A. Schneider, A. Korber, S. Grabbe, J. Dissemond, *Arch. Dermatol. Res.* **2007**, *298*, 413.
[132] S. Schreml, R.-M. Szeimies, S. Karrer, J. Heinlin, M. Landthaler, P. Babilas, *J. Eur. Acad. Dermatol. Venereol.* **2010**, *24*, 373.
[133] T. M. D. Le, H. T. T. Duong, T. Thambi, V. H. Giang Phan, J. H. Jeong, D. S. Lee, *Biomacromolecules* **2018**, *19*, 3536.
[134] L. Chang, R. Chang, X. Liu, X. Ma, D. Chen, Y. Wang, W. Li, J. Qin, *Biomater. Adv.* **2022**, *139*, 212974.
[135] G. A. Hudalla, W. L. Murphy, *Adv. Funct. Mater.* **2011**, *21*, 1754.
[136] B. Huang, Y. Yuan, C. Liu, *Appl. Mater. Today* **2020**, *19*, 100599.
[137] A. Nuschke, M. Rodrigues, J. Rivera, C. Yates, D. Whaley, D. Stolz, L. Griffith, A. Wells, *Stem Cells Transl. Med.* **2016**, *5*, 1580.
[138] B. K. Mann, R. H. Schmedlen, J. L. West, *Biomaterials* **2001**, *22*, 439.
[139] C. Siverino, S. Fahmy-Garcia, D. Mumcuoglu, H. Oberwinkler, M. Muehlemann, T. Mueller, E. Farrell, G. J. V. M. van Osch, J. Nickel, *Int. J. Mol. Sci.* **2022**, *23*, 3928.
[140] B. Huang, Z. Wu, S. Ding, Y. Yuan, C. Liu, *Acta Biomater.* **2018**, *71*, 184.
[141] A. Zieris, S. Prokoph, K. R. Levental, P. B. Welzel, K. Chwalek, K. Schneider, U. Freudenberg, C. Werner, in *Proteins Interfaces III State Art 2012* (Eds.: T. Horbett, J. L. Brash, W. Norde), American Chemical Society, Washington, DC, **2012**, pp. 525–541.
[142] GBD 2019 Diseases and Injuries Collaborators, *The Lancet* **2020**, *396*, 1204.
[143] L. Haglund, J. Moir, L. Beckman, K. R. Mulligan, B. Jim, J. A. Ouellet, P. Roughley, T. Steffen, *Tissue Eng. Part C Methods* **2011**, *17*, 1011.
[144] H. J. Wilke, P. Neef, M. Caimi, T. Hoogland, L. Claes, *Spine* **1999**, *24*, 755.
[145] C. J. Panebianco, S. Rao, W. W. Hom, J. H. Meyers, T. Y. Lim, D. M. Laudier, A. C. Hecht, M. D. Weir, J. R. Weiser, J. C. Iatridis, *Biomaterials* **2022**, *287*, 121641.
[146] B. R. Freedman, A. Kuttler, N. Beckmann, S. Nam, D. Kent, M. Schuleit, F. Ramazani, N. Accart, A. Rock, J. Li, *Nat. Biomed. Eng.* **2022**, 1.
[147] K. A. Tomaszewski, K. Saganiak, T. Gładysz, J. A. Walocha, *Folia Morphol. (Warsz.)* **2015**, *74*, 157.
[148] A. N. Khan, H. E. Jacobsen, J. Khan, C. G. Filippi, M. Levine, R. A. Lehman Jr., K. D. Riew, L. G. Lenke, N. O. Chahine, *Ann. N. Y. Acad. Sci.* **2017**, *1410*, 68.
[149] V. H. Pomin, B. Mulloy, *Pharmaceuticals* **2018**, *11*, 23.
[150] B. Yang, G. D. O'Connell, *Acta Biomater.* **2019**, *100*, 61.

[151] K. A. Tomaszewski, K. Saganiak, T. Gładysz, J. A. Walocha, *Folia Morphol. (Warsz.)* **2015**, *74*, 157.
[152] N. Newell, J. P. Little, A. Christou, M. A. Adams, C. J. Adam, S. D. Masouros, *J. Mech. Behav. Biomed. Mater.* **2017**, *69*, 420.
[153] S. Roberts, J. Menage, J. P. G. Urban, *Spine* **1989**, *14*, 166.
[154] K. A. Tomaszewski, J. A. Walocha, E. Mizia, T. Gładysz, R. Głowacki, R. Tomaszewska, *Pol. J. Pathol.* **2015**, *66*, 296.
[155] B. M. Minogue, S. M. Richardson, L. A. H. Zeef, A. J. Freemont, J. A. Hoyland, *Arthritis Care Res.* **2010**, *62*, 3695.
[156] R. Gawri, F. Mwale, J. Ouellet, P. J. Roughley, T. Steffen, J. Antoniou, L. Haglund, *Spine* **2011**, *36*, 1835.
[157] J. P. G. Urban, S. Smith, J. C. T. Fairbank, *Spine* **2004**, *29*, 2700.
[158] T. Liebscher, M. Haefeli, K. Wuertz, A. G. Nerlich, N. Boos, *Spine* **2011**, *36*, 153.
[159] M. D. Humzah, R. W. Soames, *Anat. Rec.* **1988**, *220*, 337.
[160] S. C. W. Chan, S. J. Ferguson, B. Gantenbein-Ritter, *Eur. Spine J.* **2011**, *20*, 1796.
[161] K. Sato, S. Kikuchi, T. Yonezawa, *Spine* **1999**, *24*, 2468.
[162] K. A. Tomaszewski, K. Saganiak, T. Gładysz, J. A. Walocha, P. P. Raj, M. D. Humzah, R. W. Soames, M. A. Adams, P. J. Roughley, S. C. W. Chan, S. J. Ferguson, B. Gantenbein-Ritter, *Eur. Spine J.* **2006**, *31*, 2151.
[163] H. Ishihara, D. S. Mcnally, J. P. G. Urban, A. C. Hall, *J. Appl. Physiol.* **1996**, *80*, 839.
[164] J. P. G. Urban, J. F. McMullin, *Spine* **1988**, *13*, 179.
[165] Y. Zhang, A. Chee, E. J. M. A. Thonar, H. S. An, *PM R* **2011**, *3*, 88.
[166] Y. Moriguchi, M. Alimi, T. Khair, G. Manolarakis, C. Berlin, L. J. Bonassar, R. Härtl, *Glob. Spine J.* **2016**, *6*, 497.
[167] D. Sakai, G. B. J. Andersson, *Nat. Rev. Rheumatol.* **2015**, *11*, 243.
[168] J. L. Drury, D. J. Mooney, *Biomaterials* **2003**, *24*, 4337.
[169] R. D. Bowles, K. Masuda, L. A. Bonassar, L. A. Setton, *Tissue Engineering for Regeneration and Replacement of the Intervertebral Disc*, **2014**.
[170] C. T. Buckley, J. A. Hoyland, K. Fujii, A. Pandit, J. C. Iatridis, S. Grad, *JOR Spine* **2018**, *1*, e1029.
[171] R. D. Bowles, L. A. Setton, *Biomaterials* **2017**, *129*, 54.
[172] K. Sing, K. Masuda, E. J. M. A. Thonar, H. S. An, G. Cs-Szab, *Spine Phila Pa 1976* **2009**, *34*, 10.
[173] Y. Alinejad, A. Adoungotchodo, M. P. Grant, L. M. Epure, J. Antoniou, F. Mwale, S. Lerouge, *Tissue Eng. - Part A* **2019**, *25*, 303.
[174] X. Yang, X. Li, *Eur. Spine J.* **2009**, *18*, 1564.
[175] S. S. Sivan, S. Roberts, J. P. G. Urban, J. Menage, J. Bramhill, D. Campbell, V. J. Franklin, F. Lydon, Y. Merkher, A. Maroudas, B. J. Tighe, *Acta Biomater.* **2014**, *10*, 1124.
[176] N. L. Nerurkar, D. M. Elliott, R. L. Mauck, *J. Biomech.* **2010**, *43*, 1017.
[177] Y. Peng, D. Huang, S. Liu, J. Li, X. Qing, Z. Shao, *Front. Bioeng. Biotechnol.* **2020**, *8*, DOI 10.3389/fbioe.2020.00056.
[178] G. Chang, H. J. Kim, D. Kaplan, G. Vunjak-Novakovic, R. A. Kandel, *Eur. Spine J.* **2007**, *16*, 1848.
[179] C. Zeng, Q. Yang, M. Zhu, L. Du, J. Zhang, X. Ma, B. Xu, L. Wang, *Mater. Sci. Eng. C* **2014**, *37*, 232.
[180] R. Tsaryk, A. Gloria, T. Russo, L. Anspach, R. De Santis, S. Ghanaati, R. E. Unger, L. Ambrosio, C. J. Kirkpatrick, *Acta Biomater.* **2015**, *20*, 10.

[181] D. H. Rosenzweig, R. Fairag, A. P. Mathieu, L. Li, D. Eglin, M. D'este, T. Steffen, M. H. Weber, J. A. Ouellet, L. Haglund, *Eur. Cell. Mater.* **2018**, *36*, 200.
[182] S. M. Richardson, N. Hughes, J. A. Hunt, A. J. Freemont, J. A. Hoyland, *Biomaterials* **2008**, *29*, 85.
[183] H. Mizuno, A. K. Roy, C. A. Vacanti, K. Kojima, M. Ueda, L. J. Bonassar, *Spine* **2004**, *29*, 1290.
[184] A. E. Baer, J. Y. Wang, V. B. Kraus, L. A. Setton, *J. Orthop. Res.* **2001**, *19*, 2.
[185] S. Wan, S. Borland, S. M. Richardson, C. L. R. Merry, A. Saiani, J. E. Gough, *Acta Biomater.* **2016**, *46*, 29.
[186] L. J. Nesti, W. J. Li, R. M. Shanti, Y. J. Jiang, W. Jackson, B. A. Freedman, T. R. Kuklo, J. R. Giuliani, R. S. Tuan, *Tissue Eng. - Part A* **2008**, *14*, 1527.
[187] J. Zhu, K. Xia, W. Yu, Y. Wang, J. Hua, B. Liu, Z. Gong, J. Wang, A. Xu, Z. You, Q. Chen, F. Li, H. Tao, C. Liang, *Acta Biomater.* **2019**, *86*, 300.
[188] C. L. Gilchrist, E. M. Darling, J. Chen, L. A. Setton, *PLoS ONE* **2011**, *6*, DOI 10.1371/journal.pone.0027170.
[189] W. Johannessen, D. M. Elliott, *Spine* **2005**, *30*, 724.
[190] K. H. Yang, V. L. Kish, *J. Biomech.* **1988**, *21*, 865.
[191] J. M. Cloyd, N. R. Malhotra, L. Weng, W. Chen, R. L. Mauck, D. M. Elliott, *Eur. Spine J.* **2007**, *16*, 1892.
[192] P. Y. Hwang, J. Chen, L. Jing, B. D. Hoffman, L. A. Setton, *J. Biomech. Eng.* **2014**, *136*, DOI 10.1115/1.4026360.
[193] J. C. Iatridis, L. A. Setton, M. Weidenbaum, V. C. Mow, *J. Orthop. Res.* **1997**, *15*, 318.
[194] J. C. Iatridis, M. Weidenbaum, L. A. Setton, C. Van Mow, in *Spine*, **1996**, pp. 1174–1184.
[195] Y. Hu, D. W. Grainger, S. R. Winn, J. O. Hollinger, *J. Biomed. Mater. Res.* **2002**, *59*, 563.
[196] W. L. Murphy, D. H. Kohn, D. J. Mooney, *J. Biomed. Mater. Res.* **2000**, *50*, 50.
[197] L. E. Freed, G. Vunjak-Novakovic, B. R. J., D. B. Eagles, D. C. Lesnoy, S. K. Barlow, R. Langer, *Biotechnology* **1994**, *12*, 689.
[198] H. Y. Kim, H. N. Kim, S. J. Lee, J. E. Song, S. Y. Kwon, J. W. Chung, D. Lee, G. Khang, *J. Tissue Eng. Regen. Med.* **2017**, *11*, 44.
[199] F. J. Lyu, K. M. Cheung, Z. Zheng, H. Wang, D. Sakai, V. Y. Leung, *Nat. Rev. Rheumatol.* **2019**, *15*, 102.
[200] D. Sakai, Y. Nakamura, T. Nakai, T. Mishima, S. Kato, S. Grad, M. Alini, M. V. Risbud, D. Chan, K. S. E. Cheah, K. I. Yamamura, K. Masuda, H. Okano, K. Ando, J. Mochida, *Nat. Commun.* **2012**, *3*, DOI 10.1038/ncomms2226.
[201] D. Sakai, G. B. J. Andersson, *Nat. Rev. Rheumatol.* **2015**, *11*, 243.
[202] D. Sakai, J. Mochida, T. Iwashina, T. Watanabe, T. Nakai, K. Ando, T. Hotta, *Spine* **2005**, *30*, 2379.
[203] D. Sakai, J. Mochida, Y. Yamamoto, T. Nomura, M. Okuma, K. Nishimura, T. Nakai, K. Ando, T. Hotta, *Biomaterials* **2003**, *24*, 3531.
[204] C. Le Visage, S. H. Yang, L. Kadakia, A. N. Sieber, J. P. Kostuik, K. W. Leong, *Spine* **2006**, *31*, 2423.
[205] G. Crevensten, A. J. L. Walsh, D. Ananthakrishnan, P. Page, G. M. Wahba, J. C. Lotz, S. Berven, *Ann. Biomed. Eng.* **2004**, *32*, 430.
[206] L.-C. Wu, Y.-J. Kuo, F.-W. Sun, C.-H. Chen, C.-J. Chiang, P.-W. Weng, Y.-H. Tsuang, Y.-Y. Huang, *Cell Tissue Bank.* **2017**, *18*, 383.
[207] R. Borem, A. Madeline, J. Walters, H. Mayo, S. Gill, J. Mercuri, *Acta Biomater.* **2017**, *58*, 254.

[208] R. Borem, A. Madeline, C. Theos, R. Vela Jr., A. Garon, S. Gill, J. Mercuri, *J. Biomed. Mater. Res. B Appl. Biomater.* **2022**, *110*, 1056.
[209] M.-D. Nie, Z.-B. Huang, N.-Z. Zhang, L.-J. Fu, C.-K. Cheng, *Front. Bioeng. Biotechnol.* **2023**, *11*, 1104015.
[210] S. Naahidi, M. Jafari, M. Logan, Y. Wang, Y. Yuan, H. Bae, B. Dixon, P. Chen, *Biotechnol. Adv.* **2017**, *35*, 530.
[211] N. Isobe, T. Komamiya, S. Kimura, U.-J. Kim, M. Wada, *Int. J. Biol. Macromol.* **2018**, *117*, 625.
[212] O. Guillaume, A. Daly, K. Lennon, J. Gansau, S. F. Buckley, C. T. Buckley, *Acta Biomater.* **2014**, *10*, 1985.
[213] T. J. DiStefano, J. O. Shmukler, G. Danias, J. C. Iatridis, *ACS Biomater. Sci. Eng.* **2020**, *6*, 6556.
[214] M. A. Cruz, W. W. Hom, T. J. DiStefano, R. Merrill, O. M. Torre, H. A. Lin, A. C. Hecht, S. Illien-Junger, J. C. Iatridis, *Tissue Eng. Part A* **2018**, *24*, 187.
[215] D. A. Frauchiger, R. D. May, E. Bakirci, A. Tekari, S. C. Chan, M. Wöltje, L. M. Benneker, B. Gantenbein, *J. Funct. Biomater.* **2018**, *9*, 40.
[216] B. Pennicooke, I. Hussain, C. Berlin, S. R. Sloan, B. Borde, Y. Moriguchi, G. Lang, R. Navarro-Ramirez, J. Cheetham, L. J. Bonassar, R. Härtl, *Spine* **2018**, *43*, E208.
[217] J. Bian, F. Cai, H. Chen, Z. Tang, K. Xi, J. Tang, L. Wu, Y. Xu, L. Deng, Y. Gu, W. Cui, L. Chen, *Nano Lett.* **2021**, *21*, 2690.
[218] D. R. Pereira, J. Silva-Correia, J. M. Oliveira, R. L. Reis, A. Pandit, M. J. Biggs, *Nanomedicine Nanotechnol. Biol. Med.* **2018**, *14*, 897.
[219] K. Zheng, D. Du, *J. Tissue Eng. Regen. Med.* **2021**, *15*, 299.
[220] B. K. Bhunia, B. B. Mandal, *Mater. Des.* **2018**, *158*, 74.
[221] Z. Liu, H. Wang, Z. Yuan, Q. Wei, F. Han, S. Chen, H. Xu, J. Li, J. Wang, Z. Li, Q. Chen, J. Fuh, L. Ding, H. Wang, B. Li, *Biofabrication* **2022**, *15*, 015015.
[222] T. R. Christiani, E. Baroncini, J. Stanzione, A. J. Vernengo, *Regen. Biomater.* **2019**, *6*, 175.
[223] A. Zhang, Z. Cheng, Y. Chen, P. Shi, W. Gan, Y. Zhang, *Acta Biomater.* **2023**, *167*, 1.
[224] S. E. Gullbrand, B. G. Ashinsky, E. D. Bonnevie, D. H. Kim, J. B. Engiles, L. J. Smith, D. M. Elliott, T. P. Schaer, H. E. Smith, R. L. Mauck, *Sci. Transl. Med.* **2018**, *10*, eaau0670.
[225] A. L. A. Binch, J. C. Fitzgerald, E. A. Growney, F. Barry, *Nat. Rev. Rheumatol.* **2021**, *17*, 158.
[226] J. J. MacLean, C. R. Lee, M. Alini, J. C. Iatridis, *J. Orthop. Res.* **2004**, *22*, 1193.
[227] J. J. MacLean, C. R. Lee, M. Alini, J. C. Iatridis, *J. Orthop. Res.* **2005**, *23*, 1120.
[228] A. J. L. Walsh, J. C. Lotz, *J. Biomech.* **2004**, *37*, 329.
[229] C.-Y. C. Huang, P. M. Reuben, H. S. Cheung, *Stem Cells* **2005**, *23*, 1113.
[230] S. D. Thorpe, C. T. Buckley, T. Vinardell, F. J. O'Brien, V. A. Campbell, D. J. Kelly, *Biochem. Biophys. Res. Commun.* **2008**, *377*, 458.
[231] V. Terraciano, N. Hwang, L. Moroni, H. Bin Park, Z. Zhang, J. Mizrahi, D. Seliktar, J. Elisseeff, *Stem Cells* **2007**, *25*, 2730.
[232] Z. Li, L. Kupcsik, S. J. Yao, M. Alini, M. J. Stoddart, *Tissue Eng. - Part A* **2009**, *15*, 1729.
[233] J. D. Kisiday, D. D. Frisbie, C. W. McIlwraith, A. J. Grodzinsky, *Tissue Eng. - Part A* **2009**, *15*, 2817.
[234] Y. Jung, S. H. Kim, Y. H. Kim, S. H. Kim, *Biomed. Mater.* **2009**, *4*, DOI 10.1088/1748-6041/4/5/055009.
[235] R. Gawri, J. Moir, J. Ouellet, L. Beckman, T. Steffen, P. Roughley, L. Haglund, *PLoS ONE* **2014**, *9*, 1.

[236] L. Haglund, J. Moir, L. Beckman, K. R. Mulligan, B. Jim, J. A. Ouellet, P. Roughley, T. Steffen, *Tissue Eng. - Part C Methods* **2011**, *17*, 1011.
[237] B. Gantenbein, S. Illien-Jünger, S. Chan, J. Walser, L. Haglund, S. Ferguson, J. Iatridis, S. Grad, *Curr. Stem Cell Res. Ther.* **2015**, *10*, 339.
[238] M. Peroglio, D. Gaspar, D. I. Zeugolis, M. Alini, *J. Orthop. Res.* **2018**, *36*, 10.
[239] X. Zhao, *Soft Matter* **2014**, *10*, 672.
[240] J.-Y. Sun, X. Zhao, W. R. K. Illeperuma, O. Chaudhuri, K. H. Oh, D. J. Mooney, J. J. Vlassak, Z. Suo, *Nature* **2012**, *489*, 133.
[241] H. Yuk, T. Zhang, S. Lin, G. A. Parada, X. Zhao, *Nat. Mater.* **2016**, *15*, 190.
[242] J. Caldeira, A. Celiz, N. Newell, *J. Mech. Behav. Biomed. Mater.* **2022**, *129*, 105150.
[243] R. S. Rivlin, A. G. Thomas, in *Collect. Pap. RS Rivlin Vol. II* (Eds.: G. I. Barenblatt, D. D. Joseph), Springer, New York, NY, **1997**, pp. 2615–2642.
[244] L. Haglund, J. Moir, L. Beckman, K. R. Mulligan, B. Jim, J. A. Ouellet, P. Roughley, T. Steffen, *Tissue Eng. Part C Methods* **2011**, *17*, 1011.
[245] J. S. Mort, P. J. Roughley, in *Arthritis Res. Methods Protoc. Vol. 1* (Ed.: A. P. Cope), Humana Press, Totowa, NJ, **2007**, pp. 201–209.
[246] R. G. Long, A. Bürki, P. Zysset, D. Eglin, D. W. Grijpma, S. B. Blanquer, A. C. Hecht, J. C. Iatridis, *Acta Biomater.* **2016**, *30*, 116.
[247] W. W. Hom, M. Tschopp, H. A. Lin, P. Nasser, D. M. Laudier, A. C. Hecht, S. B. Nicoll, J. C. Iatridis, *PloS One* **2019**, *14*, e0217357.
[248] K. Fujii, A. Lai, N. Korda, W. W. Hom, T. W. Evashwick-Rogler, P. Nasser, A. C. Hecht, J. C. Iatridis, *J. Biomech.* **2020**, *113*, 110100.
[249] T. Di Pauli von Treuheim, L. Zengerle, A. C. Hecht, J. C. Iatridis, H. J. Wilke, *J. Biomech.* **2021**, *129*, 110756.
[250] D. Rosenzweig, R. Gawri, J. Moir, L. Beckman, D. Eglin, T. Steffen, P. Roughley, J. Ouellet, L. Haglund, *Eur. Cell. Mater.* **2016**, *31*, 26.
[251] H. Cherif, D. G. Bisson, M. Mannarino, O. Rabau, J. A. Ouellet, L. Haglund, *eLife* **2020**, *9*, e54693.
[252] S. O. Blacklow, J. Li, B. R. Freedman, M. Zeidi, C. Chen, D. J. Mooney, *Sci. Adv.* **2019**, *5*, eaaw3963.
[253] B. R. Freedman, A. Kuttler, N. Beckmann, S. Nam, D. Kent, M. Schuleit, F. Ramazani, N. Accart, A. Rock, J. Li, M. Kurz, A. Fisch, T. Ullrich, M. W. Hast, Y. Tinguely, E. Weber, D. J. Mooney, *Nat. Biomed. Eng.* **2022**, *6*, 1167.
[254] S. R. Sloan Jr, C. Wipplinger, S. Kirnaz, R. Navarro-Ramirez, F. Schmidt, D. McCloskey, T. Pannellini, A. Schiavinato, R. Härtl, L. J. Bonassar, *Sci. Transl. Med.* **2020**, *12*, eaay2380.
[255] J. L. Bron, L. A. Vonk, T. H. Smit, G. H. Koenderink, *J. Mech. Behav. Biomed. Mater.* **2011**, *4*, 1196.
[256] M. J. Kibble, M. Domingos, J. A. Hoyland, S. M. Richardson, *Int. J. Mol. Sci.* **2022**, *23*, 6915.
[257] G. D. O'Connell, E. J. Vresilovic, D. M. Elliott, *Spine* **2007**, *32*, 328.
[258] M. Kobielarz, S. Szotek, M. Głowacki, J. Dawidowicz, C. Pezowicz, *J. Mech. Behav. Biomed. Mater.* **2016**, *62*, 45.
[259] C. Kiani, L. Chen, Y. J. Wu, A. J. Yee, B. B. Yang, *Cell Res.* **2002**, *12*, 19.
[260] G. G. H. van den Akker, M. I. Koenders, F. A. J. van de Loo, P. L. E. M. van Lent, E. Blaney Davidson, P. M. van der Kraan, *Eur. Spine J.* **2017**, *26*, 2053.
[261] M. Alini, S. M. Eisenstein, K. Ito, C. Little, A. A. Kettler, K. Masuda, J. Melrose, J. Ralphs, I. Stokes, H. J. Wilke, *Eur. Spine J.* **2008**, *17*, 2.

[262] B. L. Showalter, N. R. Malhotra, E. J. Vresilovic, D. M. Elliott, *J. Biomech.* **2014**, *47*, 2633.
[263] H.-J. Wilke, P. Neef, M. Caimi, T. Hoogland, L. E. Claes, *Spine* **1999**, *24*, 755.
[264] K. Sato, S. Kikuchi, T. Yonezawa, *Spine* **1999**, *24*, 2468.
[265] J. J. Costi, E. H. Ledet, G. D. O'Connell, *JOR SPINE* **2021**, *4*, e1138.
[266] S. Campana, E. Charpail, J. A. de Guise, L. Rillardon, W. Skalli, D. Mitton, *J. Mech. Behav. Biomed. Mater.* **2011**, *4*, 593.
[267] M. Driscoll, L. Blyum, *Clin. Biomech.* **2019**, *69*, 164.
[268] I. E. Bojairami, M. Driscoll, *Spine* **2022**, *47*, E423.
[269] H. Lee, L. Gu, D. J. Mooney, M. E. Levenston, O. Chaudhuri, *Nat. Mater.* **2017**, *16*, 1243.
[270] J. C. Iatridis, L. A. Setton, M. Weidenbaum, V. C. Mow, *J. Orthop. Res.* **1997**, *15*, 318.
[271] J. P. G. Urban, S. Holm, A. Maroudas, A. Nachemson, *Clin. Orthop. Relat. Res.* **1982**, *170*, 296.
[272] C. M. De Geer, *J. Chiropr. Med.* **2018**, *17*, 97.
[273] Y. Alinejad, A. Adoungotchodo, E. Hui, F. Zehtabi, S. Lerouge, *Int. J. Biol. Macromol.* **2018**, *113*, 132.
[274] D. H. Rosenzweig, R. Gawri, J. Moir, L. Beckman, D. Eglin, T. Steffen, P. J. Roughley, J. A. Ouellet, L. Haglund, *Eur. Cell. Mater.* **2016**, *31*, 26.
[275] B. A. Walter, S. Illien-Jünger, P. R. Nasser, A. C. Hecht, J. C. Iatridis, *J. Biomech.* **2014**, *47*, 2095.
[276] J. J. Cassidy, A. Hiltner, E. Baer, *Connect. Tissue Res.* **1989**, *23*, 75.
[277] S. Chae, U. Yong, W. Park, Y. Choi, I.-H. Jeon, H. Kang, J. Jang, H. S. Choi, D.-W. Cho, *Bioact. Mater.* **2023**, *19*, 611.
[278] S. Chae, Y. Sun, Y.-J. Choi, D.-H. Ha, I. Jeon, D.-W. Cho, *Biofabrication* **2021**, *13*, 035005.
[279] G. D. O'Connell, H. L. Guerin, D. M. Elliott, *J. Biomech. Eng.* **2009**, *131*, 111007.
[280] E. R. Acaroglu, J. C. Latridis, L. A. Setton, R. J. Foster, V. C. Mow, and M. Weidenbaum, *Spine* **1995**, *20*, 2690.
[281] S. Mohanty, C. L. Dahia, *WIREs Dev. Biol.* **2019**, *8*, e343.
[282] J. Li, W. R. K. Illeperuma, Z. Suo, J. J. Vlassak, *ACS Macro Lett.* **2014**, *3*, 520.
[283] P. Sabouri, A. Hashemi, *Med. Eng. Phys.* **2021**, *88*, 1.
[284] A. M. Dydyk, R. Ngnitewe Massa, F. B. Mesfin, in *StatPearls*, StatPearls Publishing, Treasure Island (FL), **2023**.
[285] X. Li, Y. Liu, L. Li, R. Huo, F. Ghezelbash, Z. Ma, G. Bao, S. Liu, Z. Yang, M. H. Weber, N. Y. K. Li-Jessen, L. Haglund, J. Li, *Mater. Horiz.* **2023**, *10*, 1705.
[286] T. Boontheekul, H.-J. Kong, D. J. Mooney, *Biomaterials* **2005**, *26*, 2455.
[287] E. Y. Jiang, S. R. Sloan, C. Wipplinger, S. Kirnaz, R. Härtl, L. J. Bonassar, *Acta Biomater.* **2019**, *97*, 428.
[288] R. M. Schek, A. J. Michalek, J. C. Iatridis, *Eur. Cell. Mater.* **2011**, *21*, 373.
[289] S. Virk, T. Chen, K. N. Meyers, V. Lafage, F. Schwab, S. A. Maher, *Spine J.* **2020**, *20*, 1344.
[290] A. R. Dixon, J. P. Warren, M. P. Culbert, M. Mengoni, R. K. Wilcox, *J. Mech. Behav. Biomed. Mater.* **2021**, *123*, 104703.
[291] A. T. Francisco, R. J. Mancino, R. D. Bowles, J. M. Brunger, D. M. Tainter, Y.-T. Chen, W. J. Richardson, F. Guilak, L. A. Setton, *Biomaterials* **2013**, *34*, 7381.
[292] A. T. Francisco, P. Y. Hwang, C. G. Jeong, L. Jing, J. Chen, L. A. Setton, *Acta Biomater.* **2014**, *10*, 1102.
[293] Y. Deng, X. Zhang, R. Li, Z. Li, B. Yang, P. Shi, H. Zhang, C. Wang, C. Wen, G. Li, L. Bian, *Biomaterials* **2022**, *281*, 121316.

[294] C. C. Shu, A. Dart, R. Bell, C. Dart, E. Clarke, M. M. Smith, C. B. Little, J. Melrose, *JOR Spine* **2018**, *1*, e1037.
[295] C. C. Shu, M. M. Smith, S. M. Smith, A. J. Dart, C. B. Little, J. Melrose, *Int. J. Mol. Sci.* **2017**, *18*, E1049.
[296] S. E. Bulman, C. M. Coleman, J. M. Murphy, N. Medcalf, A. E. Ryan, F. Barry, *Stem Cell Res. Ther.* **2015**, *6*, 34.
[297] Y. Liu, M. Wang, Y. Luo, Q. Liang, Y. Yu, F. Chen, J. Yao, *Gels* **2021**, *7*, 263.
[298] L. Zhou, P. Guo, M. D'Este, W. Tong, J. Xu, H. Yao, M. J. Stoddart, G. J. V. M. van Osch, K. K.-W. Ho, Z. Li, L. Qin, *Engineering* **2022**, *13*, 71.
[299] W. A. Azab, K. Nasim, M. Najibullah, *Acta Neurochir. (Wien)* **2016**, *158*, 749.
[300] C. Daly, P. Ghosh, G. Jenkin, D. Oehme, T. Goldschlager, *BioMed Res. Int.* **2016**, *2016*, 5952165.
[301] J. C. Beckstein, S. Sen, T. P. Schaer, E. J. Vresilovic, D. M. Elliott, *Spine* **2008**, *33*, E166.
[302] H. Cherif, L. Li, J. Snuggs, X. Li, C. Sammon, J. Li, L. Beckman, L. Haglund, C. L. L. Maitre, *Acta Biomater.* **2023**, S1742.
[303] F. Han, Q. Yu, G. Chu, J. Li, Z. Zhu, Z. Tu, C. Liu, W. Zhang, R. Zhao, H. Mao, F. Han, B. Li, *Adv. Healthc. Mater.* **2022**, *11*, 2200895.
[304] S. Lin, C. Cao, Q. Wang, M. Gonzalez, J. E. Dolbow, X. Zhao, *Soft Matter* **2014**, *10*, 7519.